THE ROLE OF LRP2 IN EMBRYONIC DEVELOPMENT OF ZEBRAFISH AND MOUSE

Dissertation zur Erlangung des akademischen Grades
des Doktors der Naturwissenschaften
(Dr. rer. nat.)

eingereicht im Fachbereich Biologie, Chemie, Pharmazie
der Freien Universität Berlin

vorgelegt von

ESTHER KUR
2012

Diese Arbeit wurde von November 2007 bis Juli 2011 unter der Leitung von Prof. Dr. Thomas Willnow am Max-Delbrück-Centrum für Molekulare Medizin durchgeführt.

1. Gutachter: Prof. Dr. Volker Haucke, Freie Universität Berlin

2. Gutachter: Prof. Dr. Thomas Willnow, Max-Delbrück-Centrum Berlin-Buch

Disputation am 22. November 2011

DANKSAGUNG

Ich möchte mich bei Prof. Thomas Willnow für die Möglichkeit, in seiner Arbeitsgruppe zu promovieren, sowie für die intensive Betreung bedanken.
Dr. Annette Hammes danke ich ebenfalls für ausgezeichnete Betreuung.
Mein Dank geht auch an Prof. Volker Haucke von der freien Universität Berlin für die Betreuung und Begutachtung meiner Dissertation.
Außerdem möchte ich meinen Kollegen aus der AG Willnow für ihre Hilfsbereitschaft und die sehr gute Atmosphäre im Labor danken.

CONTENTS

LIST OF ABBREVIATIONS

AEP	Anterior entopeduncular area
AME	Axial mesendoderm
ANOVA	Analysis of variance
ANR	Anterior neural ridge
APOER2	Apolipoprotein receptor 2
AVE	Anterior visceral endoderm
BAC	Bacterial artificial chromosome
BMP	Bone morphogenetic protein
BOC	Brother of CDO
BSA	Bovine serum albumin
CDO	Cell adhesion molecule-related/downregulated by oncogenes
C. elegans	*Caenorhabditis elegans*
CNS	Central nervous system
DAB2	Disabled 2
DBP	Vitamin D binding protein
DBS	Donnai-Barrow syndrome
DLG1	Discs large homolog 1
D. melanogaster	*Drosophila melanogaster*
E	Embryonic day
EGF	Epidermal growth factor
EGFP	Enhanced green fluorescent protein
EMX2	Empty spiracles 2
ES cells	Embryonic stem cells
EST	Expressed sequence tag
FDR	False discovery rate
FGF	Fibroblast growth factor
FOX	Forkhead box protein
HPE	Holoprosencephaly
hpf	Hours post fertilization
hrs	Hours
ICD	Intracellular domain
IOP	Intraocular pressure

ISH	In situ hybridization
LCM	Laser capture microdissection
LDL	Low density lipoprotein
LDLR	LDL receptor
LMO	LIM domain only protein
LRP	LDLR related protein
MHP	Medial hinge point
MIH	Midline interhemispheric HPE
min	Minutes
NDS/NGS	Normal donkey/goat serum
NKX	NK homeobox protein
NLS	Nuclear localization signal
NTD	Neural tube defect
PBS	Phosphate buffered saline
PCP	Prechordal plate
PCR	Polymerase chain reaction
PDZ	PSD95/DLG1/ZO-1
PFA	Paraformaldehyde
PSD95	Post synaptic density protein 95
RA	Retinoic acid
RBP	Retinol/vitamin A binding protein
RIP	Regulated intramembraneous proteolysis
sec	Seconds
SHBG	Sex hormone binding globulin
SHH	Sonic hedgehog
SorLA	Sortilin-related receptor, LA-repeats containing
SOX	SRY-box containing
tm	targeted mutation
WNT	Wingless-related/MMTV integration site protein
WT1	Wilms tumor 1
ZIC	Zinc finger protein of the cerebellum
ZO-1	Zona occludens-1 protein

LIST OF FIGURES

LIST OF TABLES

SUMMARY

LRP2 is a member of the LDL receptor gene family expressed on the apical surface of several epithelia in vertebrate organisms. In the adult, it has important functions in renal protein reabsorption and vitamin homeostasis. In the embryo, the receptor regulates forebrain formation through control of BMP4, SHH and FGF8, morphogens that form a signaling network and reciprocally regulate each other's expression. Loss of LRP2 expression results in deregulation of forebrain signaling and holoprosencephaly. My aim was to describe potential molecular functions for LRP2 in controlling this morphogenetic network. Towards this goal, I generated and validated novel transgenic animal models: receptor deficient zebrafish lines and a LRP2 reporter mouse line.

In zebrafish deficient for Lrp2, I analyzed the role of this receptor in zebrafish embryogenesis, and I compared my findings to phenotypes observed in mouse models. I uncovered that expression of Lrp2 in zebrafish embryos recapitulates spatial, but not temporal aspects of the pattern seen in mammals. Furthermore, I identified and described a novel LDL receptor family member, Lrp2b, that is unique to fish and highly homologous to Lrp2. Finally, my studies revealed that the function of Lrp2 in renal tubular clearance, but not in forebrain development, is conserved between fish and mammals.

To more clearly define the role of LRP2 in mammalian forebrain development, I generated a new mouse model expressing EGFPcre under the control of the endogenous *Lrp2* promoter. Using this model, I showed that the *Lrp2* promoter is most active in the ventral midline cells of the forebrain. These cells show distinct morphological defects upon loss of LRP2 function, leading to impaired neuroepithelial hingepoint formation and ultimately resulting in a delay of neural tube closure. To globally assess the defects in ventral midline cells lacking LRP2, I performed microarray analysis of forebrain midline tissue from LRP2 deficient embryos and controls and identified several novel gene pathways affected in *Lrp2* mutants previously not considered, such as WNT and notch signaling. Furthermore, analysis of my data showed that loss of receptor activity results in a dorsalization as well as a posteriorization of the forebrain at the expense of telencephalic identity.

Taken together, my studies demonstrated that a role in forebrain development is unique to mammalian LRP2. My findings provide an important explanatory model for the consequences of LRP2 deficiency in mammalian forebrain development, thus helping to guide further studies aimed at unraveling the molecular mechanism of this critical receptor pathway.

Parts of this thesis were published/accepted for revision:

Loss of Lrp2 in Zebrafish Disrupts Pronephric Tubular Clearance But Not Forebrain Development. Esther Kur, Anna Christa, Kerry N. Veth, Chandresh R. Gajera, Miguel A. Andrade-Navarro, Jingjing Zhang, Jason R. Willer, Ronald G. Gregg, Salim Abdelilah-Seyfried, Sebastian Bachmann, Brian A. Link, Annette Hammes, and Thomas E. Willnow. *Dev Dyn* 240(6): 1567-77, Mar 2011

LRP2 is a Component of the SHH Receptor Complex Required to Condition the Forebrain Ventral Midline for Inductive Signals. Annabel Christ, Anna Christa, Esther Kur, Oleg Lioubinski, Sebastian Bachmann, Thomas E. Willnow, and Annette Hammes. *Dev Cell,* in revision

ZUSAMMENFASSUNG

LRP2 ist ein Mitglied der LDL-Rezeptorfamilie und wird in Wirbeltieren auf der apikalen Oberfläche zahlreicher Epithelien exprimiert. Im adulten Organismus ist LRP2 wichtig für die Reabsorption von Proteinen in der Niere, sowie für die rezeptorvermittelte Endozytose zahlreicher Vitamine und Steroidhormone. Während der Embryonalentwicklung steuert der Rezeptor die Ausbildung des Vorderhirns, indem er die Signaltransduktion durch die Morphogene BMP4, SHH und FGF8 beeinflusst. Der genetisch bedingte Verlust der LRP2 Expression im Mausmodell und in Patienten verursacht eine Störung der Vorderhirnentwicklung und führt zu Holoprosenzephalie. Ziel meiner Arbeit war es, mögliche molekulare Funktionen von LRP2 bei der Kontrolle der genannten Morphogene zu beschreiben. Ich habe zu diesem Zweck neue Tiermodelle generiert bzw. validiert: eine Rezeptor-defiziente Zebrafischlinie sowie eine LRP2 Reportermauslinie.

In Lrp2-defizienten Zebrafischen habe ich die Rolle des Rezeptors in der Embryonalentwicklung untersucht. Ich konnte zeigen, dass die Expressionsdomänen von Lrp2 im Zebrafisch und in der Maus übereinstimmen, aber dass der Rezeptor im Zebrafisch zu einem deutlich späteren Zeitpunkt exprimiert wird. Desweiteren habe ich ein neues Mitglied der LDL-Rezeptorfamilie identifiziert, das nur in Fischen existiert. Dieser Rezeptor ist eng mit Lrp2 verwandt und wurde deshalb Lrp2b genannt. Meine Studien ergaben, dass die Funktion von Lrp2 bei Reabsorptionsprozessen in der Niere zwischen Fischen und Säugetieren konserviert ist, nicht aber seine Funktion bei der Vorderhirnentwicklung.

Um die Rolle von LRP2 während der Vorderhirnentwicklung von Säugetieren näher zu untersuchen, habe ich ein Mausmodell generiert, in welchem EGFPcre unter der Kontrolle des endogenen *Lrp2*-Promotors exprimiert wird. Anhand dieses Modells konnte ich zeigen, dass die *Lrp2*-Promotoraktivität in den Zellen der ventralen Mittellinie des Vorderhirns am stärksten ist. In LRP2-defizienten Mäusen weisen diese Zellen morphologische Defekte auf, die die weitere Morphogenese des Neuroepithels beeinflussen und letztlich eine verzögerte Schließung des Neuralrohrs bewirken. Ich die Genexpression der Mittellinienzellen mithilfe von Microarray-Analysen untersucht und konnte zeigen, dass mehr Signalwege von dem Verlust der LRP2-Expression betroffen sind, als bisher beschrieben, so wie die WNT- und Notch-Signalwege. Außerdem zeigt meine Analyse, dass der Phänotyp LRP2-defizienter Mäuse mit einer Dorsalisierung und einer Posteriorisierung des Vorderhirns einhergeht, die eine eingeschränkte Ausbildung des Telenzephalons zur Folge hat.

Zusammenfassend legen meine Ergebnisse dar, dass die Funktion von LRP2 in der Vorderhirnentwicklung auf Säugetiere beschränkt zu sein scheint. Außerdem konnte ich mithife meiner Daten ein Modell entwickeln, das die Auswirkungen des LRP2-Verlustes in Säugetieren darstellt. Somit liefert diese Arbeit die Grundlage für weitere Analysen der molekularen Funktion dieses wichtigen Rezeptors.

1. INTRODUCTION

1.1 THE LDLR FAMILY

The low density lipoprotein (LDL) receptor family represents a group of cell surface receptors with diverse biological functions (Herz and Bock, 2002). The first family member to be identified was the low density lipoprotein receptor (LDLR), a key component of cholesterol metabolism (Goldstein and Brown, 1979; Goldstein and Brown, 1986). Several structurally related proteins were identified since, and accordingly called LDLR-related proteins (LRPs). The LDLR family consists of seven core family members and three more distantly related family members (Figure 1). In vertebrates, the core family members are LDLR, LRP1, LRP1B, LRP2, LRP4, LRP8 (apolipoprotein E receptor-2, APOER2) and very low density lipoprotein receptor (VLDLR). The more distantly related family members are LRP5, LRP6 and SorLA (sortilin-related receptor, LA repeats containing) (Herz and Bock, 2002).

1.1.1 Structural hallmarks of LDLR family members

In the core family members, the extracellular domain is composed of either one or multiple copies of a distinct module consisting of complement-type repeats, epidermal growth factor (EGF)-type repeats and YWTD-motif containing β-propellers (Figure 1). The complement-type repeats are the site of ligand binding, whereas the β-propellers are implicated in pH-dependent ligand release in endosomes. In the more distant family members, this module is either inverted (LRP5/6) or combined with motifs that are not present in the other receptors (SorLA). All members of the LDLR family are anchored to the plasma membrane by a single transmembrane domain (May et al., 2003).
The short carboxy-terminal cytoplasmic domains are characteristic of the individual receptors. Here, the sequence homology between family members is much lower than in the extracellular domains. The cytoplasmic domains are crucial for the function of the LDLR family members since they harbor regulatory phosphorylation sites (Li et al., 2001b) as well as motifs implicated in endocytosis (NPxY, YxxΦ, dileucin) and protein interactions (PxxP, PDZ domain binding motif) (Chen et al., 1990) (Li et al., 2001a). Compared to classical signaling receptors, the cytoplasmic tails are very short and do not contain any kinase domains. However, signal transduction can be archieved via clustering

of the receptors and binding of adaptor proteins to the protein interaction motifs (Li et al., 2001a).

1.1.2 Evolution of the LDLR family

While no homologs have been identified in *Saccharomyces cerevisiae*, all organisms from *Caenorhabditis elegans (C. elegans)* and *Drosophila melanogaster (D. melanogaster)* to mammals express members of the LDLR family. This finding suggests that LDL receptors are required for the functional integrity of multicellular organisms while being dispensable for unicellular organisms (Christensen and Verroust, 2002).
Several LDLR family members are described in *C. elegans*, e.g. RME 2 (receptor mediated endocytosis 2) (Grant and Hirsh, 1999), a homolog of mammalian VLDLR, and Ce-LRP1, that has virtually the same structure as mammalian LRP2 (Yochem et al., 1999) (Grigorenko et al., 2004). Also in *D. melanogaster*, multiple family members have been identified, such as LRP1, LRP2, LpR1/2 (homologous to LDLR) (Khaliullina et al., 2009), arrow (homologous to LRP5/6), and yolkless, a receptor variant that is not present in vertebrates (Herz and Bock, 2002) (Schonbaum et al., 1995). In mice, all family members depicted in figure 1 are expressed.

1.1.3 Functions of LDLR family members

Multiple ligands have been described to bind to LDLR family members, including lipoproteins, vitamins, hormones, protease/protease inhibitor complexes, extracellular matrix proteins and signaling molecules (May et al., 2005). This multitude of ligands is consistent with the diverse biological functions of the receptors. Loss-of-function of LDLR family members results in diverse phenotypes including defects in lipid metabolism and development. An overview of LDLR family loss-of-function models is given in table 1.

Functions in the adult organism
The prototype of the receptor family, the LDLR, mediates cellular uptake of cholesterol-rich lipoproteins. In humans, an inheritable gene defect in LDLR leads to high plasma cholesterol levels (hypercholesterolemia) and consequently to an increased risk of atherosclerosis and coronary artery disease (Goldstein et al., 2001). Since other LDLR family members also bind lipoproteins and mediate their uptake, it was initially assumed

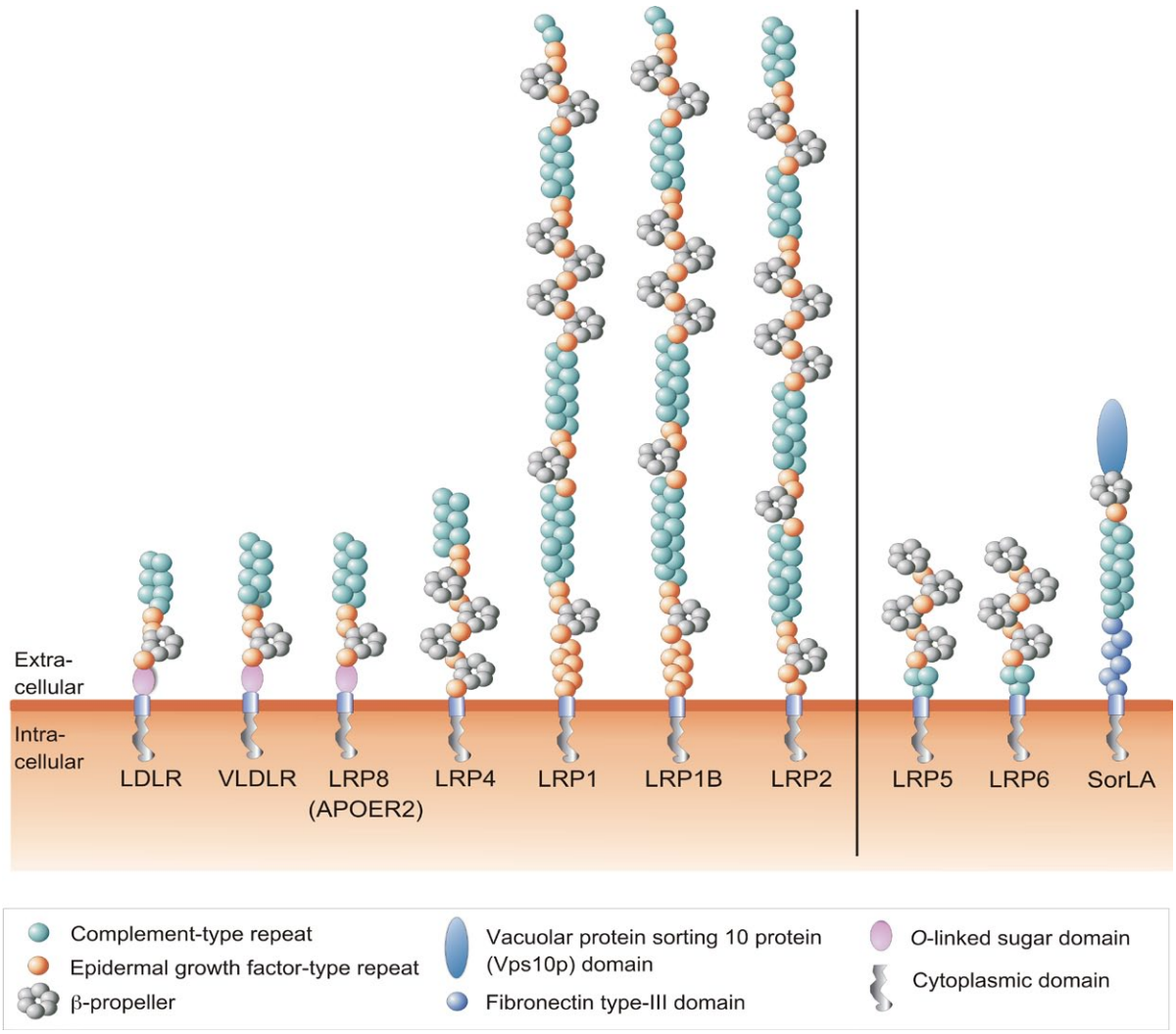

Figure 1. The low density lipoprotein receptor (LDLR) family.
The structural organization of members of the LDLR family is depicted. Receptors on the left are considered core family members, receptors on the right are more distantly related. VLDLR: very low density lipoprotein receptor, LRP: LDLR related protein, SorLA: sortilin-related receptor, LA repeats containing. (Modified from Willnow et al., 2007)

that they would mainly act in lipid transport. However, their functions turned out to be much more diverse.

For instance, LRP1 is not only a receptor for chylomicrons, large triglyceride-rich proteins that carry lipids from the gut to the liver, but also plays an important role in regulation of proteases and their inhibitors and in phagocytosis (Herz and Bock, 2002). Not much is known about the function of LRP1B, but it has been described to be silenced in several human tumors, indicating a role as a tumor suppressor (Liu et al., 2000) (Langbein et al., 2002) (Sonoda et al., 2004). In recent years, a protective role for the LDLR family members

LRP1, LRP2 and SorLA in Alzheimer's disease was reported. The current hypothesis is that these LDLR family members influence the intracellular trafficking of the amyloid precursor protein (Li et al., 2001a) (May et al., 2005) (Willnow et al., 2008). Thus, they inhibit the accumulation of amyloid plaques, which are a hallmark of Alzheimer's disease and presumably toxic for neurons (Kadowaki et al., 2005).

Table 1. Loss-of-function models of the low density lipoprotein receptor (LDLR) family.
Receptors for which loss-of function is associated with developmental defects is highlighted. (Modified from Willnow et al., 2007)

Receptor	Expression	Organism	Phenotype	References
LDLR	Vertebrates	Rabbit	Hypercholesterolemia Hypercholesterolemia	Tanzawa et al., 1980 Ishibashi et al., 1993
VLDLR	Vertebrates	Mouse Chicken	Dysplastic cerebellum, reduced adipose tissue mass Impaired vitellogenesis, female sterility	Trommsdorff et al., 1999 Bujo et al., 1995
Yolkless	Insects	*D. melanogaster*	Impaired vitellogenesis, female sterility	Schonbaum et al., 1995
RME-2	Nematodes	C. elegans	Impaired yolk deposition, reduced embryonic viability	Grant and Hirsch, 1999
LRP8	Vertebrates	Mouse	Dysplastic hippocampus and cerebellum	Trommsdorff et al., 1999
LRP4	Vertebrates	Mouse Cattle	Impaired limb formation, polysyndaktyly, neuromuscular junction defects Syndaktyly	Johnson et al., 2005 Simon-Chazottes et al., 2006 Zhang et al., 2008 Duchesne et al., 2006
LRP5	Vertebrates, Invertebrates	Mouse	Low bone mass, hypercholesterolemia, impaired insulin secretion	Fujino et al., 2003 Kato et al., 2002
LRP6	Vertebrates, Invertebrates	Mouse Xenopus *D. melanogaster*	Abnormal body axis Impaired dorsal axis and neural crest formation Inhibition of Wingless-dependant patterning	Pinson et al., 2000 Tamai et al., 2000 Wehrli et al., 2000
LRP1	Vertebrates	Mouse	Embryonic lethality	Herz et al., 1992 Roebroeck et al., 2006
LRP1B	Vertebrates	Mouse	Unknown	Marschang et al., 2004
LPR2	Vertebrates, Invertebrates	Mouse Rat Zebrafish *D. melanogaster* *C. elegans*	Holoprosencephaly, impaired maturation of reproductive organs, renal dysfunction Glomerular nephrits Adult onset ocular pathogenesis Death at larval stages Molting defects, larval growth arrest	Willnow et al., 1996 Nykjaer et al., 1999 Hammes et al., 2005 Raychowdhury et al., 1989 Veth et al., 2011 Riedel et al., 2011 Yochem et al., 1999
SorLA	Vertebrates, Invertebrates	Mouse	Increased risk for Alzheimer's disease	Andersen et al., 2005

Functions in the developing organism

It was known early on that lipoproteins and their receptors have an important function in embryonic development, since studies in humans and experimental animal models showed that the inactivation of key factors in lipoprotein metabolism severely affects normal embryonic development. Examples are the Smith-Lemli-Opitz syndrome and desmosterolosis, which are caused by mutations in 7-dehydrocholesterol reductase and desmosterol reductase, respectively (Smith et al., 1964) (Irons et al., 1993) (FitzPatrick et al., 1998). The syndromes include developmental phenotypes like cleft palate, microcephaly, global developmental delay, polydactyly and heart defects. This was supposed to be mainly due to inadequate supply of cholesterol from endogenous biosynthesis or from maternal sources absorbed via the yolk sac (Kelley, 2000). Today, the view has emerged that LDLR family members actively participate in signaling pathways by regulating the distribution and local delivery of key regulators of cellular differentiation, such as sterols and lipid-linked morphogens (Willnow et al., 2007).

While the LDLR itself seems to be dispensable for embryogenesis, the loss of other family members has severe consequences for developmental processes (see table 1). For instance, LRP1 deficient embryos die around midgestation (Herz et al., 1993), likely due to abnormal development of the liver (Roebroek et al., 2006).

LRP4 deficient embryos show impaired limb formation and polysyndaktyly, probably due to suppression of WNT signaling in the apical ectodermal ridge, an important structure for growth and patterning of the limb (Johnson et al., 2005). In addition, it was reported that LRP4 acts as a receptor for agrin, a motor neuron-derived ligand that induces the formation of neuromuscular junctions (Kim et al., 2008) (Zhang et al., 2008).

VLDLR and LRP8 (APOER2) influence neuronal migration by binding to reelin, a neuronal guidance factor in the central nervous system (CNS) (D'Arcangelo et al., 1999) (Hiesberger et al., 1999). Signaling through reelin and VLDLR/LRP8 is important for correct layering of the brain. Accordingly, mice deficient for both VLDLR and LRP8 exhibit a dysplastic cerebellum as well as a disturbed architecture of cortex and hippocampus (Curran and D'Arcangelo, 1998) (Trommsdorff et al., 1999). Human patients homozygous for a mutation in the VLDLR gene display cerebellar hypoplasia (Boycott et al., 2005).

LRP5 and LRP6 are important components of the WNT signaling pathway since they bind WNT proteins and act as coreceptors to frizzled. Phosphorylation of the cytoplasmic tail of LRP6 recruits axin, a component of the β-catenin destruction complex, to the cell membrane (Davidson et al., 2005) (Zeng et al., 2005). This inhibits the degradation of

β-catenin so that β-catenin can translocate to the nucleus and activate the transcription of WNT target genes.
Like the LDLR family members mentioned above, also LRP2 plays an important role during development. The function of LRP2 in the embryonic as well as in the adult organism will be the subject of the next chapter.

1.2 LRP2

LRP2 is the largest member of the LDLR family. Loss-of-function-models of LRP2 exist in several organisms including *C. elegans*, *D. melanogaster*, zebrafish and mouse. Furthermore, also patients with mutations in LRP2 have been described. Studying the impact of LRP2 deficiency in these different organisms provided important insights into the diverse molecular functions of this receptor.

1.2.1 Invertebrate animal models for LRP2 deficiency

In *C. elegans*, LRP2 (misleadingly called Ce-LRP1) is expressed in the larval epidermis. Embryos deficient for the receptor hatch and initiate development, but at the mold from the third to the fourth larval stage or even earlier they stop growing and die. Probably, this is due to an inability to shed and degrade the old cuticle during molting. The phenotype of the mutant can be copied by sterol starvation, suggesting that the major function of LRP2 is endocytosis of sterols (Yochem et al., 1999). On the other hand, a similar phenotype is caused by deficiency for imp-2, a secretase that releases the LRP2 intracellular domain (ICD) by regulated intramembraneous proteolysis (RIP). Imp-2 deficiency can be rescued by expression of the LRP2 ICD, suggesting that LRP2 is not only needed for endocytosis, but that some important functions are carried out by its ICD (Grigorenko et al., 2004). Recently, it was shown that the LRP2 ICD regulates gene expression in the nucleus, similar as described for the Notch ICD (Li et al., 2008).
LRP2 deficiency also affects development of *D. melanogaster*. Mutant larvae die before adulthood and rarely reach the crawling third instar larval stage (Riedel et al., 2011), indicating that LRP2 fulfils a crucial function in the developing organism. Specific knock-down of LRP2 in the wing disc, the embryonic structure giving rise to the wing, results in altered pigmentation and stiffness of the cuticle. Here, LRP2 is needed for endocytosis and spatial restriction of Yellow, a protein important for melanization. In the absence of LRP2,

Yellow persists at higher levels and ectopic melanization occurs (Riedel et al., 2011).

1.2.2 Lrp2 deficient zebrafish

Recently, two zebrafish lines deficient for Lrp2 have been identified in mutagenesis screens. As adults, these Lrp2 deficient fish develop abnormally enlarged eyes and exhibit risk factors for glaucoma including severe myopia, elevated intraocular pressure (IOP), and progressive retinal ganglion cell loss with upregulation of stress genes. The authors suggest that Lrp2, which is expressed in the retinal pigmented epithelium, is needed for regulation of fluid homeostasis in the eye. Consequently, Lrp2 deficiency results in elevated IOP which then causes excessive eye growth (Veth et al., 2011). The impact of Lrp2 deficiency in zebrafish at earlier developmental stages has not been thoroughly analyzed so far.

1.2.3 LRP2 deficient mice

Mice deficient for LRP2 have been first described in 1996 (Willnow et al., 1996). Except for occasional survivors, *Lrp2*$^{-/-}$ mice die perinatally on the commonly used C57BL/6N and 129SvEmcTer genetic backgrounds. So far, it is unclear whether the cause of death is respiratory insufficiency or defects in brain development. The complex phenotypes of LRP2 deficient mice will be summarized in this chapter.

Impaired renal protein reabsorption in Lrp2$^{-/-}$ mice

The site of highest LRP2 expression in the adult mouse is the brush border surface of kidney proximal tubule cells. In LRP2 deficient mice surviving to adulthood, the kidney develops normally, however electronmicroscopic analysis shows that endocytic structures are drastically reduced (Nykjaer et al., 1999), indicating that LRP2 plays an important role in protein reabsorption from the glomerular filtrate. Indeed, LRP2 deficient mice suffer from low-molecular-weight proteinuria (Willnow et al., 1996).

The physiological relevance of LRP2 in retrieval of filtered metabolites is best described for the vitamin D_3 precursor 25-OH vitamin D_3. LRP2-mediated uptake of 25-OH vitamin D_3/ DBP (vitamin D binding protein) complexes from the lumen of the renal tubules prevents urinary excretion of the vitamin D_3 precursor. Following internalization, the carrier DBP is degraded in lysosomes of the tubular cells, while 25-OH vitamin D_3 is released

into the cytosol and converted into the active hormone 1,25-$(OH)_2$ vitamin D_3, a potent regulator of calcium homeostasis (Brown et al., 2002). In LRP2 deficient mice, the vitamin D_3 precursor cannot be reabsorbed from the glomerular filtrate and is therefore excreted and lost, resulting in vitamin D deficiency and bone-calcification defects (Nykjaer et al., 1999). Similar functions for LRP2 have been described for reabsorption of vitamin A and vitamin B_{12} metabolites bound to their respective carrier proteins, indicating a general role of LRP2 in hormone homeostasis.

Impaired sex hormone signaling in Lrp2$^{-/-}$ mice

LRP2 deficient mice exhibit anomalies in genital maturation. Male *Lrp2$^{-/-}$* mice show incomplete descent of the testes into the scrotum, while female *Lrp2$^{-/-}$* mice exhibit impaired opening of the vaginal cavity . Both phenotypes are consistent with an insensitivity to sex hormones. Strikingly, LRP2 is highly expressed in the male and female reproductive organs (epidydimis, prostate, ovaries and uterus), suggesting a function for the receptor in mediating sex hormone action (Hammes et al., 2005).

In the blood, androgens and estrogens are transported bound to the carrier protein sex hormone binding globulin (SHBG). According to the free hormone hypothesis, only free steroids are biologically relevant, because binding to carrier proteins prevents them from entering cells by free diffusion. Contrary to this hypothesis, it was shown that LRP2 can mediate the uptake of sex hormone/SHBG complexes, thereby delivering carrier bound but biologically active steroids to their target cells (Hammes et al., 2005). Consequently, in LRP2 deficient mice, androgen and estrogen signaling is impaired due to inefficient steroid uptake into target cells, leading to impaired maturation of the reproductive organs.

Defective forebrain development in Lrp2$^{-/-}$ mice

Besides the roles of LRP2 in the adult organism (renal protein reabsorption) and during late embryonic/postnatal stages (genital maturation), LRP2 is also crucial during early embryonic development. In the developing mouse brain, LRP2 is expressed on the apical surface of the neuroepithelium. Mice that lack expression of LRP2 show severe facial dysgenesis and brain malformations (Willnow et al., 1996). Newborns are characterized by a shortened snout and occasional cleft lip/palate. Histological sections of the brain reveal improper separation of the forebrain hemispheres and expanded lateral ventricles (Spoelgen et al., 2005). This phenotype is consistent with features observed in holoprosencephaly (HPE) (see box 1).

Box1. Pathogenesis of holoprosencephaly (HPE)

HPE is a common brain malformation resulting from a failure to delineate the midline of forebrain and face (Roach et al., 1975) (Muenke and Beachy, 2000). In humans, it occurs in 1 in 250 conceptuses and 1 in 16,000 live births, revealing that most affected embryos are eliminated by spontaneous abortion. According to its severity, HPE can be grouped into distinct forms. In alobar HPE, no lateral separation of the brain occurs. The whole forebrain is monoventricular, and the face can be cyclopic. Affected individuals are generally not viable. In semi-lobar HPE, the hemispheres and ventricles partially separate, but only posteriorly. In lobar HPE, the hemispheres separate, but the ventricles are dysmorphic. Additionally, anterior structures such as corpus callosum and the olfactory bulbs are missing or hypoplastic (Cohen, 2006). The recently defined microforms of HPE include combinations of mild craniofacial features of HPE (like hypotelorism, cleft lip/palate, single central incisor) and mild neurological defects like absent septum pellucidum, optic nerve abnormalities and pituitary dysfunction (Rosenfeld et al., 2010). Finally, besides these forms of 'classical' HPE, there is also the so-called midline interhemispheric (MIH) HPE or syntelecephaly, which is characterized by failure of the posterior regions to separate while the anterior structures develop normally.

HPE can be caused by genetic and environmental factors. Environmental risk factors are maternal diabetes, maternal alcoholism and prenatal exposure to drugs (Cohen and Shiota, 2002). Genetic causes include mutations in components of the nodal, sonic hedgehog (SHH), fibroblast growth factor (FGF), bone morphogenetic protein (BMP), wingless/int (WNT) and retinoic acid (RA) signaling pathways (Rosenfeld et al., 2010) (Geng and Oliver, 2009). Evidence for involvement of these pathways in the emergence of HPE comes from both patient data and the analysis of mouse models (Schachter and Krauss, 2008). In contrast to humans, in mice, usually only homozygous mutations in HPE genes produce a phenotype, but not heterozygous mutations (Fernandes and Hebert, 2008).

The clinical manifestation of HPE in patients is highly variable. In family members carrying the same mutation, the whole spectrum of HPE can be observed (Krauss, 2007). The explanation for this variability might be the multiple-hit model, which states that HPE is not a monogenic disease, but that more than two genetic or environmental factors contribute to its phenotype (Geng and Oliver, 2009).

Initially, if was hypothesized that the defect underlying the HPE phenotype in LRP2 deficient mice is insufficient uptake of cholesterol from the maternal circulation resulting in starvation of neuroepithelial cells for cholesterol. This was a plausible explanation since LRP2 is highly expressed in the yolk sac (Willnow et al., 1996). However, generation of conditional *Lrp2* mutants deficient for LRP2 in the embryo, but not in the yolk sac, demonstrated that sustained LRP2 expression in the yolk sac does not prevent forebrain malformations. This result suggests that expression of LRP2 on the neuroepithelium is crucial for normal brain development (Spoelgen et al., 2005).

The severity of the holoprosencephalic phenotype in LRP2 deficient mice is dependent on the genetic background. While a mild phenotype resembling lobar HPE is observed on the FVB/N background (Gajera et al., 2010), the phenotype on the C57Bl/6N or 129SvEmcTer background can be described as semilobar, sometimes even alobar (see Box1), with basically all $Lrp2^{-/-}$ animals dying perinatally. This variability is likely to be explained by the presence of genetic modifiers, additional gene variants that affect the severity and

penetrance of the phenotype.
On the molecular level, the phenotype of *Lrp2*$^{-/-}$ embryos comprises increased bone morphogenetic protein 4 (BMP4) expression and dorsally extended fibroblast growth factor 8 (FGF8) expression at embryonic day (E) 9.5, as well as decreased cell proliferation and reduced sonic hedgehog (SHH) expression in the anterior entopeduncular area (AEP) at E10.5. These findings indicate disturbed dorsoventral patterning (Spoelgen et al., 2005).

1.2.4 *LRP2* mutations in humans

In recent years, several patients with mutations in the *LRP2* gene have been described. A study by Kantarci et al. reports that mutations in *LRP2* cause the Donnai-Barrow syndrome (DBS) (Kantarci et al., 2007). This rare autosomal recessive syndrome comprises several malformations, including agenesis of the corpus callosum, coloboma (a gap in the eye's structures), congenital diaphragmatic hernia, facial dysmorphology, ocular anomalies, proteinuria and developmental delay (Donnai, 1996) (Chassaing et al., 2003) (Kantarci et al., 2007). Another recent study describes that mutations in *LRP2* cause microforms of HPE (see Box1) (Rosenfeld et al., 2010). The authors hypothesize that in a specific genetic background or upon certain environmental influences, mutations in *LRP2* may also lead to more severe forms of HPE.
In summary, both studies show that LRP2 plays an important developmental role not only in animal models, but also in humans. To appreciate the function of LRP2 in forebrain development and in the emergence of HPE, it is crucial to understand the complex processes involved in normal forebrain development. Therefore, these processes will be summarized in the following chapter.

1.3 FOREBRAIN DEVELOPMENT AND MIDLINE SPECIFICATION

The forebrain is the most anterior derivative of the embryonic neural tissue. It gives rise to telencephalon and diencephalon, comprising brain centers that control functions like perception, memory, emotions, voluntary movements and regulation of endocrine homeostasis. Its development involves the integration of signals from multiple neural and non-neural patterning centers as well as regulated cell proliferation, cell differentiation, cell migration and cell shape changes. The principles underlying forebrain development are highly conserved and therefore common to all vertebrates.

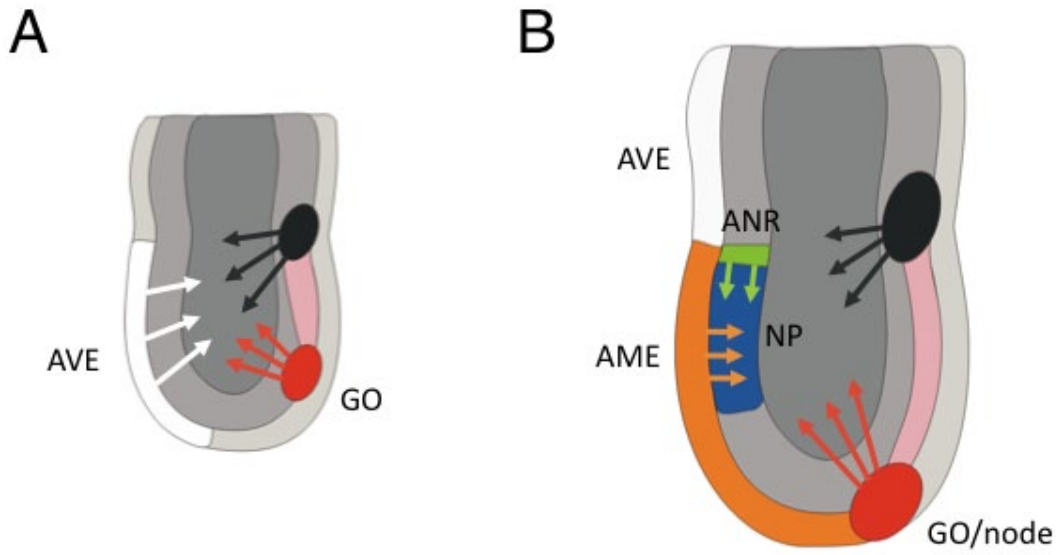

Figure 2. Forebrain induction by anti-BMP and FGF signals.
(A) At embryonic day (E) 6.5, BMP signals (black) from posterior mesodermal tissue are antagonized by anti-BMP activity (white and red) from the gastrula organizer (GO) and the anterior visceral endoderm (AVE). **(B)** At E7.25, the neural plate (NP) has formed. It receives anti-BMP signals (orange and red) from the anterior mesendoderm (AME) and the GO/node. FGF signals (green) from the anterior neural ridge (ANR) establish anterior identity within the NP.

1.3.1 Forebrain induction

The first steps of forebrain development occur very early in embryogenesis, during a process called gastrulation. During gastrulation, the simple two-layered embryonic body plan (epiblast and hypoblast) is reorganized into the three-layered body plan of the mature organism, consisting of the outer ectoderm, the inner endoderm and the interstitial mesoderm. The process of gastrulation involves complex cell movements and rearrangements, thereby enabling novel interactions between the repositioned tissues.
Since BMP signals from posterior mesodermal tissue inhibit formation of neural tissues, signals that antagonize BMP signaling are required for forebrain development. These anti-BMP signals are secreted by specialized tissues, which are the gastrula organizer, the AVE (anterior visceral endoderm) and at slightly later stages the AME (axial mesendoderm) (Figure 2). The secreted molecules include the BMP antagonists chordin and noggin (Yang and Klingensmith, 2006), as well as nodal, which can also negatively interact with BMP signaling (Yang et al., 2010). These signals are crucial for the division of the ectoderm into surface ectoderm (giving rise to the epidermis) and neuroectoderm (giving rise to the neural plate).

Besides anti-BMP signals, another prerequisite for induction of forebrain identity are FGF signals. In the newly formed neural plate, the anterior neural ridge (ANR), a region at the anterior junction of neural plate and surface ectoderm, begins to express FGF8 (Figure 2 B). FGF8 expression is induced by signals from the AME that antagonize the posteriorizing effect of wingless/int (WNT) signals from lateral mesoderm and posterior ectoderm (Kazanskaya et al., 2000). There is also evidence that cranial neural crest cells are important for induction and maintenance of FGF8 expression in the ANR (Creuzet et al., 2004). Once FGF8 expression is established, its role is to induce forebrain markers in the anterior part of the neural plate (Shanmugalingam et al., 2000).

1.3.2 Neurulation

Neurulation is the process during which the neural plate is transformed into a hollow neural tube beneath the overlying ectoderm. At the beginning of neurulation, the neural plate cells elongate into a columnar shape which distinguishes them from the flatter non-neural ectoderm cells (Smith and Schoenwolf, 1989). Subsequently, the edges of the neural plate thicken and move upward to form the neural folds. The so-called medial hingepoint (MHP) cells at the center of the neural plate shorten and constrict apically, thereby becoming wedge-shaped (van Straaten et al., 1988). Additional hingepoints are formed laterally. The neural folds migrate towards the midline of the embryo and eventually fuse to form the neural tube, so that medial becomes ventral and lateral becomes dorsal.
The process of neurulation requires drastic cell shape changes which are mediated by the cytoskeleton, namely actin filaments, microtubles and their respective regulatory proteins (Zolessi and Arruti, 2001). In addition, pinching off of the neural tube from the surface ectoderm requires differential expression of cell adhesion molecules: E-cadherin in the surface ectoderm and N-cadherin in the neural tube (Detrick et al., 1990).
Neural tube closure does not occur simultaneously throughout the embryo. The neural tube in the most anterior and posterior regions is still open when it has already closed in medial regions. The two open ends of the neural tube are called the anterior and posterior neuropore. Failure of neural tube closure results in congenital malformations called neural tube defects (NTDs). After congenital heart defects, NTDs are the second most prevalent malformations in human pregnancies. Failure of posterior neuropore closure results in a defect called spina bifida, while failure of anterior neuropore closure results in degeneration of the forebrain and anencephaly (Copp et al., 2003).

1.3.3 Midline specification and dorsoventral patterning

The forebrain midline is a specialized structure in the developing brain. It comprises the ventral midline, the dorsal midline and between them the anterior midline or ANR. When the telencephalic vesicle expands, the midline cells undergo reduced proliferation, thereby enabling the separation of the telencephalon into two bilateral vesicles, the hemispheres. As forebrain development proceeds, the dorsal midline cells differentiate into the choroid plexus, a structure which secretes the cerebrospinal fluid, and into the adjacent cortical hem, a signaling center which induces formation of the hippocampus. Rostrally and ventrally, midline cells contribute to the septum and ganglionic eminences, which give rise to parts of the basal ganglia (Fernandes and Hebert, 2008).
The midline gives not only rise to important structures, it also has a crucial function in establishing dorsal and ventral domains of the forebrain. This is achieved by secretion of distinct signaling molecules from the midline cells. As illustrated in figure 3, these are: SHH (from the ventral midline), FGFs (from the ANR), BMPs and WNTs (from the dorsal midline).

SHH signals from the ventral midline

During early forebrain development, nodal signaling induces expression of SHH in the prechordal plate (PCP) underlying the neural tube. Consequently, SHH from the PCP induces its own expression in the ventral neuroepithelium (Roelink et al., 1995). SHH secreted from the ventral midline (Figure 3, red) forms a gradient across the neural tube, with high ventral concentrations and low dorsal concentrations. SHH acts as a morphogen, meaning that it induces the expression of target genes in a concentration dependent manner. In more dorsal domains, SHH induces only its low-threshold targets, whereas in the ventral neuroepithelial cells it induces high-threshold targets like FOXA2, an important factor for the specification of ventral cells (Fuccillo et al., 2006).
Compared to the spinal cord, where ventral identity is thought to exclusively rely on SHH signals, patterning processes in the forebrain are more complicated, mainly due to the complex three dimensional architecture. Here, also FGF signals are needed to specify ventral cells (Gutin et al., 2006). FGF8 and SHH reciprocally regulate each other, rendering the interpretation of their functions complicated. In addition, there is evidence that retinoic acid (RA) signaling from the anterior forebrain modulates the expression of both FGF8 and SHH (Ribes and Briscoe, 2009), and there are also ventral BMP/WNT

signaling centers, in particular in the anlage of the ventral hippocampus (Hoch et al., 2009). However, regardless whether additional factors are needed and whether the effects of SHH are direct or via FGF8, it is clear that expression of SHH by the ventral midline cells is crucial for forebrain patterning. An indication for the important role of SHH is the phenotype of SHH deficient mice, which show a dramatic loss of midline structures with cyclopia (Chiang et al., 1996). Although less dramatic, also Shh deficient zebrafish show defects in the formation of midline structures like the optic chiasm (Schauerte et al., 1998).

FGF signals from the anterior neural ridge

The ANR expresses several FGF molecules (FGF3, 8, 15, 17, 18) (Figure 3, green). As mentioned above, their secretion plays an important role in specifying dorsoventral identities and in inducing anterior midline character (Storm et al., 2006) (Gutin et al., 2006). Mice defective for FGF signaling show lack of midline structures (Smith et al., 2006) (Tole et al., 2006) and in Fgf8 deficient zebrafish midline defects are observed (Shanmugalingam et al., 2000). In chick embryos, gain-of-function studies indicate that FGF8 induces formation of midline structures (Crossley et al., 2001). In SHH deficient mice, ectopic FGF8 signaling is able to induce expression of ZIC2 and LHX5, two transcription factors important for midline specification (Okada et al., 2008). Interestingly, ZIC2 is one of the genes causative for HPE in humans (Brown et al., 1998). Since SHH is known to positively regulate expression of FGF8, these results suggest that absence of midline structures in SHH deficient mice at least partly results from reduced FGF8 expression.

BMP and WNT signals from the dorsal midline

Several BMP molecules (BMP2, 4, 5, 6, 7) are expressed in the dorsal midline. In the spinal cord, BMP signals play an active role in conveying positional information along the dorsoventral axis to neuroepithelial cells. Similar to the ventral SHH gradient, a dorsal BMP4 gradient is formed. High BMP4 concentrations induce expression of transcription factors like MATH1, while lower BMP4 concentrations induce expression of transcription factors like neurogenin 1 and 2 (Liu and Niswander, 2005).

Again, the situation in the forebrain differs from the situation in the spinal cord. BMP signaling is clearly necessary for the formation of the dorsal-most structure, the choroid plexus, but beyond that it seems to be dispensable for dorsoventral patterning of the forebrain (Fernandes et al., 2007). Rather, the important aspect seems to be that BMP4

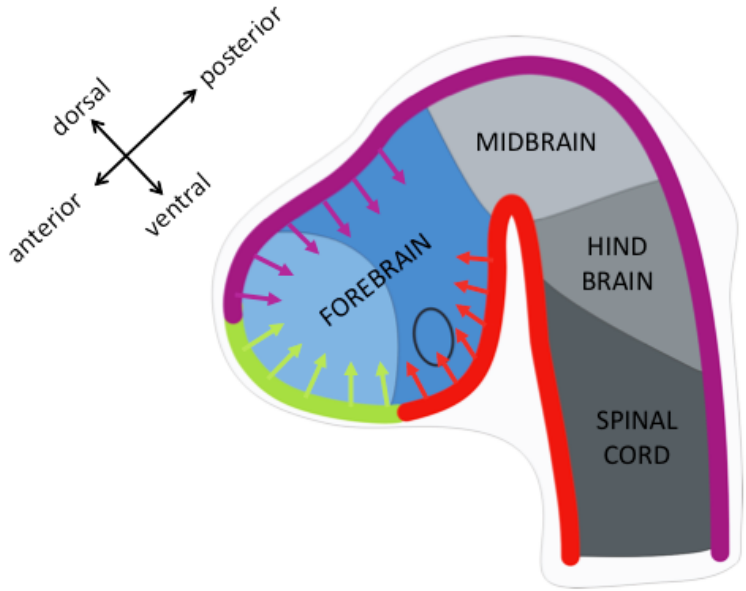

Figure 3. Dorsoventral and anterioposterior patterning by signals from the forebrain midline. At embryonic day 9.5, diencephalon (blue) and telencephalon (light blue) can be distinguished within the forebrain. From midline tissue, the forebrain receives dorsoventral and anterioposterior patterning information: WNT and BMP signals from the dorsal midline (purple), FGF signals from the anterior neural ridge (green) as well as SHH signals from the ventral midline (red).

downregulates the expression of SHH and FGF8 and therefore has to be restricted to the dorsal neuroepithelium (Liu and Niswander, 2005).

Besides BMP molecules, also WNT molecules (WNT1, 2b, 3a, 5a, 8b) are expressed in the dorsal midline. A direct role for *Wnt* genes in midline formation has not been demonstrated. However, there is evidence that WNT signaling interacts with the other key morphogen pathways, e.g. by maintaining FGF8 expression and thereby counteracting BMP4 signals (Paek et al., 2011).

Deregulation of forebrain patterning can result in HPE

Many mutations in pathways governing specification and patterning of the forebrain (nodal, SHH, FGF, BMP, WNT and RA signaling) have been reported to cause HPE (Geng and Oliver, 2009) (Rosenfeld et al., 2010). Here, a correlation can be seen between when and where a signaling pathway is crucial during development, and the severity of the HPE phenotype caused by its disruption. Alterations in pathways that are active during early stages (e.g. nodal or SHH) are likely to promote alobar HPE. Alterations in pathways that are active during or after neural tube closure (e.g. FGF or RA) disturb rostral and ventral patterning centers, thereby causing semilobar HPE. Alterations in dorsal patterning centers (i.e. BMP or WNT) cause failure of the dorsal midline structures to develop, but do not affect ventral patterning, thereby causing MIH HPE (Geng and Oliver, 2009). However, this classification is not clear-cut, since most of the pathways are interconnected and thus disturbances in one pathway also impair patterning processes controlled by another pathway.

2. AIM

Forebrain development is a tightly regulated process whereby a simple neuroepithelial cell sheet is transformed into a highly specialized tissue during early stages of ontogeny. Defects in forebrain formation can result in holoprosencephaly (HPE), a devastating disorder in which the cerebral hemispheres fail to separate along the midline. Patients carrying mutations in the *LRP2* gene display microforms of HPE, a feature recapitulated in mice with targeted *Lrp2* gene disruption.

The underlying developmental defect has been linked to impaired dorsoventral patterning of the murine neural tube associated with altered expression of the morphogens SHH, BMP4 and FGF8. However, due to the complex nature of interactions, it was so far unclear which morphogenic pathway was primarily affected by receptor deficiency. Furthermore, the exact mechanism of LRP2 action at the cellular level remained enigmatic. Thus, the aim of my project was to characterize the molecular function of LRP2 in early forebrain development and to unravel the reasons for patterning defects and HPE caused by LRP2 deficiency. Towards these goals, I chose two experimental approaches:

1) The first approach was to validate the zebrafish as novel model organism of LRP2 deficiency as it offers a range of experimental possibilities, especially with respect to imaging, knock-down and overexpression approaches. These techniques may help to dissect the morphogen pathway network underlying the HPE phenotype caused by LRP2 deficiency in mice and humans. An additional goal was to determine the extent of conservation of LRP2 function from fish to mammals.

2) My second approach aimed at an in depth molecular and cellular analysis of the forebrain defects in LRP2 deficient mice that extends beyond the mere description of target pathways by in situ hybridization. I generated a reporter mouse line (*Lrp2*$^{tm(EGFPcre)}$) to visualize single LRP2 expressing cells and to investigate LRP2 function by employing novel experimental techniques, like lineage tracing, live cell imaging and cell sorting by flow cytometry. Furthermore, I performed gene expression profiling of forebrain midline tissue to achieve a global and unbiased representation of the pathways affected by LRP2 deficiency.

3. RESULTS

3.1 ZEBRAFISH LRP2 IS CRUCIAL FOR KIDNEY FUNCTION, BUT NOT FOR FOREBRAIN DEVELOPMENT

In several model organisms including *C. elegans*, *D. melanogaster* and mice, LRP2 is known to be crucial for normal embryonic development (Yochem et al., 1999) (Riedel et al., 2011) (Willnow et al., 1996). However, not much is known about its role during early development of another common model organism, the zebrafish. Due to their transparent nature, their rapid development and the possibility to easily perform knock-down, rescue and overexpression experiments, zebrafish embryos are perfectly suited for studying developmental processes. Therefore, I decided to explore the usefulness of the zebrafish as a model to analyze the function of *Lrp2* and its gene product LRP2 (designated *lrp2* and Lrp2 in zebrafish, respectively).

3.1.1 Detailed expression analysis of Lrp2 in the zebrafish

Before starting to investigate the role of Lrp2 in zebrafish, it was important to clarify whether its expression pattern was comparable to the expression pattern of LRP2 in mammals. Towards this aim I performed in situ hybridization (ISH) experiments on zebrafish embryos.

Zebrafish Lrp2 recapitulates spatial aspects of mammalian LRP2 expression

By whole-mount ISH, expression of *lrp2* mRNA was detected in the developing brain, the embryonic kidney (pronephros) as well as in the otic vesicles at 48 hours post fertilization (hpf) (Figure 4). Thus, expression of *lrp2* nicely recapitulated the expression pattern seen in mammals. This conservation of expression domains in zebrafish was an important indication that the function of Lrp2 may be conserved as well.

To further define the site of Lrp2 expression in the developing brain, I performed immunohistology. For detection of Lrp2 I used two different polyclonal antibodies raised against the full-length receptor purified from rabbit. On coronal sections at 48 hpf, expression of Lrp2 was detected on the apical surface of cells lining the brain ventricles (Figure 5 B). Since these cells are known to be radial glia cells, I also stained for brain lipid binding protein (Blbp), a radial glia marker (Figure 5 C). Indeed, colocalization of Lrp2

and Blbp was observed (Figure 5 D), demonstrating that the Lrp2 expressing cells in the zebrafish brain were radial glia cells.

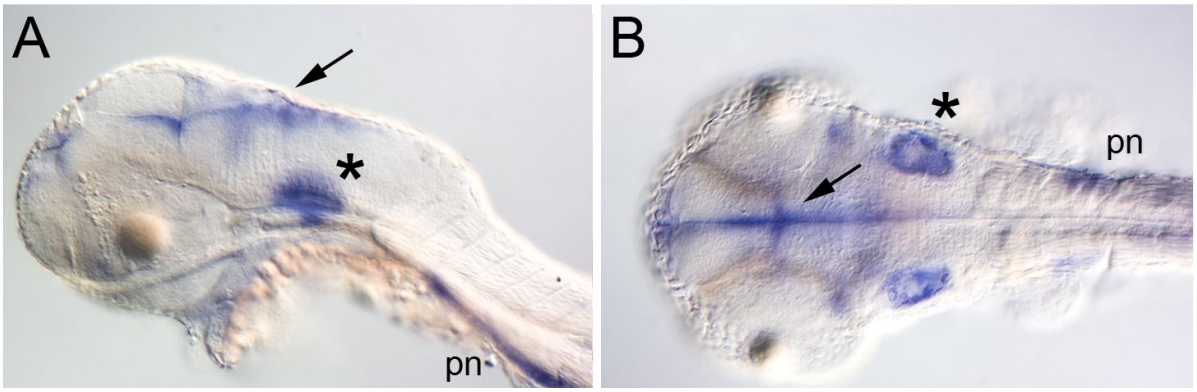

Figure 4. Expression of *lrp2* mRNA in zebrafish embryos at 48 hpf.
(A, B) Lateral and dorsal views of a zebrafish embryo at 48 hpf. Expression of *lrp2* is detected by whole-mount in situ hybridization. Asterisks mark expression in the otic vesicle, pn indicates expression in the pronephros, arrows highlight expression in the central nervous system.

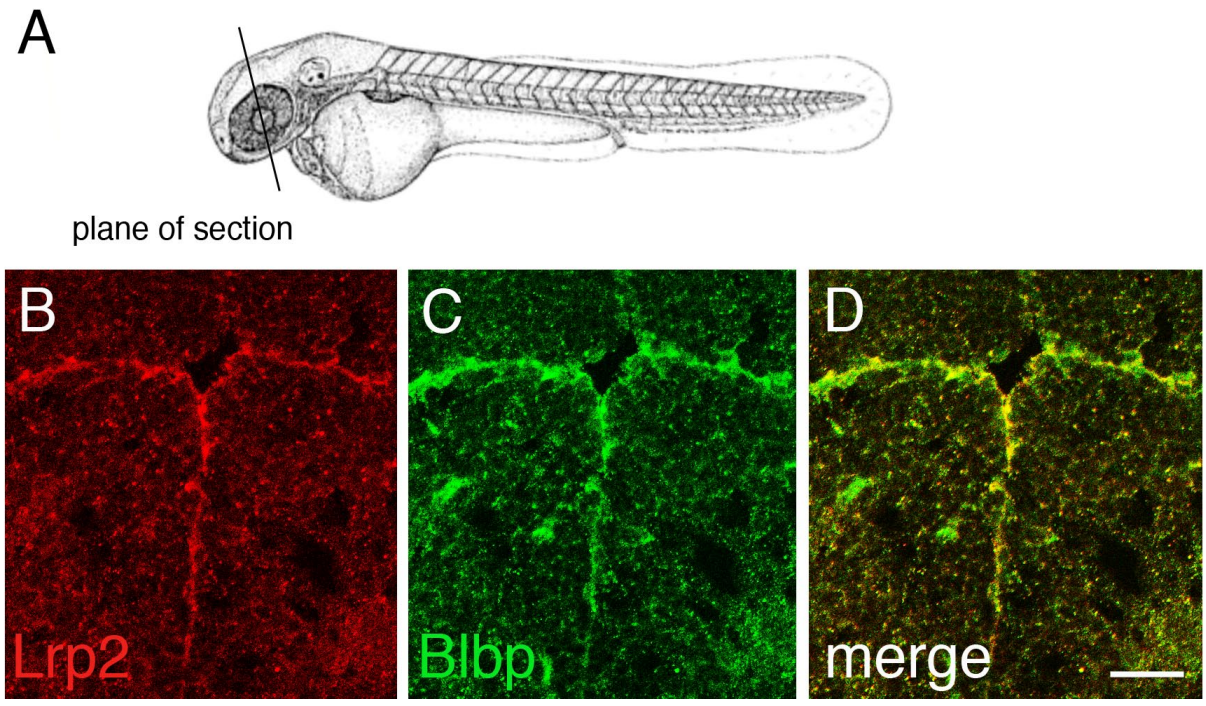

Figure 5. Expression of Lrp2 in the ventricular system.
(A) Scheme of a zebrafish embryo at 48 hpf indicating the plane of section shown in (B-D). **(B, C)** Immunohistological detection of Lrp2 and brain lipid binding protein (Blbp) on coronal forebrain sections. **(D)** Merge of Lrp2 and Blbp staining demonstrating co-localization of both proteins. Scale bar: 25 µm. (Modified from Kur et al., 2011)

Zebrafish Lrp2 does not recapitulate temporal aspects of mammalian LRP2 expression

To further characterize the expression of *lrp2* in the zebrafish during different stages of ontogeny, ISH was carried out at several time points. Prominent expression of the receptor in the pronephros was apparent as early as 20 hpf and persisted throughout all analyzed embryonic stages (Figure 6 A-D, F-H). *Lrp2* expression in the otic vesicles appeared slightly later at 24 hpf and also persisted (Figure 6 B-D, F-H). In contrast to the early onset of expression at these sites, in the brain, very low expression of *lrp2* was first seen at 36 hpf (Figure 6 D, E). Expression levels in the brain peaked at 48 hpf (Figure 6 F) and again decreased at later stages (Figure 6 G, H). This temporal aspect clearly distinguishes the expression pattern of the receptor in the zebrafish brain from the expression pattern of LRP2 in the mouse brain, where it is robustly expressed from neurulation on (Annabel Christ, personal communication).

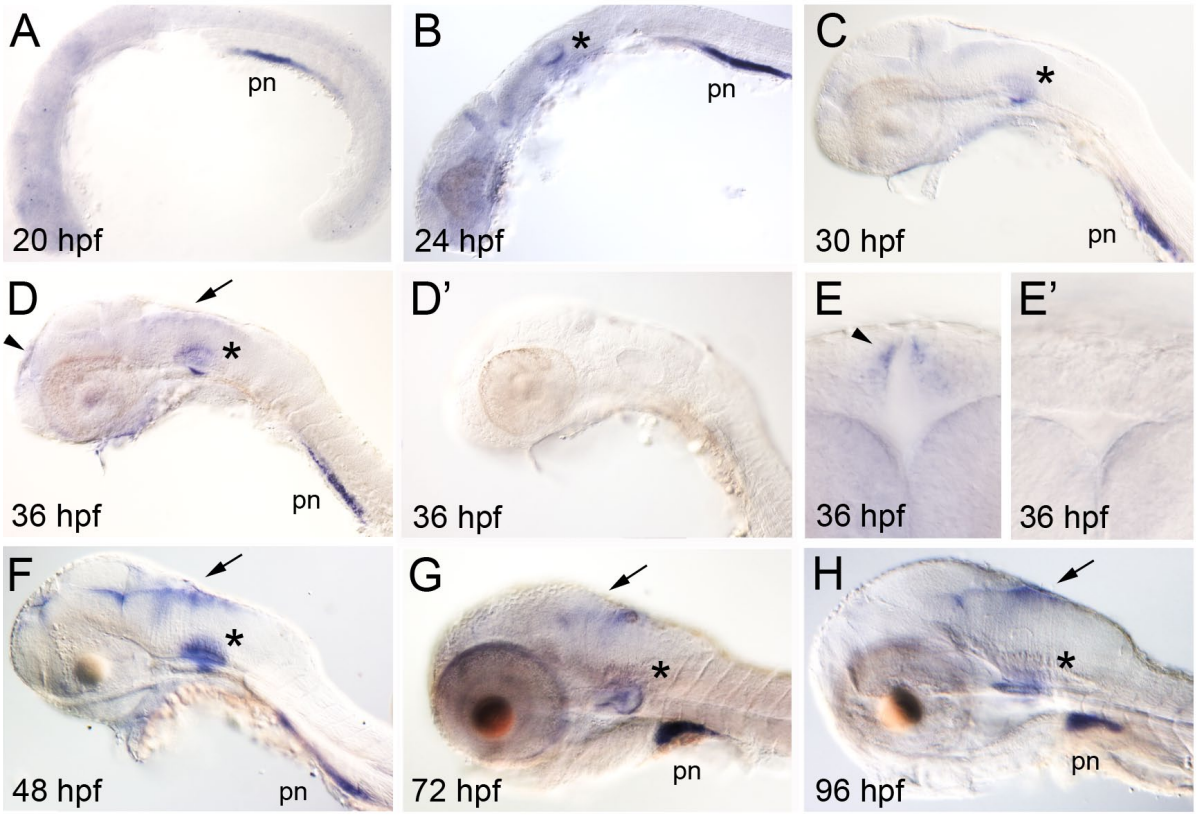

Figure 6. Expression of *lrp2* mRNA in zebrafish embryos at different developmental stages.
(A-H, but not D', E') Whole mount in situ hybridization (ISH) for *lrp2* in zebrafish embryos at the indicated time points. Asterisks mark expression in the otic vesicle, pn indicates expression in the pronephros, arrows highlight expression in the central nervous system. Arrowheads indicate faint *lrp2* expression in the telencephalon at 36 hpf in lateral (D) and frontal (E) views. **(D', E')** ISH at 36 hpf using the *lrp2* sense probe as negative control. (Kur et al., 2011)

Having confirmed that the expression of zebrafish Lrp2 spatially recapitulates the pattern seen in mammals, I decided to analyze the consequences of loss of Lrp2 function during embryonic development of the zebrafish.

3.1.2 Analysis of Lrp2 deficient zebrafish

Targeted gene disruption is more difficult in the zebrafish than in the mouse, since zebrafish embryonic stem (ES) cell lines have not been successfully established yet. Approaches to permanently disrupt specific genes at the one cell stage by zinc finger nucleases are promising (Doyon et al., 2008), but until now, analysis of zebrafish deficient for a protein of interest mainly depends on morpholino knock-down approaches and mutants identified in mutagenesis screens.

Bugeye and 5cben zebrafish lines are deficient for Lrp2

Recently, two zebrafish lines *bugeye (lrp2^{mw1})* and *5cben (lrp2^{p5bnc})* were identified in independent forward-genetic screens for adult ocular defects (Veth et al., 2011). Starting from three months of age, these fish develop considerably enlarged eyes (Figure 7 B-D).

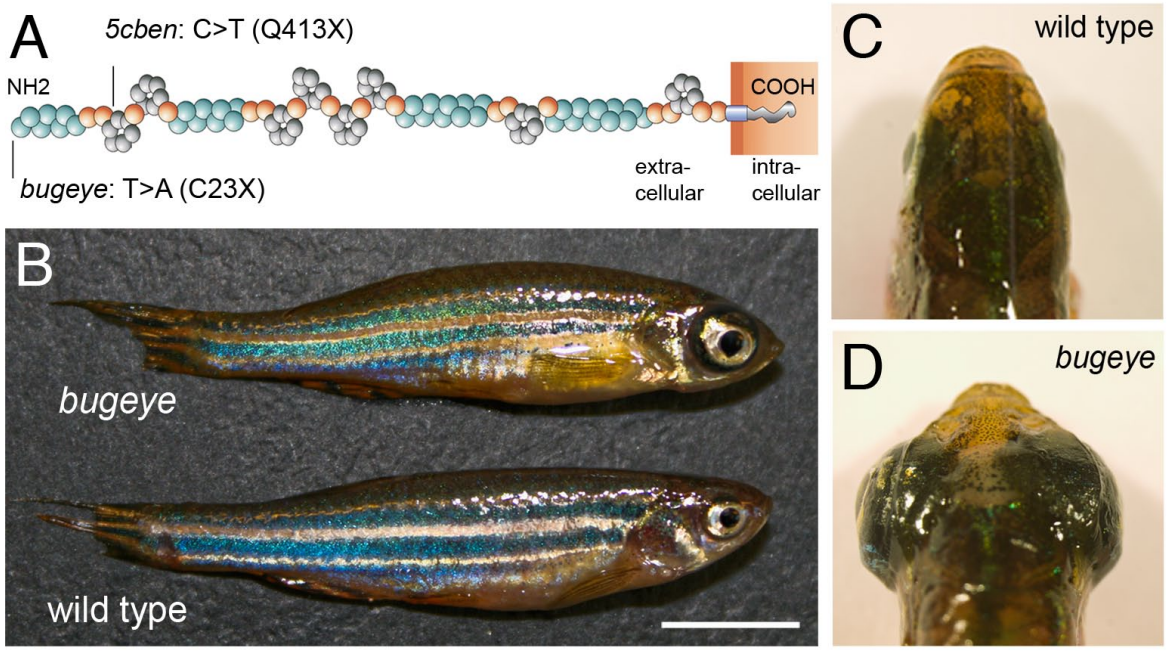

Figure 7. Lrp2 deficient zebrafish lines *bugeye* and *5cben*.
(A) Structure of Lrp2 indicating amino acid changes in *bugeye* and *5cben* lines. **(B)** Adult wild type and *bugeye* zebrafish in lateral view. Scale bar: 0.5 cm **(C, D)** Adult wild type and *bugeye* zebrafish in dorsal view highlighting the large eye phenotype in mutants. (Modified from Kur et al., 2011)

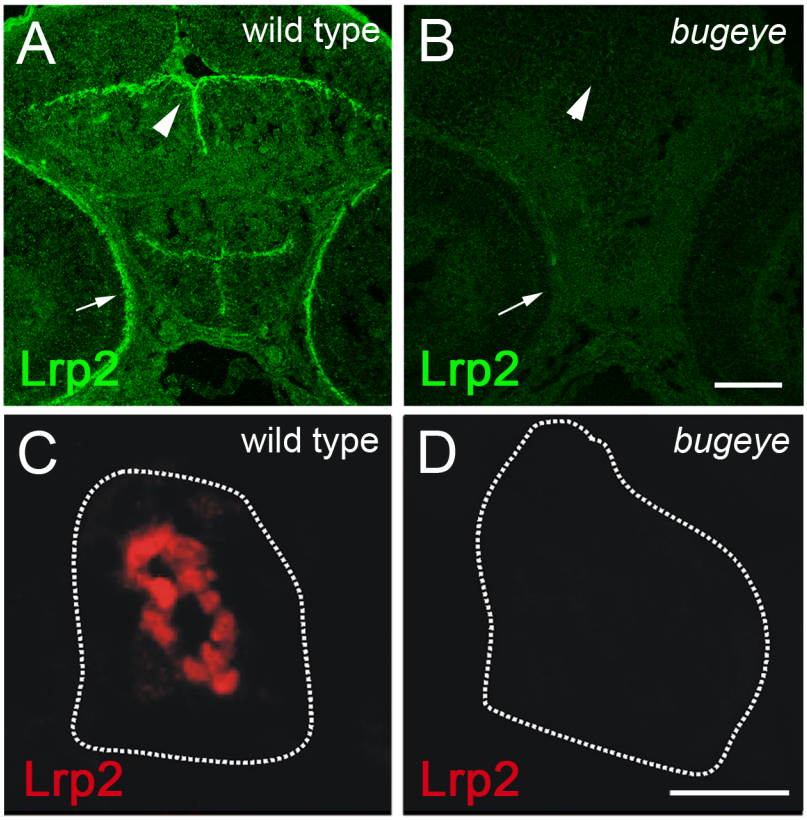

Figure 8. Loss of Lrp2 expression in *bugeye* mutants.
(A, B) Immunohistological detection of Lrp2 in the retinal pigment epithelium (arrow) and the ventricular system (arrowhead) on coronal sections of wild type (A) but not *bugeye* (B) embryos at 48 hpf. scale bar: 50 µm. **(C, D)** Immunohistological detection of Lrp2 on coronal sections of the pronephros in wild type (C) but not *bugeye* (D) larvae at 96 hpf. Scale bar: 25 µm. White lines indicate the outline of the pronephric ducts. (Modified from Kur et al., 2011)

Positional cloning efforts uncovered nonsense mutations in *lrp2* as the cause underlying the large eye phenotype (Veth et al., 2011). Both the *bugeye* and the *5cben* mutation lead to stop codons close to the amino terminus of the receptor (C23X and Q413X, respectively) (Figure 7 A). As shown by immunohistology, the mutations completely disrupt expression of Lrp2 in the zebrafish brain (Figure 8 A, B) and pronephros (Figure 8 C, D). Therefore, the *lrp2*^{mw1} and *lrp2*^{p5bnc} alleles can be considered as null alleles.
Overall, Lrp2 deficiency does not impact growth, viability, or reproduction of affected fish. The adult-onset eye phenotype has been described by Veth et al. and is summarized in chapter 1.2.2. In my study, I analyzed the consequences of Lrp2 deficiency for embryonic development. I focused on the structural and functional integrity of the kidney and the forebrain, since in these organs, the receptor has important functions in mammals.

Loss of Lrp2 disrupts clearance pathways in the zebrafish embryonic kidney

Robust expression of *lrp2* mRNA was seen in the zebrafish pronephros throughout ontogeny (Figure 6). To evaluate the consequences of receptor deficiency for this organ, I analyzed the development as well as the function of the embryonic kidney in *lrp2* mutant lines. To see whether there are morphological alterations in the Lrp2 deficient kidney, I

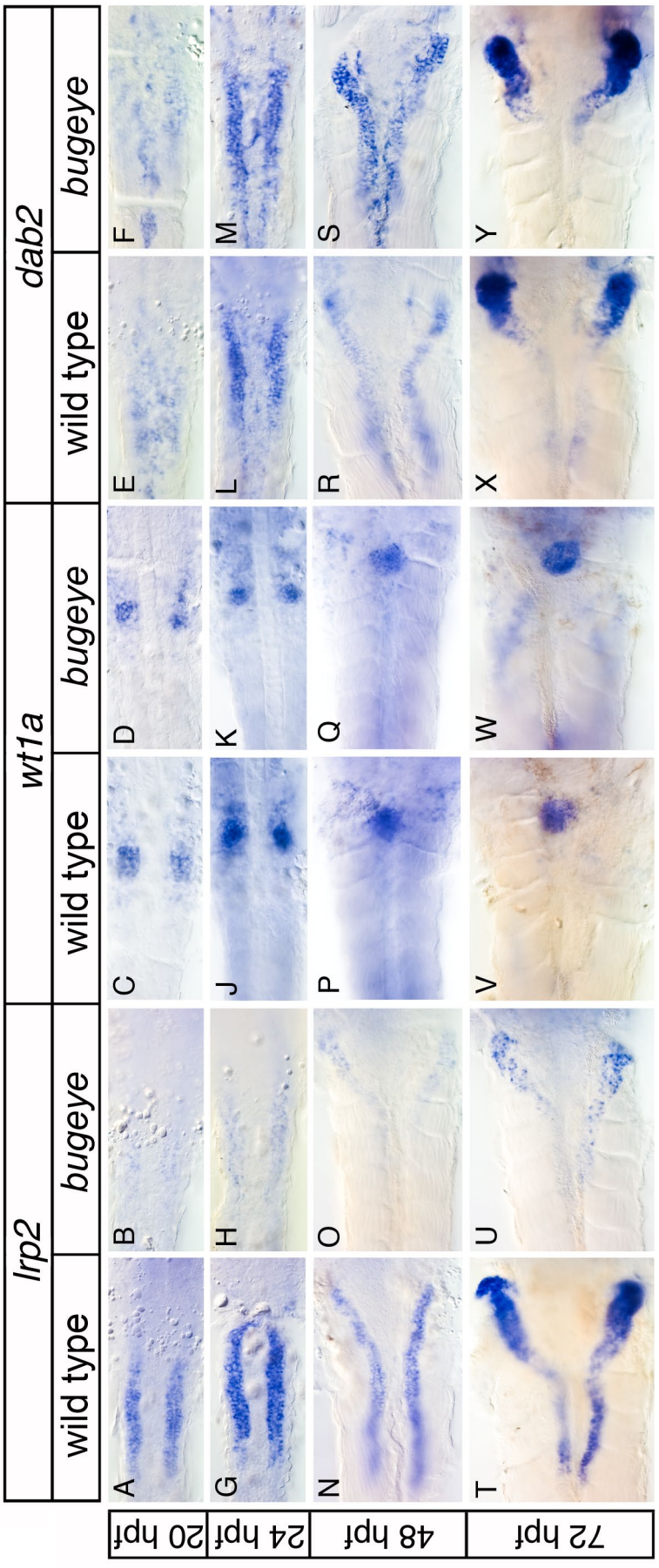

Figure 9. Loss of Lrp2 does not affect development of the pronephros.
(A-Y) Whole-mount in situ hybridization for *lrp2*, *wilms tumor 1a (wt1a)*, and *disabled 2 (dab2)* in wild type and *bugeye* embryos at the indicated time points. Ventral views of the pronephric region are shown. Signals for *lrp2* transcripts are reduced in *bugeye* embryos (B, H, O, U) compared to wild type controls (A, G, N, T). No discernable differences are seen in the expression domains of *wt1a* and *dab2* between mutant and wild type embryos. (Kur et al., 2011)

tested the mRNA expression patterns of the kidney markers *lrp2*, *disabled 2 (dab2)*, and *wilms tumor 1a (wt1a)* in wild type and mutant embryos from 20 to 72 hpf (Figure 9). *Wt1a* marks cells in the nephric primordia (20-24 hpf) that later fuse to form the central pronephric glomeruli (48-72 hpf) (Serluca and Fishman, 2001). *Lrp2* and *dab2* are co-expressed in the anterior part of the pronephric duct at 20-24 hpf. The expression domain becomes more restricted as the tubular system of the pronephros condenses (48-72 hpf). Signals for *lrp2* transcripts were significantly reduced but not absent in bugeye embryos suggesting that loss of receptor activity negatively impacts receptor gene transcription or that the non-sense mutation renders the RNA less stable. No discernable differences were seen in *dab2* and *wt1a* expression domains in mutant compared to wild type embryos.

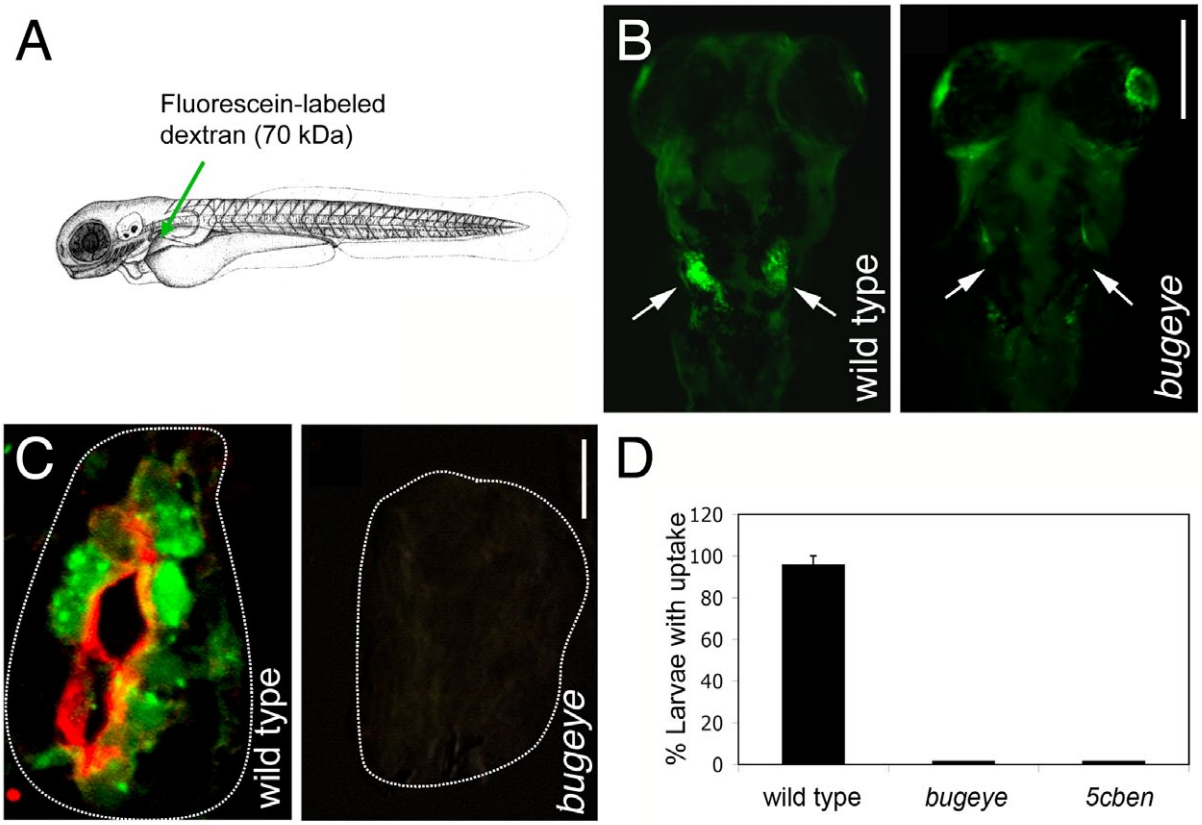

Figure 10. Lrp2 deficiency disrupts clearance pathways in the pronephros.
(A) Scheme depicting injection of fluorescein-labeled dextran into the cardinal vein of a zebrafish embryo. **(B)** Whole mount fluorescence microscopy showing accumulation of fluid phase marker fluorescein-labeled dextran (green) in the wild type but not in the Lrp2 deficient pronephros (arrows). Scale bar: 0.5 mm. **(C)** Immunohistochemical detection of Lrp2 (red) and fluorescein-labeled dextran (green) in the pronephros of wild type and *bugeye* larvae. White lines highlight the position of the pronephric ducts. Scale bar: 25 µm. **(D)** Wild type, *bugeye* and *5cben* larvae at 96 hpf were injected with fluorescein-labeled dextran and the number of larvae with tubular accumulation of tracer was evaluated by fluorescence microscopy. Data are given as % ± SEM of all larvae injected. n= 53 (wild type), 15 (*bugeye*), 23 (*5cben*). (Modified from Kur et al., 2011)

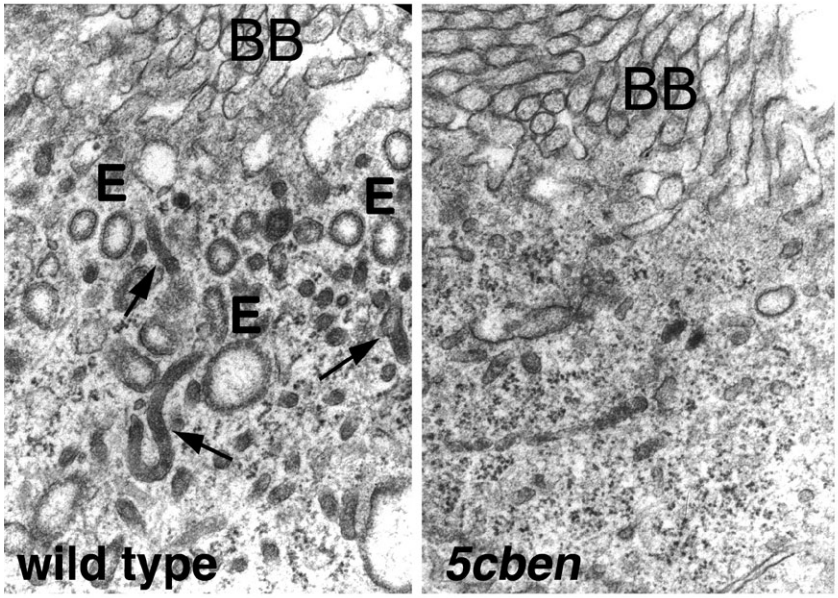

Figure 11. Lrp2 deficiency causes loss of the endocytic apparatus in the pronephros.
Electron microscopical analysis of the wildtype and *5cben* pronephros at 96 hpf. The endocytic apparatus including endosomes (E) and dense apical tubules (arrows) is almost completely lost in the *5cben* pronephros compared to the wild type control. BB: brush border of the tubular epithelium. (Kur et al., 2011)

In zebrafish, the onset of blood filtration in the kidney starts at 48 hpf (Drummond et al., 1998). Clearance of metabolites from the glomerular filtrate takes place in the pronephric duct regions that express Lrp2, suggesting a role for the receptor in reabsorptive processes. Tubular clearance pathways in the zebrafish pronephros can be analyzed by injection of fluid-phase tracers such as fluorescein-labeled dextran into the cardinal vein and by subsequent visualization of reabsorption of the dye from the primary urin into the pronephric duct (Figure 10 A) (Drummond et al., 1998).
Whereas in wild type embryos uptake of fluorescein-labeled dextran was detected by fluorescence microscopy on whole mounts (Figure 10 B) and on transverse sections through the kidney (Figure 10 C), loss of Lrp2 in *bugeye* embryos resulted in complete absence of pronephric uptake. This phenotype was also confirmed in *5cben* embryos. Figure 10 D shows a quantification of the results obtained in wild type, *bugeye* and *5cben* embryos.
To further define possible defects in the endocytic machinery of Lrp2 deficient zebrafish, we performed electron microscopical analysis of embryonic kidneys in the lab of Prof. Bachmann (Charité Berlin). In wild types, components of the endocytic apparatus such as endosomes or dense apical tubules (the recycling membrane compartment) were visible just below the apical surface of tubule cells. In contrast, these structures were drastically reduced or absent in *lrp2* mutants (Figure 11). The loss of the endocytic machinery in tubule cells lacking Lrp2 suggested that renal tubular endocytosis crucially depends on Lrp2 activity.

Loss of Lrp2 does not impair forebrain patterning in zebrafish

In mice, LRP2 deficiency leads to HPE with severe craniofacial malformations due to mispatterning of the forebrain (Spoelgen et al., 2005). To explore whether Lrp2 has a similar function in controling forebrain formation in zebrafish, I performed detailed histo-anatomical characterization of early forebrain development in *bugeye* and *5cben*. Surprisingly, no obvious alterations in head and forebrain anatomy were evident in whole

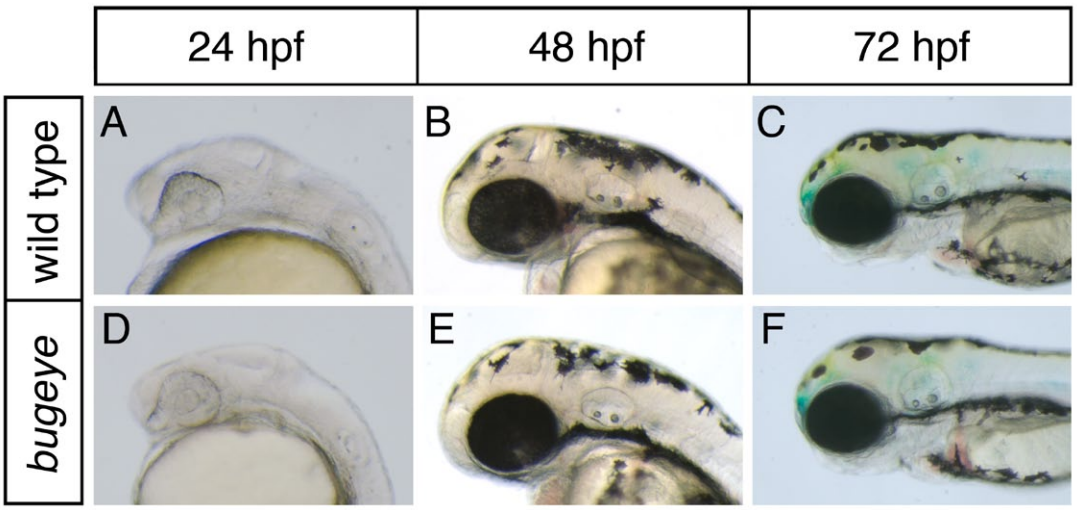

Figure 12. Head structures of wild type and Lrp2 deficient embryos.
Lateral head aspects of wild type and *bugeye* embryos at the indicated time points are shown. No obvious malformations in head anatomy are seen comparing both genotypes. (Modified from Kur et al., 2011)

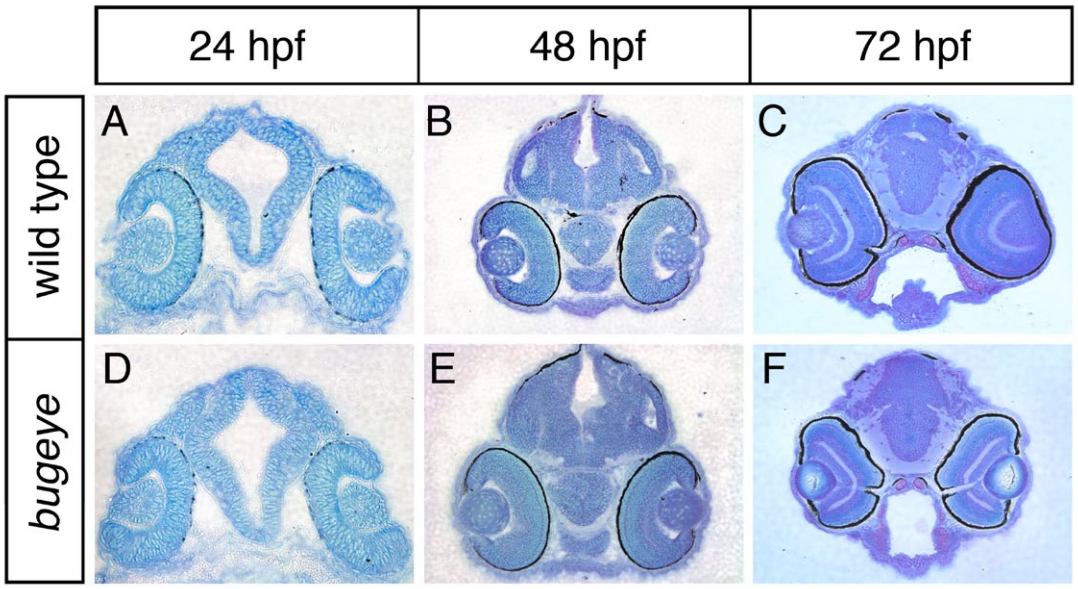

Figure 13. Brain anatomy of wild type and Lrp2 deficient embryos.
Coronal sections of wild type and *bugeye* embryos at the indicated time points are shown. Staining with toluidine blue does not reveal obvious brain malformations comparing both genotypes. (Modified from Kur et al., 2011)

mounts of Lrp2 deficient fish compared to wild type fish at 24, 48 and 72 hpf (Figure 12). To identify less pronounced morphological alterations, I prepared histological sections from mutant and control embryos. However, also on brain sections no differences in brain morphology were observed in mutant embryos (Figure 13).

To investigate whether there were subtle patterning alterations in Lrp2 deficient embryos compared to control embryos, the expression pattern of markers of forebrain development was analyzed. I performed ISH for *one-eyed pinhead (oep), paired box 6b (pax6b), empty spiracles 3 (emx3), forkhead box a1 (foxa1), sonic hedgehog a (shha), sonic hedgehog b (shhb), nk2 homeobox 1b (nkx2.1b), fibroblast growth factor 8 (fgf8), netrin* and *axial*. I first focused on early developmental stages when patterning of the embryonic zebrafish brain occurs. However, ISH for forebrain markers failed to reveal any discernable differences at 20 hpf comparing wild type and mutant embryos, indicating that ventral and dorsal diencephalic and telencephalic domains were correctly patterned (Figure 14). Also at 30 hpf, I did not detect any alterations in marker gene expression (Figure 15). Since robust expression of Lrp2 in the zebrafish brain starts at 36 hpf, I also analyzed later developmental stages. However, neither at 72 nor at 96 hpf differences in the expression pattern of forebrain markers were visible (Figure 16).

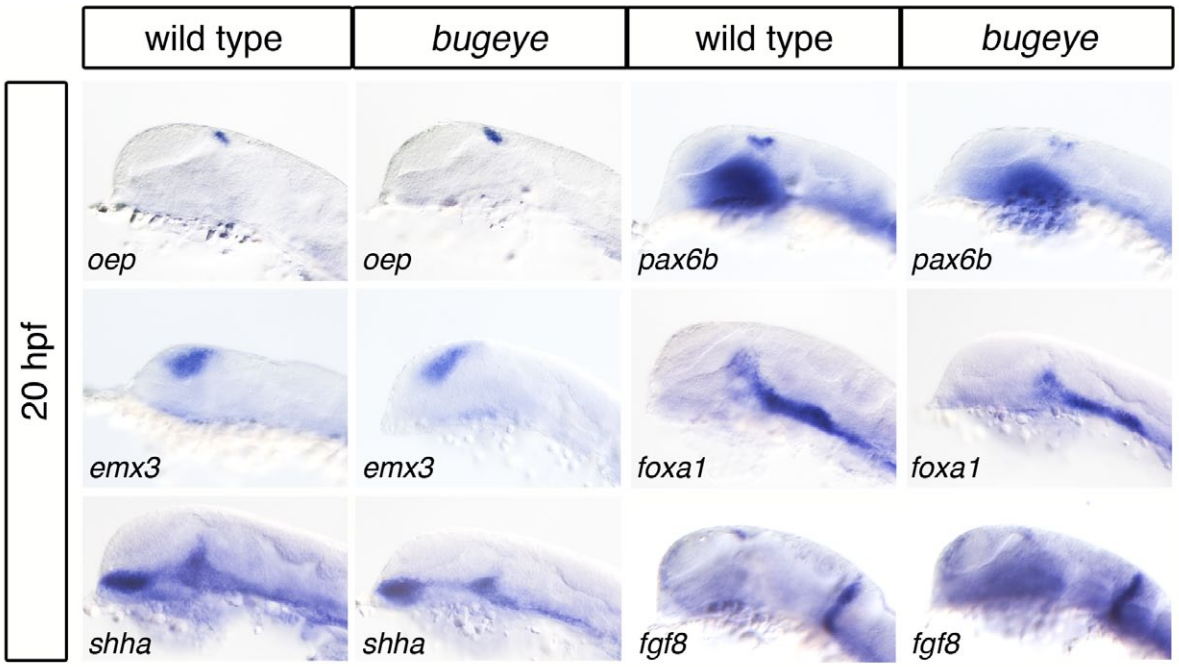

Figure 14. Expression analysis of forebrain markers at 20 hpf.
Whole mount in situ hybridization of *one-eyed pinhead (oep), paired box 6b (pax6b), empty spiracles 3 (emx3), forkhead box a1 (foxa1), sonic hedgehog a (shha)* and *fibroblast growth factor 8 (fgf8)* in wild type and *bugeye* embryos at 20 hpf. No differences are observed comparing both genotypes. (Modified from Kur et al., 2011)

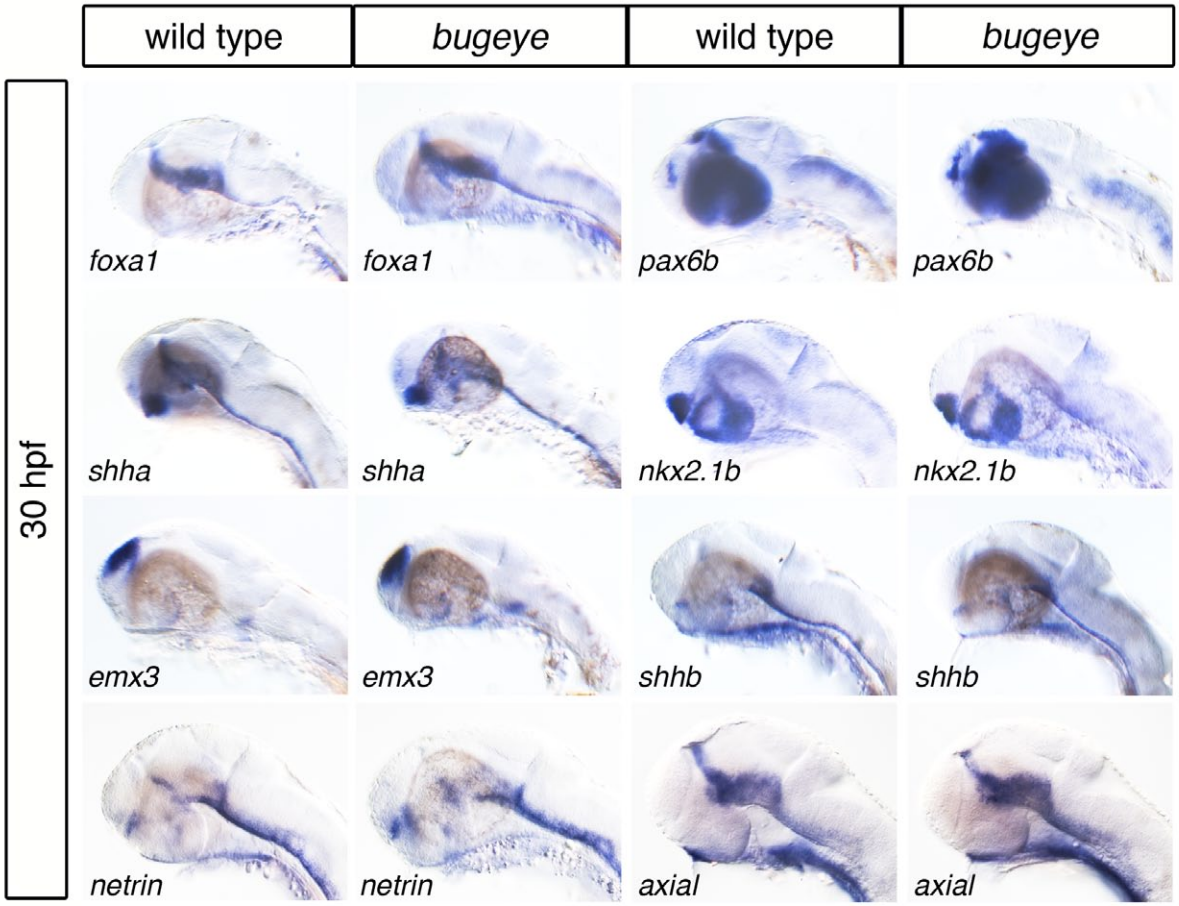

Figure 15. Expression analysis of forebrain markers at 30 hpf.
Whole mount in situ hybridization of *forkhead box a1 (foxa1), paired box 6b (pax6b), sonic hedgehog a (shha), nk2 homeobox 1b (nkx2.1b), empty spiracles 3 (emx3), sonic hedgehog b (shhb), netrin* and *axial* in wild type and *bugeye* embryos at 30 hpf. No differences are observed comparing both genotypes. (Modified from Kur et al., 2011)

There are indications that specification of the midline cells is impaired in LRP2 deficient mice (Christ et al., in revision). To analyze whether Lrp2 deficient zebrafish show a comparable phenotype, I checked for proper midline formation in *bugeye* and *5cben* embryos. In zebrafish, faulty midline specification can be investigated by visualization of the optic chiasm. Mutants lacking Shha (Schauerte et al., 1998) or Fgf8 (Shanmugalingam et al., 2000) show severe defects in the formation of the optic chiasm with the retinal axons failing to cross the midline. In contrast, the optic chiasm was normal in bugeye embryos as shown by immunohistology for marker Zn-5, which detects activated cell adhesion molecule a (Alcama), and thus visualizes axonal processes (Figure 17). Staining for radial glia marker Blbp revealed that lack of receptor expression also did not affect the appearance of radial glia in the ventricular system (Figure 18). In mice deficient for LRP2, the proliferation of neuroepithelial cells is reduced, leading to a decrease in neuroepithelial

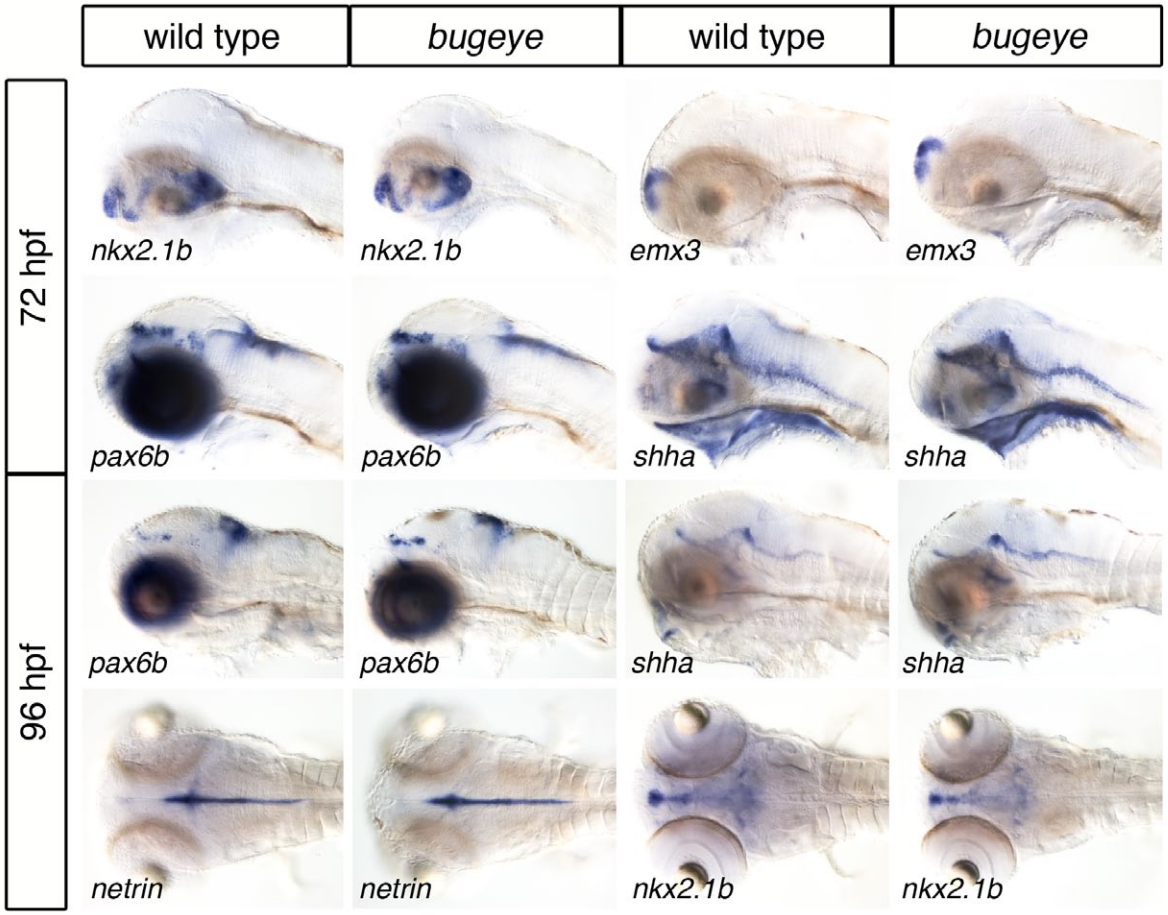

Figure 16. Expression analysis of forebrain markers at 72 and 96 hpf.
Whole mount in situ hybridization of *nk2 homeobox 1b (nkx2.1b), empty spiracles 3 (emx3), paired box 6b (pax6b), sonic hedgehog a (shha)* and *netrin* in wild type and *bugeye* embryos at 72 hpf (row 1, 2) and 96 hpf (row 3, 4). No differences are observed comparing both genotypes. Row 1-3: lateral views, row 4: dorsal views. (Modified from Kur et al., 2011)

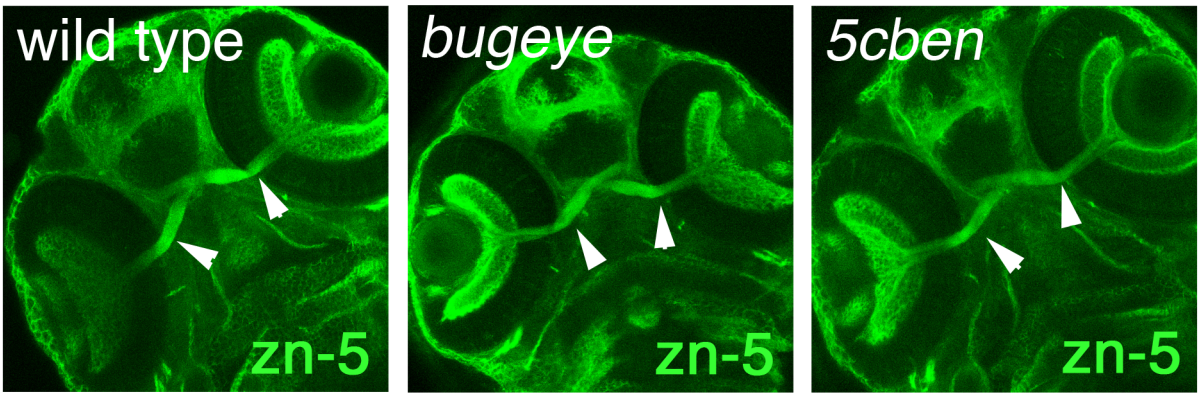

Figure 17. Correct formation of the optic chiasm in wild type and Lrp2 deficient embryos.
Immunohistolological detection of zn-5 visualizes correct formation of the optic chiasm (arrowhead) in wild type, *bugeye* and *5cben* embryos at 53 hpf. (Kur et al., 2011)

wall thickness (Spoelgen et al., 2005). To clarify whether this holds true for Lrp2 deficient zebrafish, I analyzed cell proliferation in the forebrain of bugeye and wild type embryos by staining for phospho-histone 3, a marker for mitotic cells. However, no differences in the numbers of proliferating cells were detected (Figure 19). Taken together, I could not any observe defects in forebrain formation in Lrp2 deficient embryos. This lack of an obvious phenotype in brain development caused by Lrp2 deficiency prompted the question whether in zebrafish, another member of the LDLR family might compensate for loss of Lrp2.

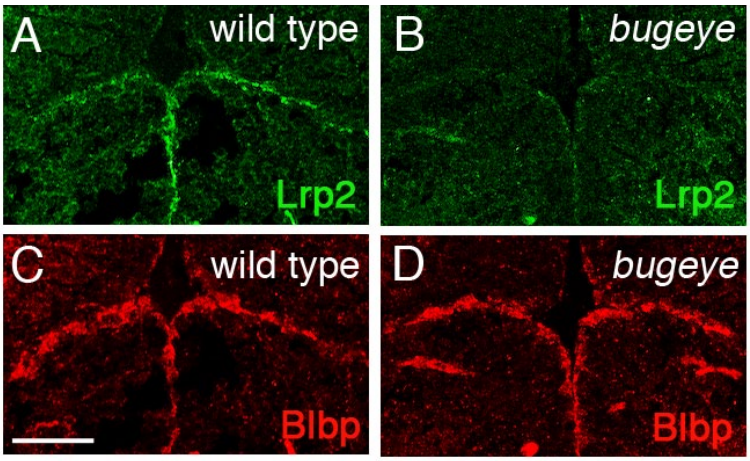

Figure 18. Appearance of radial glia in the ventricular system of wild type and Lrp2 deficient embryos. **(A, B)** Immunohistological detection of Lrp2 on coronal sections of wild type (A) but not *bugeye* (B) embryos at 48 hpf. **(C, D)** Immunohistological detection of brain lipid binding protein (Blbp) on coronal sections of wild type (C) and *bugeye* (D) embryos at 48 hpf. Scale bar: 25 µm. (Kur et al., 2011)

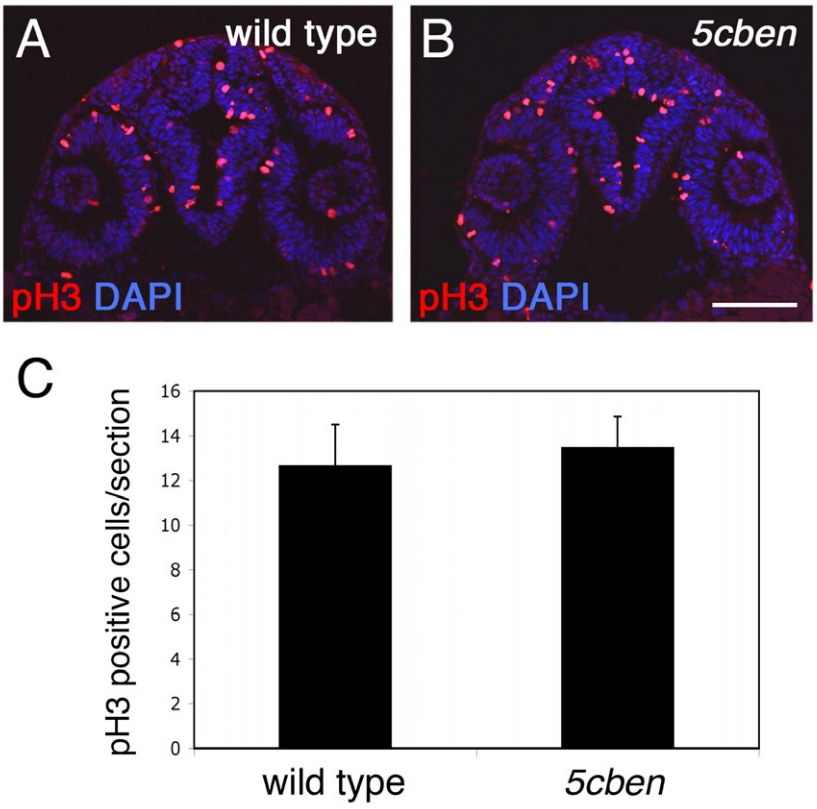

Figure 19. Quantification of proliferation in the embryonic brain of wild type and Lrp2 deficient embryos. **(A, B)** Immunohistological detection of phospho-histone 3 (pH3) on coronal sections of wild type and *5cben* brains at 24 hpf. Scale bar: 200 µm. **(C)** Quantification of the number of pH3 positive cells per section (± SEM), showing that proliferation is not affected by lack of Lrp2 expression. n= 3-6 sections each for 10 embryos per genotype. (Kur et al., 2011)

3.1.3 Zebrafish Lrp2b does not compensate for loss of Lrp2

In zebrafish, many genes exist in two copies. This fact is due to the occurrence of a whole-genome duplication in the teleost fish lineage, subsequent to its divergence from mammals (Jaillon et al., 2004). Often, this situation complicates the analysis of mutant lines, because the loss of one protein is compensated by its paralog.

The gene lrp2b encodes a receptor homologue unique to fish

Apparently, an additional copy of *lrp2* exists in zebrafish. Homology search in the NCBI genome database identified entry XR_084338.1 as possible *lrp2* gene duplication, which was termed *lrp2b* by our lab. The original entry includes an insertion of six nucleotides at position 8603-8609 resulting in a stop codon. We manually removed this insertion to derive an open reading frame encoding a full length receptor of 4579 amino acids. Obviously, the presence of the insertion raised the question whether *lrp2b* is a functional gene or a pseudogene. However, there were several lines of evidence that *lrp2b* was indeed expressed.

First of all, expression is supported by three expressed sequence tags (ESTs) from different libraries (EH509550, EH535651, AL918472), and by a similar sequence in the pufferfish *Tetraodon nigroviridis* (GenPept 47219712). Secondly, Ensembl predicts *lrp2b* to be a protein-coding gene (ENSDARG00000007906, ENSDARP00000073782). Thirdly, *lrp2b* is not included in a comprehensive list of 16,357 pseudogenes in zebrafish in relevant databases (pseudogenes.org). Lastly, the absence of several stop codons in such a large open reading frame is unlikely if the transcript is not producing a functional protein. For all these reasons, the procedure of removing the six nucleotide insertion to derive an open reading frame seemed justified.

The protein domain structure of mouse LRP2 shows a defined arrangement of complement-type repeats, EGF-type repeats and YWTD-motifs. Both zebrafish Lrp2 and Lrp2b display an identical arrangement of these structural domains (Figure 20 A). To analyze how closely Lrp2 and Lrp2b are related, we performed a multiple sequence alignment using Lrp2 and Lrp2b sequences from several species. The corresponding phylogenetic tree showed that zebrafish Lrp2 is more closely related to mouse LRP2 than to its paralog Lrp2b (Figure 20 B). This result was further underlined by comparing the amino acid sequence of the cytoplasmic tail in the three receptors. The cytoplasmic domains of LRPs are particularly well conserved in individual receptor variants across species, because

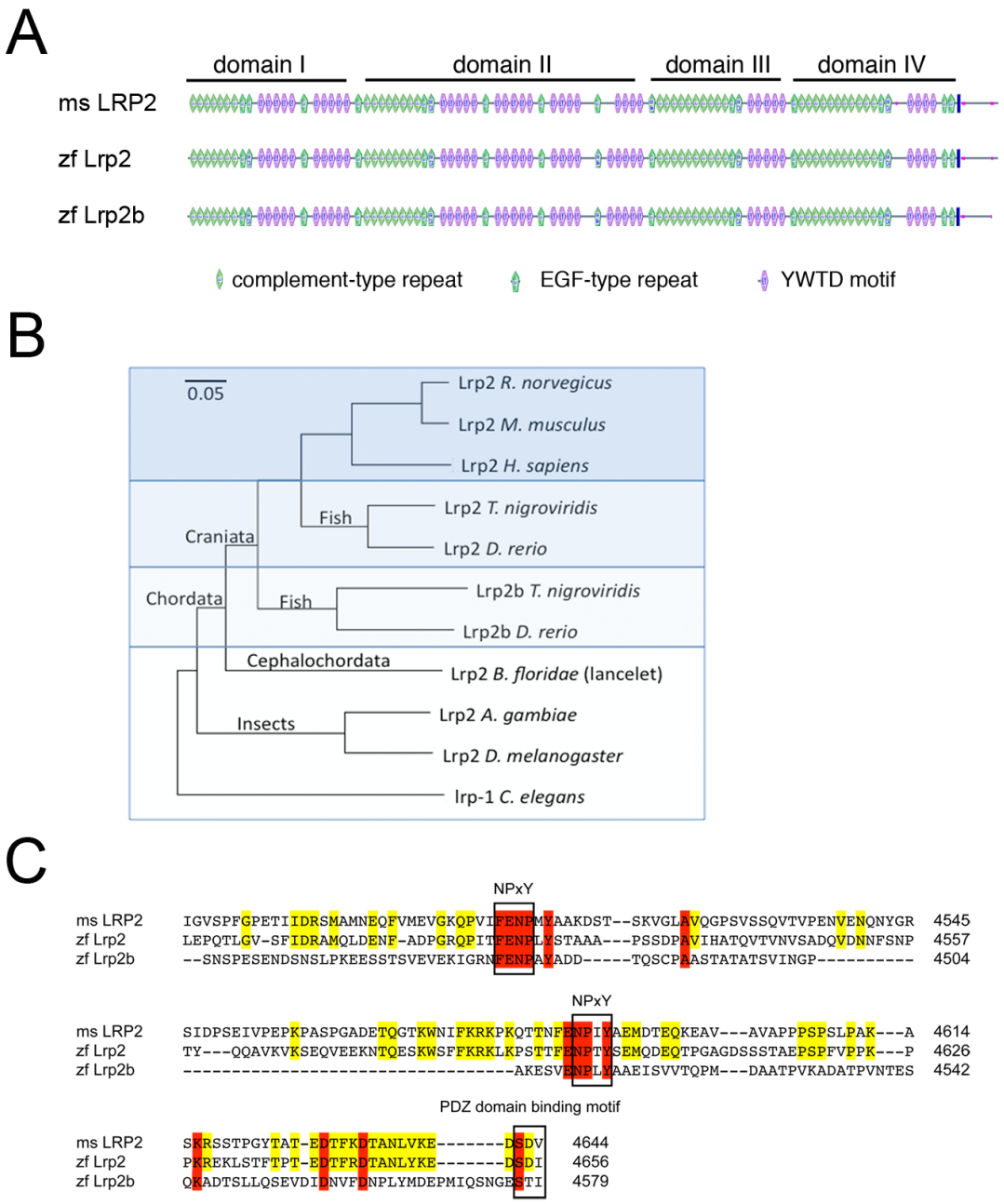

Figure 20. Comparative analysis of Lrp2 and Lrp2b.
(A) Structural organization of protein domains of mouse (ms) LRP2 as well as zebrafish (zf) Lrp2 and Lrp2b. The vertical solid line indicates the membrane anchor in the receptor polypeptides. **(B)** Phylogenetic tree of the indicated receptors based on the amino acid sequences from the following GenPept records (unless indicated): Lrp2 *Rattus norvegicus* (13562118), Lrp2 *Mus musculus* (124487372), Lrp2 *Homo sapiens* (126012573), Lrp2 *Tetraodon nigroviridis* (47210425), Lrp2 *Danio rerio* (303304950), Lrp2b *Tetraodon nigroviridis* (47219712), Lrp2b *Danio rerio* (GenBank XR_084338.1), Lrp2 *Branchiostoma floridae* (260807227), Lrp2 *Anopheles gambiae* (158300186), Lrp2 *Drosophila melanogaster* (281360654), lrp-1 *Caenorhabditis elegans* (212645014). **(C)** Amino acid sequence of the cytoplasmic domains of mouse LRP2 as well as zebrafish Lrp2 and Lrp2b indicating identity between mouse LRP2 and zebrafish Lrp2 (yellow) or between all three receptor variants (red). The NPxY protein-protein interaction sites and the PDZ domain-binding motif common to all three receptor species are highlighted. (Kur et al., 2011)

they carry protein-protein interaction motifs that are important for receptor function. The alignment illustrates that mouse LRP2 and zebrafish Lrp2 share a higher degree of sequence identity than zebrafish Lrp2 and Lrp2b (Figure 20 C). However, two essential NPxY motifs that interact with cytosolic adaptors (Gotthardt et al., 2000) as well as a carboxyl terminal PDZ binding domain are conserved in Lrp2b.

I used quantitative RT-PCR on whole zebrafish embryos to investigate the expression levels of *lrp2b* mRNA. As shown in figure 21 A, the levels of *lrp2b* transcript that can be detected at 24, 48, or 72 hpf are considerably lower than the levels of *lrp2* transcript. To see whether there was an upregulation of *lrp2b* mRNA in *lrp2* mutants, I compared *lrp2b* expression levels in wild type and *bugeye* embryos. However, no increase in *lrp2b* expression was detectable at 24, 48, or 72 hpf (Figure 21 B).

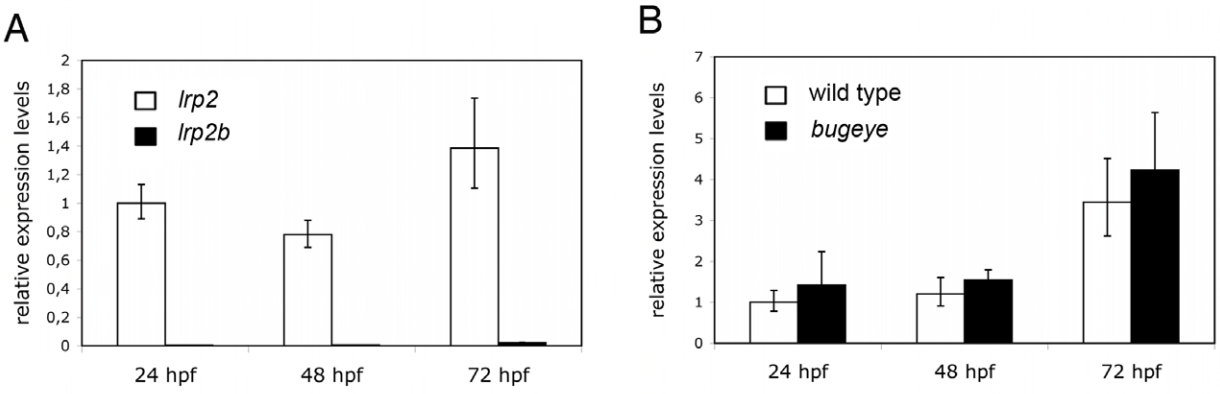

Figure 21. Relative mRNA expression levels of *lrp2* and *lrp2b*.
(A) RT-PCR of *lrp2* and *lrp2b* transcripts in wild type embryos at the indicated time points. Data are given relative to lrp2 levels in wild types at 24 hpf (set to 1). **(B)** RT-PCR of *lrp2b* transcripts in wild types and *bugeye* mutants at the indicated time points. Data are given relative to *lrp2b* levels in wild types at 24 hpf (set to 1). (Kur et al., 2011)

Lrp2b is dispensable for clearance pathways in the zebrafish kidney

To explore the role of Lrp2b during embryonic development of the zebrafish and to test whether it might compensate for loss of Lrp2 function in *bugeye* embryos, I decided to block Lrp2b expression using a morpholino knockdown approach. Morpholinos allow the analysis of phenotypes caused by blocking the expression of a certain protein of interest. There are two different kinds of morpholinos: splice morpholinos, which inhibit processing of the pre-mRNA by binding to splice acceptor/splice donor sites, and ATG morpholinos, which inhibit translation by binding to the ATG region. I decided to use ATG morpholinos, which are considered to be more efficient since they also prevent protein synthesis from maternal, already spliced mRNA.

A disadvantage of ATG morpholinos is that it is hard to assess whether they efficiently block protein synthesis if no specific antibody is available. I therefore cloned a reporter construct encoding the red fluorescent protein *mCherry* with a modified ATG region (Figure 22 A). In this construct, the *mCherry* start codon is mutated. Instead, a 46 bp sequence homologous to the *lrp2b* ATG region is cloned in frame upstream of the *mCherry* coding sequence. Thus, ATG morpholinos designed to block expression of Lrp2b, also bind to the sequence of the reporter construct and inhibit expression of mCherry protein. Injection of the *mCherry* reporter mRNA into fertilized oocytes resulted in expression of mCherry protein in zebrafish embryos (Figure 22 B). Co-injection of the reporter mRNA and an *lrp2b* ATG morpholino blocked expression of mCherry (Figure 22 C, D). This result was seen using two different *lrp2b* ATG morpholinos. It indicated that the morpholinos were functional and thus could be used to efficiently block Lrp2b expression.

To test whether Lrp2b has a role in renal clearance processes, I performed the dextran uptake assay in larvae injected with *lrp2b* morpholino, so-called Lrp2b morphants. In contrast to Lrp2, Lrp2b seems to be dispensable for kidney function, since knockdown of

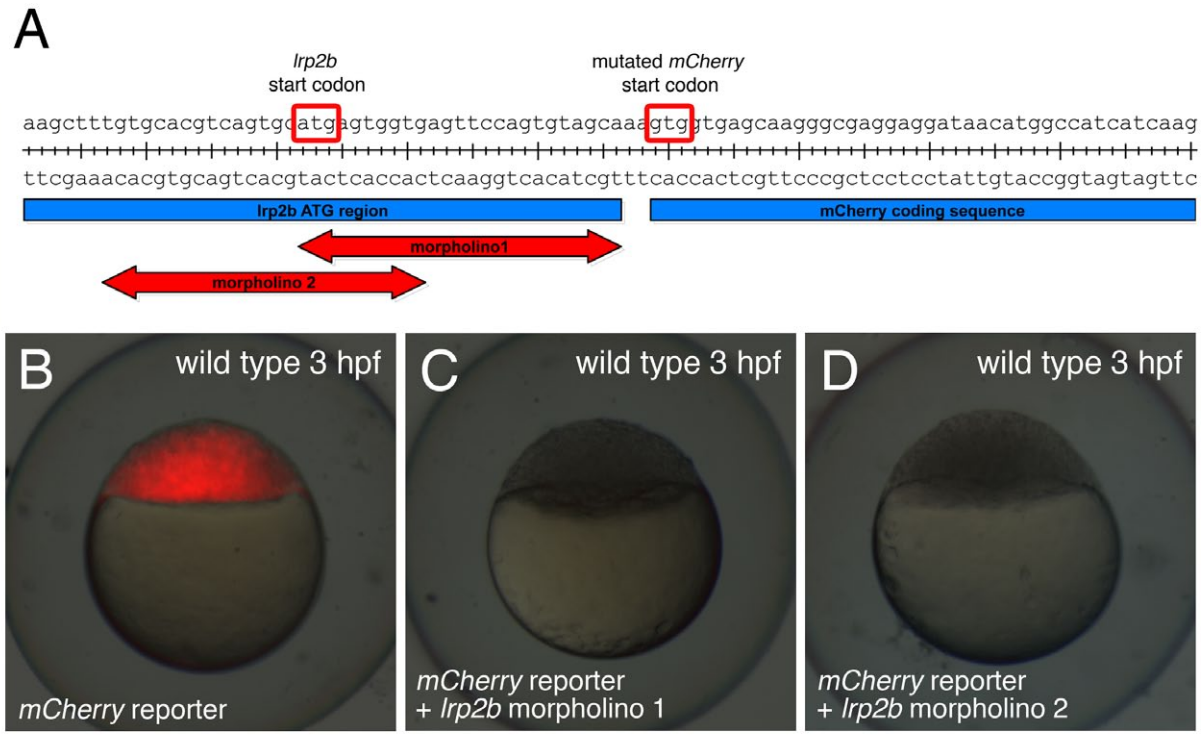

Figure 22. Test of the *lrp2b* ATG morpholinos.
(A) Sequence of the *mCherry* reporter construct indicating the reporter start codon, the mutated start codon as well as the morpholino binding sites. **(B - D)** Wild type embryos injected with the *mCherry* reporter construct and 2 different *lrp2b* ATG morpholinos (C, D). Successful knockdown of *mCherry* expression is shown 3 hrs after injection at the one cell stage by whole mount fluorescence microscopy. (Modified from Kur et al., 2011)

Lrp2b did not impair pronephric uptake of fluorescein-labeled dextran. 14 out of 15 *lrp2b* morphants were tested positive compared to 15 out of 16 wild type embryos (Figure 20). This observation indicated that tubular clearance is an activity unique to Lrp2.

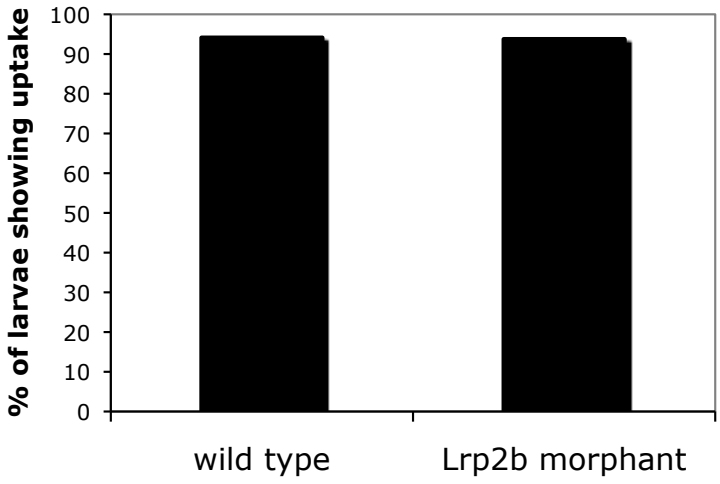

Figure 23. Loss of Lrp2b does not impair renal clearance.
Wild type embryos were injected with *lrp2b* ATG morpholino 1 at the one cell stage. At 69 hpf fluorescein-labeled dextran was injected into the cardinal vein and the number of larvae with tubular accumulation of tracer was evaluated by fluorescence microscopy. Lrp2b morphants showed normal uptake of fluorescent dextran into the pronephros (wild type: 15/16, morphants: 14/15). (Kur et al., 2011)

Simultaneous loss of Lrp2 and Lrp2b does not result in a brain phenotype

To investigate whether the loss of both homologous receptors Lrp2 and Lrp2b leads to a phenotype in brain development, I performed morpholino knockdown to block Lrp2b expression in *bugeye*. However, application of two different *lrp2b* morpholinos failed to elicit any obvious morphological alterations in *bugeye* at 24 hpf (Figure 24). This finding suggests that Lrp2b does not compensate for loss of Lrp2 in *bugeye* mutants and that even double deficiency for Lrp2 and Lrp2b does not result in a developmental phenotype.

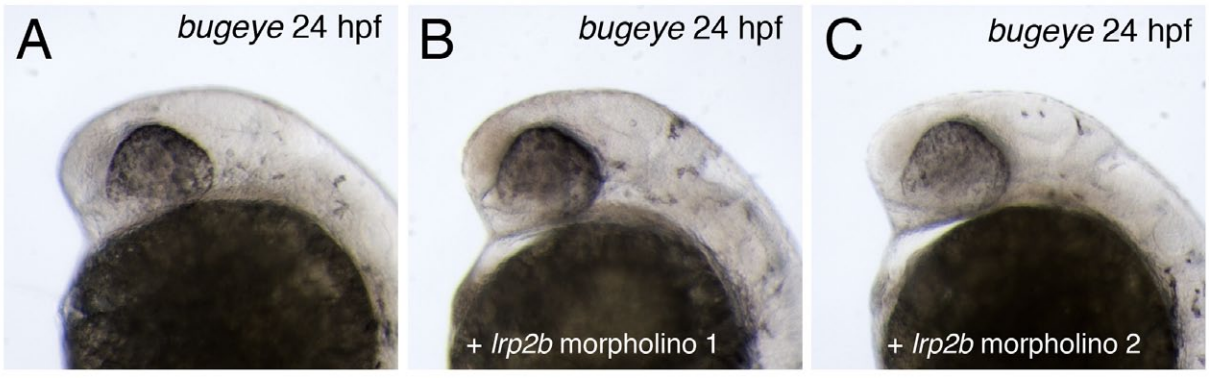

Figure 24. Simultaneous loss of Lrp2 and Lrp2b does not impair brain development.
Bugeye embryos were injected with 2 different *lrp2b* ATG morpholinos at the one cell stage. At 24 hpf, the development of embryos deficient for both Lrp2 and Lrp2b (B, C) was undisturbed compared to *bugeye* embryos (A). (Modified from Kur et al., 2011)

3.2 LRP2 IS REQUIRED FOR THE SPECIFICATION OF MIDLINE CELLS DURING MOUSE FOREBRAIN DEVELOPMENT

My analysis of Lrp2 deficient zebrafish revealed that the function of LRP2 in brain development is unique to mammals. Since my main interest was the role of LRP2 in patterning of the forebrain and the pathogenesis of HPE, I focused again on the mouse as model organism for LRP2 deficiency. Mice deficient for LRP2 exhibit severe forebrain malformations. Disturbed dorsoventral patterning due to alterations in SHH, BMP4 and FGF8 signaling has been identified as the defect underlying this phenotype (Spoelgen et al., 2005). Over the past years, significant progress has been made in elucidating the downstream effects of these morphogen signals. However, it is still unknown how these pathways are influenced by LRP2 and how the single pathways interact.

3.2.1 A new mouse model to study the function of LRP2: *Lrp2$^{tm(EGFPcre)}$*

To achieve a more thorough genetic and molecular analysis of the consequences of LRP2 deficiency, I wanted to investigate how loss of LRP2 function mechanistically manifests at the cellular level. Towards this aim, I decided to generate a knock-in reporter mouse model expressing EGFPcre (a fusion protein consisting of enhanced green fluorescent protein (EGFP) and the cre recombinase) under the control of the endogenous *Lrp2* promoter (*Lrp2$^{tm(EGFPcre)}$*). Complementary to the analysis of obligate *Lrp2* mutants, this model can be used to visualize single LRP2 expressing cells and to investigate cell intrinsic effects of LRP2 function. Furthermore, the *Lrp2$^{tm(EGFPcre)}$* mouse line offers several experimental prospects: using the cre recombinase one can perform lineage tracing studies to investigate how LRP2 expressing cells further differentiate. Using EGFP one can carry out live cell imaging to monitor the migratory and proliferative behavior of LRP2 expressing cells (fate mapping). Furthermore, EGFP positive cells can be sorted by flow cytometry and subsequently used for expression profiling or for establishing stable cell lines for biochemical studies.

Generation of the Lrp2$^{tm(EGFPcre)}$ line

To generate the *Lrp2$^{tm(EGFPcre)}$* reporter mouse, ES cells were targeted with a mini gene construct encoding the *EGFPcre* fusion gene (β-Globin intron – *EGFPcre* – polyA). The sequences mediating homologous recombination (long arm and short arm) were chosen

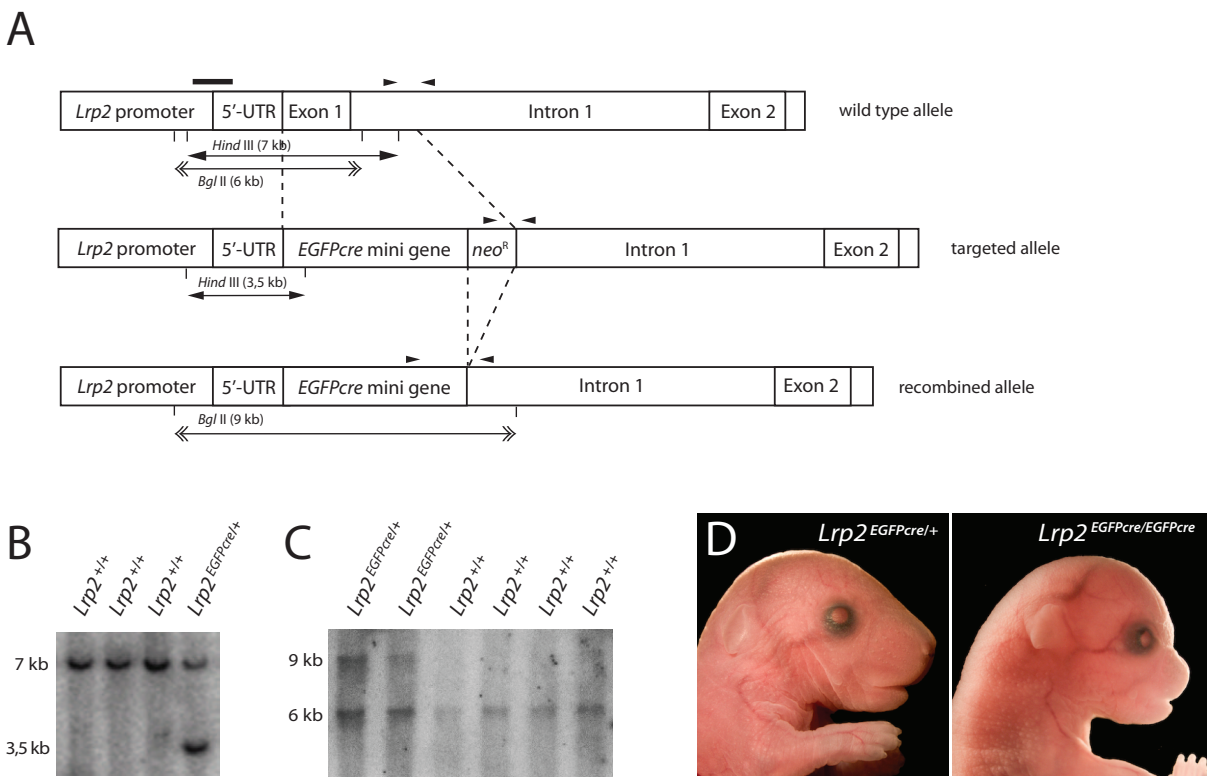

Figure 25. Generation of the *Lrp2*$^{tm(EGFPcre)}$ reporter mouse line.
(A) Genomic organization of the wild type *Lrp2* locus, the targeted gene locus and the targeted gene locus after removal of the neomycin resistance cassette (neo^R). Arrowheads indicate the position of primers used for PCR genotyping. The solid black line indicates the position of the probe used for Southern blotting. Arrows indicate the DNA fragments diagnostic for the different genotypes in Southern Blots after digestion of genomic DNA with restriction enzymes *Hind*III or *Bgl*II. **(B)** Southern Blot analysis of ES cell genomic DNA digested with *Hind*III. The 7 kb band is indicative of the wild type allele, the 3.5 kb band is indicative of the targeted allele (arrows in A). **(C)** Southern Blot analysis of adult mouse genomic DNA digested with *Bgl*II. The 6 kb band is indicative of the wild type allele and the 9 kb band is indicative of the targeted allele after removal of neo^R (arrows with double arrowhead in A). Note that no homozygous *Lrp2*$^{EGFPcre/EGFPcre}$ animals are shown since they do not survive until adulthood. **(D)** Heterozygous *Lrp2*$^{EGFPcre/+}$ and homozygous *Lrp2*$^{EGFPcre/EGFPcre}$ embryos at embryonic day 18.5. *Lrp2*$^{EGFPcre/EGFPcre}$ embryos show severe craniofacial malformations.

in a way that resulted in insertion of the *EGFPcre* mini gene immediately downstream of the *Lrp2* 5'-untranslated region. This strategy results in expression of EGFPcre under the control of the endogenous *Lrp2* promoter (Figure 25 A). Others have successfully employed this approach to generate a mouse line expressing EGFPcre under the control of the *Shh* promoter (*Shh*$^{tm(EGFPcre)}$) (Harfe et al., 2004).

After homologous recombination in murine ES cells, targeted ES cell clones were identified by Southern blot analysis (Figure 25 B). In *Hind*III digested genomic DNA hybridized with a probe from the *Lrp2* promotor region, wild type ES cells showed a 7 kb DNA fragment,

whereas targeted ES cells showed a 3.5 kb DNA fragment. Targeted ES cell clones were injected into blastocysts which were implanted into the uterus of pseudo pregnant foster mothers to obtain chimeras. Germ line transmission of the modified *Lrp2* gene locus was confirmed in offspring of the chimeras by Southern blot analysis. By crossing these animals with flp deleter mice, the neomycin resistance cassette was removed from the $Lrp2^{tm(EGFPcre)}$ allele (Figure 25 A). Removal of the neomycin resistance cassette is important, because its presence can reduce expression levels of the transgene (Nagy et al., 1998).

Breeding of $Lrp2^{EGFPcre/+}$ mice produced surviving offspring of two genotypes: $Lrp2^{+/+}$ and $Lrp2^{EGFPcre/+}$ (Figure 25 C). Animals homozygous for the transgene ($Lrp2^{EGFPcre/EGFPcre}$) displayed severe craniofacial malformations (Figure 25 D) and died perinatally. This phenotype was due to the fact that the knock-in of EGFPcre destroyed the open reading frame of *Lrp2* and thus created a null allele. As described previously for the $Lrp2^{-/-}$ mouse line, mice deficient for LRP2 are usually not viable (Willnow et al., 1996).

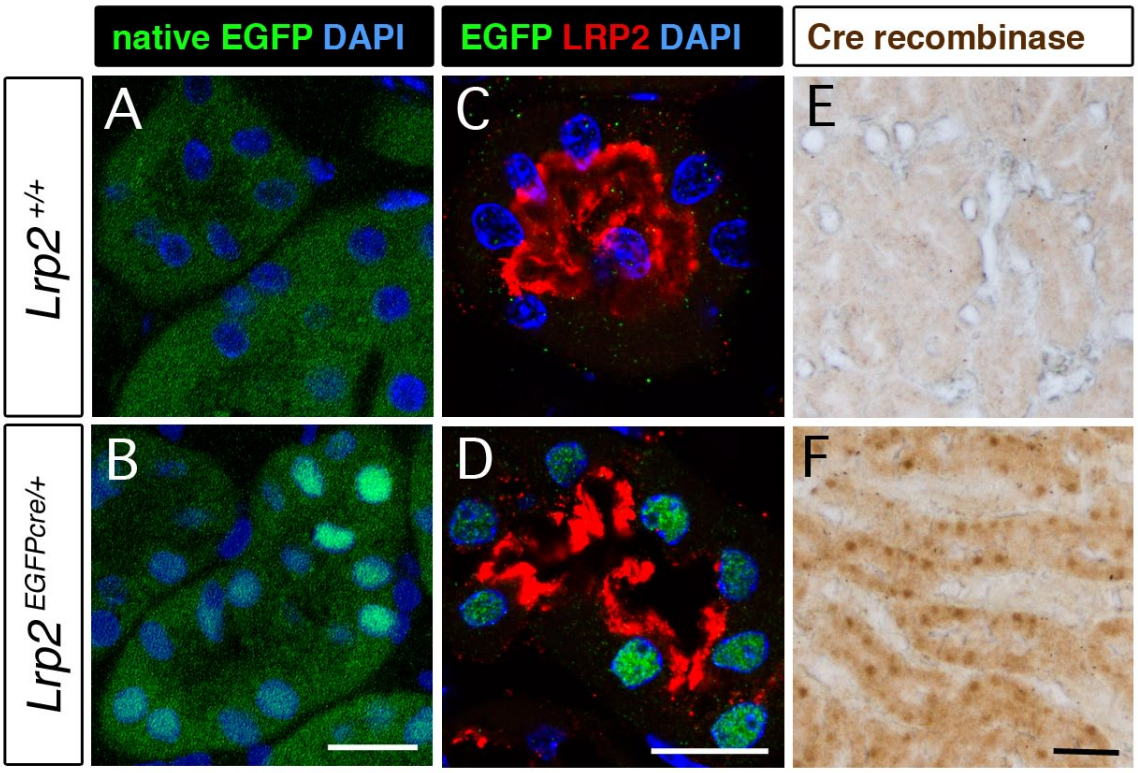

Figure 26. Expression of EGFPcre in kidney proximal tubule cells of adult $Lrp2^{EGFPcre/+}$ mice.
(A, B) Native nuclear EGFP fluorescence is visible on cryosections of $Lrp2^{EGFPcre/+}$ (B) but not $Lrp2^{+/+}$ (A) kidneys. Scale bar: 25 µm. **(C, D)** Immunohistology for EGFP and LRP2 on cryosections of $Lrp2^{EGFPcre/+}$ and $Lrp2^{+/+}$ kidneys. EGFP can be detected in Lrp2EGFPcre/+ (D) but not $Lrp2^{+/+}$ (C) embryos. Scale bar: 25 µm. **(E, F)** Immunohistology for cre on paraffin sections of $Lrp2^{EGFPcre/+}$ and $Lrp2^{+/+}$ kidneys. Cre can be detected in $Lrp2^{EGFPcre/+}$ (F) but not $Lrp2^{+/+}$ (E) embryos. Scale bar: 100 µm.

For the initial verification that EGFPcre was functionally expressed, I chose a tissue with high levels of LRP2 expression. Since in the adult mouse, LRP2 is highly expressed in the kidney, I first analyzed reporter gene expression in this organ. The EGFPcre fusion protein carries a nuclear localization signal (NLS) and is therefore supposed to be detectable in the nuclei of all cells in which the *Lrp2* promoter is active. On cryosections of fixed kidneys, I detected native EGFP fluorescence in the nuclei of *Lrp2*$^{EGFPcre/+}$ proximal tubule cells (Figure 26 B). By performing co-immunohistochemistry with antibodies directed against EGFP and LRP2, I showed that *Lrp2*$^{EGFPcre/+}$ proximal tubule cells expressed LRP2 on the apical cell surface as well as EGFPcre in the nucleus (Figure 26 D). This finding indicated that EGFPcre expression indeed faithfully recapitulated LRP2 expression in the kidney. Additional confirmation that the EGFPcre fusion protein was expressed as expected came from immunohistochemical stainings with an antibody directed against the cre recombinase: in *Lrp2*$^{EGFPcre/+}$ animals, also the cre recombinase portion of the fusion protein was detected in the nuclei of proximal tubule cells (Figure 26 F).

Cre activity indicates early onset of LPR2 expression

One possibility of using the cre recombinase expressed under the *Lrp2* promoter would be to generate conditional mouse mutants which are deficient for a certain gene product only in LRP2 expressing cells. In addition to that, one can perform lineage tracing experiments by crossing *Lrp2*$^{EGFPcre/+}$ mice with *Gt(ROSA)26Sor*^{tm1Sor} reporter mice. In *Gt(ROSA)26Sor*^{tm1Sor} mice, lacZ expression driven by the ubiquitously active Rosa26 promoter is interrupted by a LoxP site-flanked stop codon (Soriano, 1999). In any cell expressing cre, the stop codon is excised from the genomic DNA, resulting in lacZ expression in this cell and all its descendants. By crossing *Lrp2*$^{EGFPcre/+}$ mice with *Gt(ROSA)26Sor*^{tm1Sor} mice, one can thus investigate the progeny of LRP2 expressing cells.

I analyzed E8.0 embryos obtained from matings of *Lrp2*$^{EGFPcre/+}$ mice with homozygous *Gt(ROSA)26Sor*^{tm1Sor} reporter mice. All embryos were positive for the *Gt(ROSA)26Sor*^{tm1Sor} transgene and half of them were positive for EGFPcre. LacZ staining revealed that while in *Lrp2*$^{+/+}$ embryos, no expression of lacZ was detected, lacZ was expressed in all cells of the *Lrp2*$^{EGFPcre/+}$ embryos (Figure 27). This result implied that every cell in the developing *Lrp2*$^{EGFPcre/+}$ embryo is descendant from a cell that has previously expressed the cre recombinase. In conclusion, the observation argued for a very early onset of LRP2 expression, possibly during blastula stages.

This was an unexpected finding, since several studies describe the earliest expression of

LRP2 in the embryo proper at later stages (Drake et al., 2004) (Gerbe et al., 2008). While the observation that LRP2 was obviously expressed earlier than previously thought was very interesting, on the other hand it precluded lineage tracing experiments. With the cre recombinase being active that early during embryonic development and all cells being lacZ positive, one cannot compare different neuroepithelial lineages. Furthermore, it does not seem reasonable to use the *Lrp2*$^{tm(EGFPcre)}$ line for the generation of conditional mutants since they would probably phenocopy the obligate mutants.

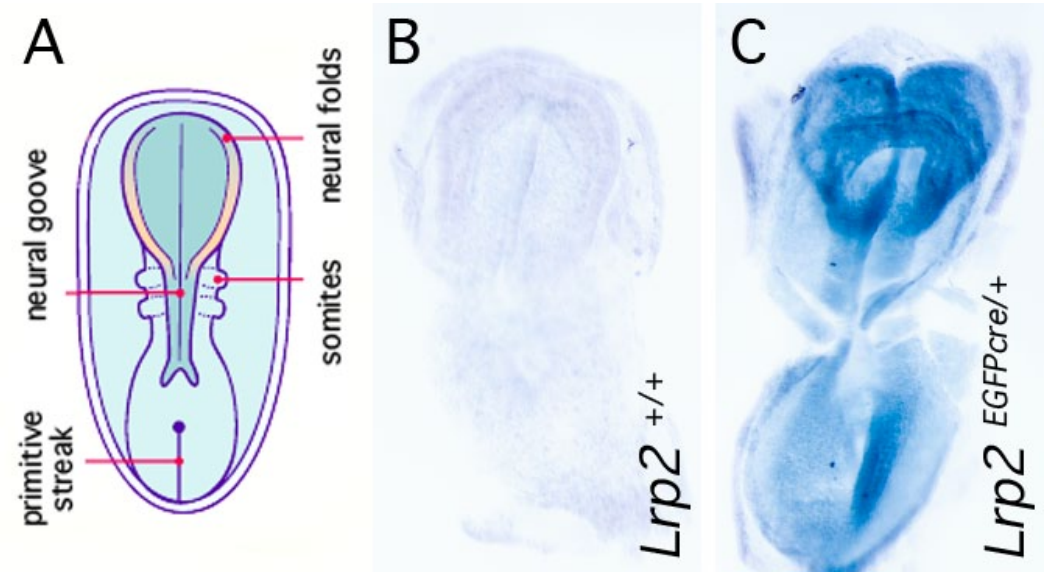

Figure 27. The *Lrp2* promoter is active in early mammalian development.
(A) Scheme depicting a mouse embryo at E8.0. **(B, C)** Whole mount lacZ staining of E8.0 embryos positive for the *ROSA26Sor*^{tm1Sor} transgene. No staining is seen in *Lrp2*$^{+/+}$ embryos (B). *Lrp2*$^{EGFPcre/+}$ embryos (C) show a uniform blue staining, indicating an early onset of cre recombinase expression in these embryos.

EGFP expression is a read-out for Lrp2 promoter activity

LRP2 has a long half-life of approximately 48 hours. In conditional *Lrp2* mutants, LRP2 can still be detected by immunohistochemistry two days after the recombination occurred (our own unpublished observation). In the developing brain, where expression domains change in the course of several hours, LRP2 protein is therefore not a reliable read-out for *Lrp2* promoter activity. In *Lrp2*$^{EGFPcre/+}$ mice, expression of EGFP could be used as an alternative indicator of promoter activity.

Until E10.0, the neuroepithelium of the brain is a pseudostratified epithelium, that looks layered, but in fact is composed of only a single layer of cells. Each cell spans the whole neuroepithelium from apical to basal, while the nuclei migrate up and down the apicobasal axis during the cell cycle (interkinetic nuclear migration). During S phase,

the nucleus is in a basal position, while during M phase, it is in an apical position. In G1 and G2 phase, the nucleus is migrating in apical or basal direction, respectively (Frade et al., 2002). For analysis of EGFP expression in the elongated neuroepithelial cells it was an obvious advantage that the EGFPcre in my reporter mouse model carried a NLS. Transport of EGFPcre to the nucleus resulted in a defined nuclear EGFP signal compared to a diffuse cytoplasmic signal spanning the whole epithelium. This localization made it easier to identify single EGFP positive cells. In addition, the position of the nucleus contains information about the cell cycle state of a certain cell. Furthermore, after the start of neurogenesis in the forebrain at E10.0, one might analyze the EGFP positive nuclei of LRP2 expressing cells to assess whether these cells have a preference for either the symmetric, proliferative division or the asymmetric, neurogenic division.

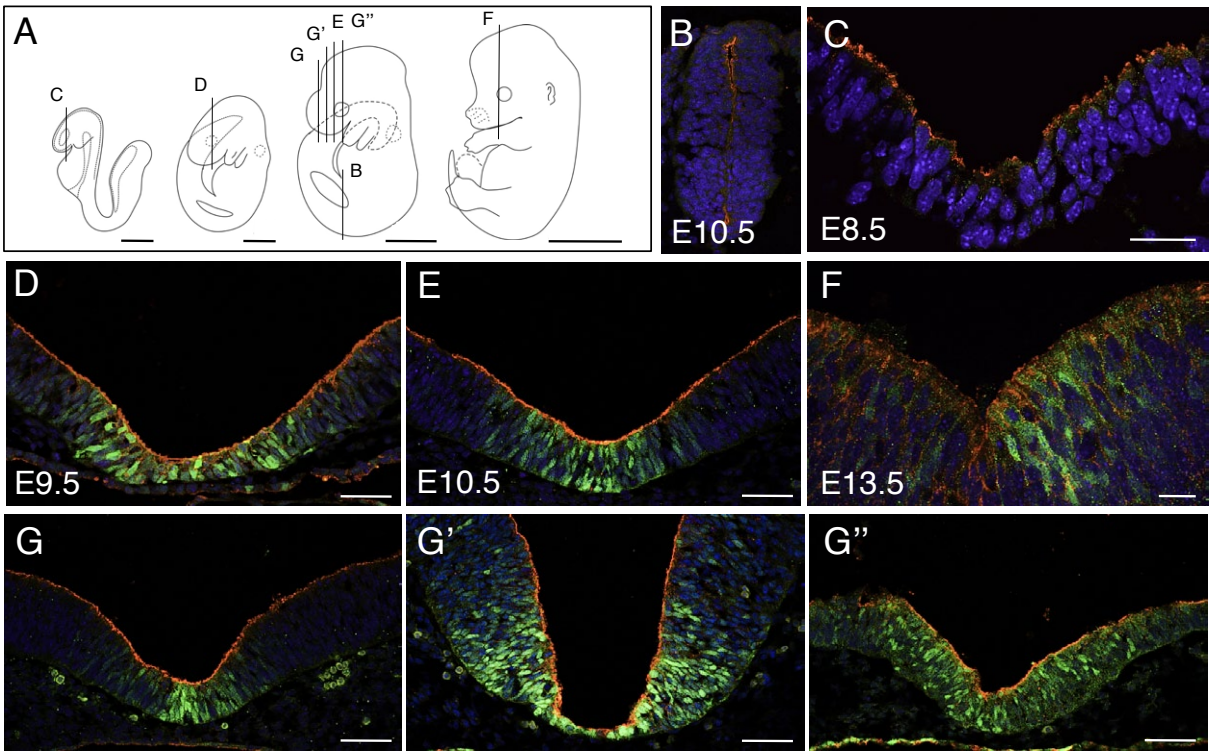

Figure 28. Expression of LRP2 and EGFP in the ventral forebrain of *Lrp2*$^{EGFPcre/+}$ embryos.
(A) Scheme depicting mouse embryos at embryonic day (E) 8.5, E9.5, E10.5 and E13.5 (left to right). The planes of the coronal sections shown in (B-G'') are indictated. Scale bars: 300 µm, 500 µm, 500 µm, 2 mm (left to right). **(B-F)** Immunohistology for LRP2 (red) and EGFP (green) in the spinal cord at E10.5 (B) and in the ventral forebrain at different embryonic stages (C-F). While LRP2 expression can be detected on all sections, EGFP expression is absent in the spinal cord (B) as well as in the forebrain at E8.5 (C). Note that EGFP expression can only be detected in the immediate ventral midline (D-F). Scale bars: 50 µm (C), 100 µm (D, E), 25 µm (F) **(G-G'')** Immunohistology for LRP2 (red) and EGFP (green) at different rostrocaudal levels of the ventral forebrain at E10.5. Scale bars: 100 µm. EGFP expression can be detected on all sections.

To visualize both EGFP and LRP2 expression in the embryonic brain, I performed co-immunohistology on brain sections of *Lrp2*$^{EGFPcre/+}$ embryos. Staining for EGFP was necessary since EGFP expression in the developing brain was not as prominent as in the adult kidney and native EGFP fluorescence could hardly be detected. I analyzed EGFP expression at different embryonic stages (E8.5 to E13.5) (Figure 28 B-G''). At all stages analyzed, expression of LRP2 could be detected at the apical surface of the neuroepithelium. In contrast to expression of LRP2, EGFP expression could not be detected at E8.5. Starting from E9.5, EGFP expression was seen in the nuclei of neuroepithelial cells. Interestingly, expression of EGFP was only detected in the immediate ventral midline, but not in regions lateral to the midline.

At E10.0, I analyzed the expression of LRP2 and EGFP at different positions along the rostrocaudal axis of the forebrain (Figure 28 E, G-G'') and in the spinal cord (Figure 28 B). On all sections analyzed, expression of LRP2 could be detected at the apical surface of the neuroepithelium. From the anterior telencephalon to the optic stalk region in the diencephalon, EGFP expression was detected in the ventral midline cells. However, in the spinal cord, no EGFP expression could be detected while LRP2 staining could readily be seen. A possible explanation for the discrepancy seen in EGFP staining versus LRP2 staining may be better immunohistological detection of LRP2 protein compared to EGFP protein. This interpretation would suggest that EGFP staining is indicative for sites of very high *Lrp2* promoter activity.

Lrp2 promoter activity is higher in the ventral than in the dorsal midline

Expression of LRP2 is seen uniformly on the apical surface of the neuroepithelium at early stages. Starting from E9.5, expression becomes restricted to the ventral and dorsal midline (Figure 29 A, B). Analysis of Lrp2$^{EGFPcre/+}$ embryos showed ventral (Figure 29 C), but not dorsal expression (Figure 29 D) of EGFP at E9.5. At E10.5, robust expression is seen ventrally (Figure 29 E) and in addition a very faint signal can be detected dorsally (Figure 29 F). In regions lateral to the midline, EGFP expression was never observed. Assuming that EGFP expression is a read-out for high *Lrp2* promoter activity, this finding suggests that LRP2 expression is high in ventral midline cells, less high in dorsal midline cells, and even lower in lateral cells. Although speculative, it might indicate that LRP2 activity is more crucial in the midline – especially the ventral midline – than in the lateral neuroepithelium.

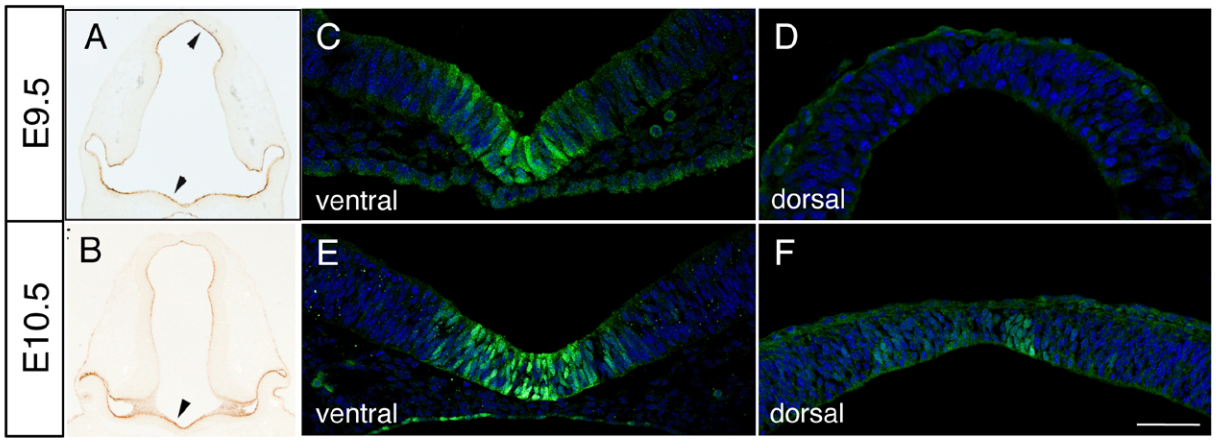

Figure 29. Expression of LRP2 and EGFP in ventral vs. dorsal forebrain.
(A, B) Immunohistological detection of LRP2 on coronal forebrain sections of *Lrp2*$^{+/+}$ embryos. LRP2 expression in the neuroepithelium is most pronounced in the ventral and dorsal midline. **(C-F)** Immunohistological detection of EGFP on coronal forebrain sections of *Lrp2*$^{EGFPcre/+}$ embryos. At embryonic day (E) 9.5, expression of EGFP can be detected in the ventral (C), but not in the dorsal (D) midline. At E10.5, a robust EGFP signal can be detected in the ventral midline (E) and a faint EGFP signal can be detected in the dorsal midline (F). Scale bar: 100 µm.

Lrp2 promoter activity is decreased in LRP2 deficient mice

An unexpected finding was made when the expression of EGFP in LRP2 deficient *Lrp2*$^{EGFPcre/-}$ mice was analyzed. These mice carry one knock-out allele and one EGFPcre knock-in allele and thus have no intact copy of the Lrp2 gene. Surprisingly, in contrast to *Lrp2*$^{EGFPcre/+}$ embryos, no EGFP expression could be detected in *Lrp2*$^{EGFPcre/-}$ embryos at E9.5 (Figure 30 A, B). At E10.5, EGFP expression could be detected in *Lrp2*$^{EGFPcre/-}$ embryos, although at lower levels compared to *Lrp2*$^{EGFPcre/+}$ embryos (Figure 27 D, E).

A possible explanation for this finding might be that LRP2 activity is needed for activation of the *Lrp2* promoter. Several scenarios could be envisioned for this positive feedback loop. One intriguing possibility would be that the ICD of LRP2 is released by RIP and subsequently transported to the nucleus where it regulates transcription of target genes, including the *Lrp2* gene itself. This model has been suggested by work on opossum kidney cells (Li et al., 2008). Recently, a mouse model expressing the LRP2 ICD under the control of the endogenous Lrp2 promoter has been generated in our lab (Christ et al., 2010). By crossing *Lrp2*$^{EGFPcre/+}$ and *Lrp2*$^{ICD/+}$ mice, I obtained *Lrp2*$^{EGFPcre/ICD}$ embryos, which were deficient for the full-length receptor, but expressed the LRP2 ICD. However, also in *Lrp2*$^{EGFPcre/ICD}$ embryos I could not detect EGFP staining at E9.5 (Figure 30 C). This finding indicated that not only the ICD, but full-length LRP2 was needed to activate the *Lrp2* promoter.

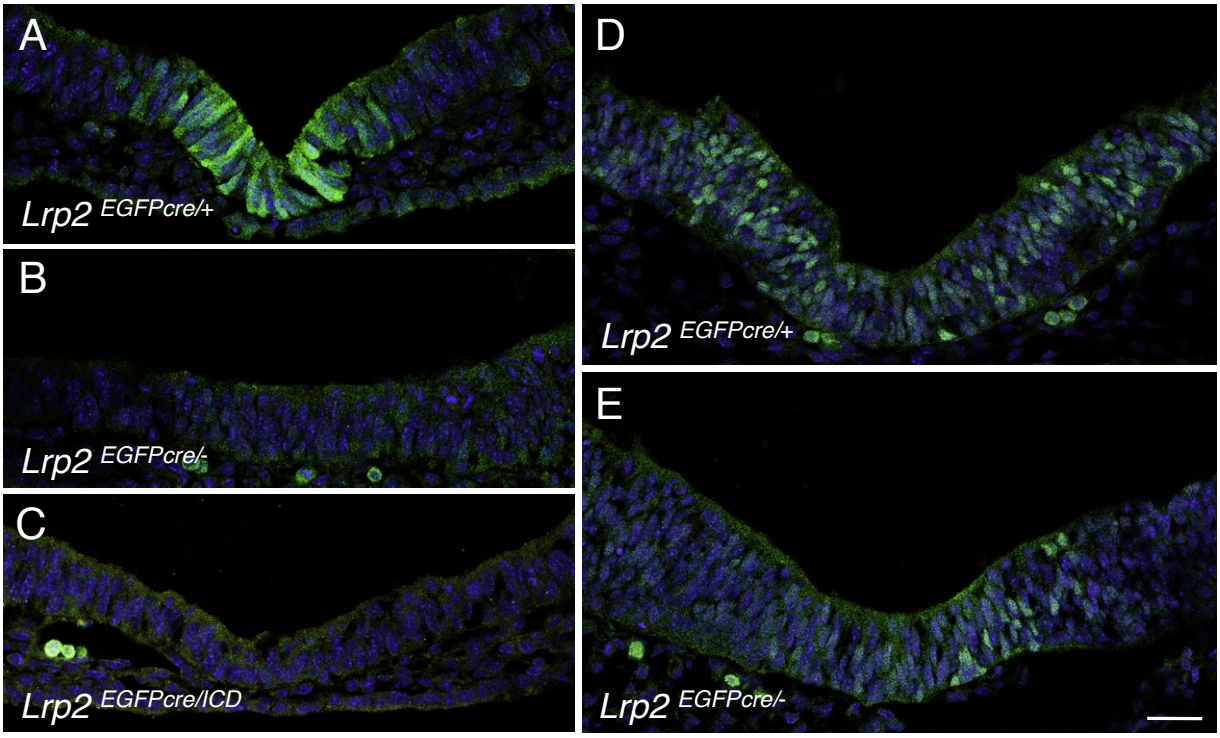

Figure 30. Expression of EGFP in *Lrp2*$^{EGFPcre/+}$, *Lrp2*$^{EGFPcre/-}$ and *Lrp2*$^{EGFPcre/ICD}$ embryos.
(A-C) Immunohistological detection of EGFP in the ventral forebrain midline of embryonic day (E) 9.5 embryos. EGFP can be detected in *Lrp2*$^{EGFPcre/+}$ embryos (A), but not in *Lrp2*$^{EGFPcre/-}$ embryos (B), which lack expression of LRP2. Also, no EGFP expression can be detected in *Lrp2*$^{EGFPcre/ICD}$ embryos (C), which lack expression of full-length LRP2, but express the LRP2 intracellular domain (ICD). **(D, E)** Immunohistological detection of EGFP in the ventral forebrain midline of E10.5 embryos. EGFP can be detected in *Lrp2*$^{EGFPcre/+}$ embryos (D) and weakly in *Lrp2*$^{EGFPcre/-}$ embryos (E). Scale bar: 50 µm.

Ventral midline cells are particularly affected by LRP2 deficiency

While comparing the expression of EGFP in the ventral midline cells of *Lrp2*$^{EGFPcre/+}$ and *Lrp2*$^{EGFPcre/-}$ embryos, I made the concomitant observation that the morphology of the ventral neuroepithelium was altered in LRP2 deficient embryos compared to controls. In *Lrp2*$^{EGFPcre/-}$ embryos, the epithelium lacked the characteristic bend caused by the medial hingepoint (Figure 30 B). Defects in hingepoint formation are compatible with a severe delay in neural tube closure observed in LRP2 deficient embryos (Willnow et al., 1996). Since establishment of apicobasal cell polarity is an important prerequisite for neurulation (Yang et al., 2009), I decided to test whether apical and basal markers are correctly localized in LRP2 deficient midline cells. Staining for laminin (basal) and prominin (apical) revealed no discernable differences between *Lrp2*$^{EGFPcre/+}$ and *Lrp2*$^{EGFPcre/+}$ embryos (Figure 31 A, B), suggesting that apicobasal polarity was correctly established in LRP2 deficient embryos. However, the defective hingepoint formation was very obvious. Visualization

of the actin cytoskeleton showed that the midline cells in control embryos were wedge-shaped (Figure 31 C), whereas the midline cells in LRP2 deficient embryos displayed a columnar shape, indicating that they did not undergo apical constriction (Figure 31 D). This defect in control of cell shape was an interesting finding since it offered a possible explanation why neural tube closure is delayed in LRP2 deficient embryos. In addition, it supported the notion that LRP2 function is especially important for the specification of ventral midline cells.

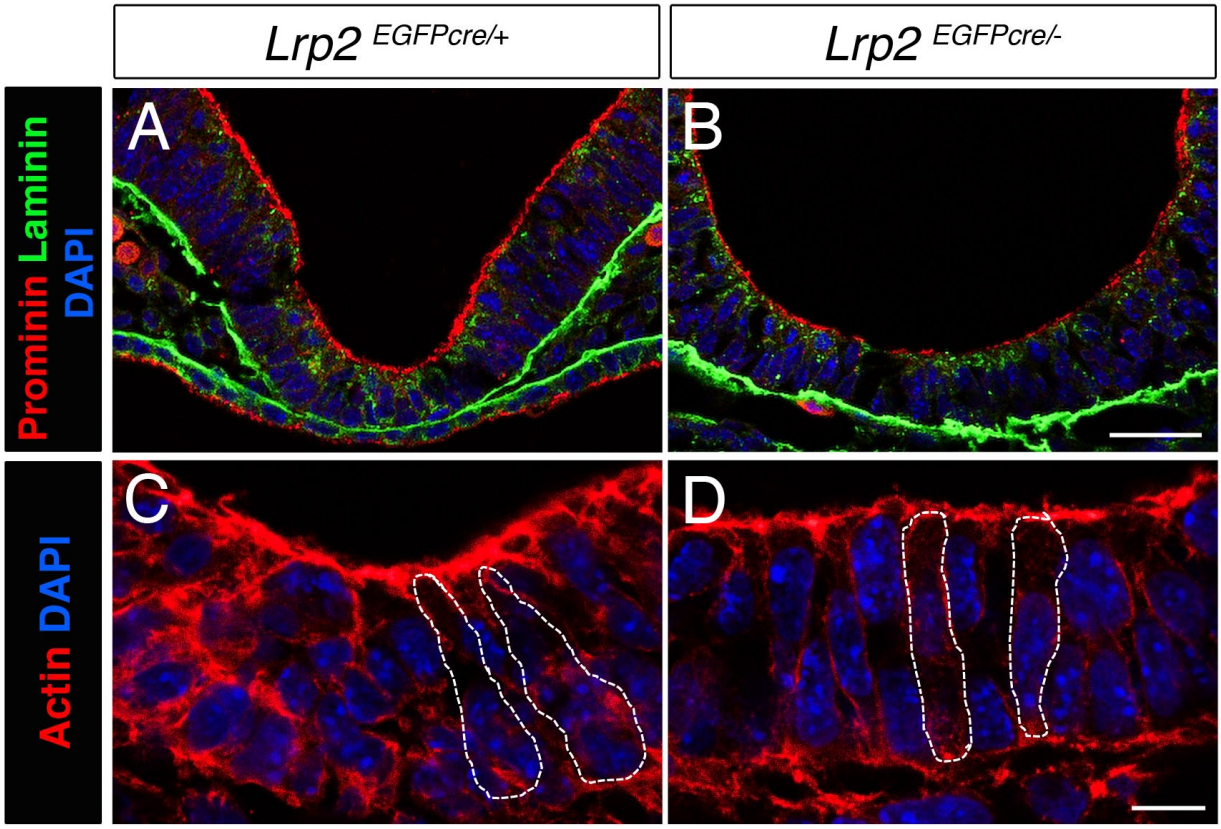

Figure 31. Ventral midline cells of *Lrp2*$^{EGFPcre/-}$ embryos exhibit normal polarity, but altered cell shape.
(A, B) Immunohistology for prominin and laminin on coronal forebrain sections of *Lrp2*$^{EGFPcre/+}$ and *Lrp2*$^{EGFPcre/-}$ embryos. Apical expression of prominin and basal expression of laminin is unchanged in LRP2 deficient embryos. Note the U-shaped ventral midline of LRP2 deficient embryos (B) in comparison to the V-shaped ventral midline of control embryos (A). Scale bar: 100 µm. **(C, D)** Visualization of actin filaments on coronal forebrain sections of *Lrp2*$^{EGFPcre/+}$ and *Lrp2*$^{EGFPcre/-}$ embryos. Note the columnar shaped ventral midline cells of LRP2 deficient embryos (D) in comparison to the wedge-shaped ventral midline cells of control embryos (C). Scale bar: 25 µm.

Low Lrp2 promoter activity prevents sorting of EGFP positive cells

A major motivation for generating the *Lrp2*$^{tm(EGFPcre)}$ line was the possibility to sort EGFP expressing neuroepithelial cells via flow cytometry and to use these cells for expression profiling or for establishing stable cell lines for biochemical studies. Sorting EGFP positive cells from *Lrp2*$^{EGFPcre/+}$ as well as *Lrp2*$^{EGFPcre/-}$ embryos would enable a comparative analysis of LRP2 deficient and control neuroepithelial cells. One drawback of this approach was the finding that in *Lrp2*$^{EGFPcre/-}$ embryos expression of EGFP was delayed. This circumstance would render it impossible to compare EGFP positive cells from *Lrp2*$^{EGFPcre/-}$ and *Lrp2*$^{EGFPcre/+}$ embryos at E9.5, because at this time point there are no such cells in *Lrp2*$^{EGFPcre/-}$ embryos. Still one could use developmental stage E10.5 or older stages for these experiments.

To see whether sorting of EGFP positive cells by flow cytometry was possible, I isolated embryonic brain cells from *Lrp2*$^{EGFPcre/+}$ embryos. A single cell suspension was produced by careful dissection of the embryonic brain, enzymatic degradation of cell adhesion molecules and mechanical dissociation of cells (see methods section for details). As a positive control I also isolated cells from *Shh*$^{EGFPcre/+}$ embryos, which expressed EGFPcre under the control of the endogenous *Shh* promoter (Harfe et al., 2004). During dissection of the embryos under a fluorescent stereomicroscope, it was obvious that *Shh*$^{EGFPcre/+}$ embryos showed a considerably higher EGFP fluorescence than the *Lrp2*$^{EGFPcre/+}$ embryos, although both knock-in lines were generated using the same EGFPcre expression construct and LRP2 and SHH have similar expression domains. Using a LSR 2 flow cytometer, I was able to identify an EGFP positive population in cells isolated from *Shh*$^{EGFPcre/+}$ embryos, but not in cells isolated from *Lrp2*$^{EGFPcre/+}$ embryos (Figure 32).

This discrepancy in EGFP expression between the two lines might be due to different levels of activity of the two promoters, with the *Shh* promoter having a very strong and the *Lrp2* promoter having a weak activity. With regard to isolation of EGFP positive cells by flow cytometry, this weak promoter activity was a clear disadvantage since it prevented efficient cell sorting. Innovations in the field of flow cytometry leading to an increased detection sensitivity may enable sorting of neuroepithelial cells from *Lrp2*$^{EGFPcre/+}$ embryos in the future. However, for the time being I decided to focus on alternative methods to generate samples for expression profiling.

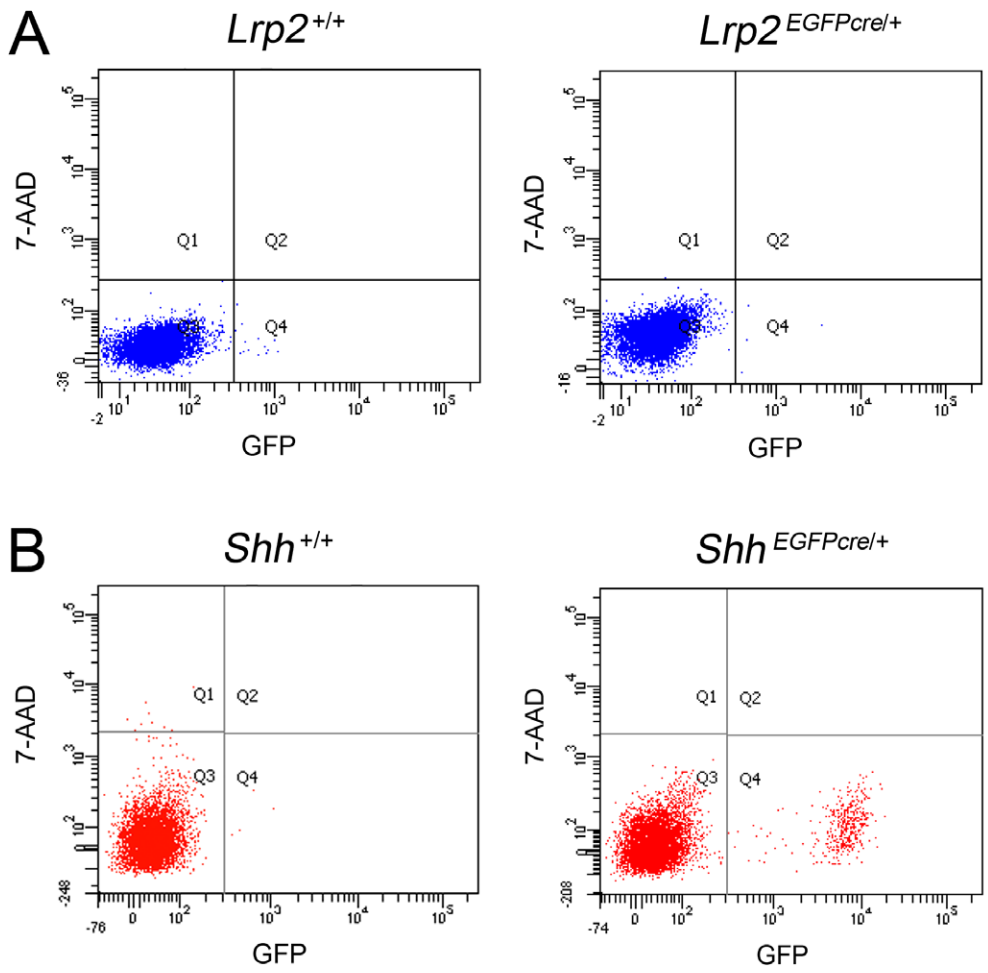

Figure 32. Analysis of EGFP expressing cells by flow cytometry.
(A) Embryonic neuroepithelial cells of embryonic day (E) 13.5 *Lrp2*$^{EGFPcre/+}$ embryos were isolated, stained for EGFP and analyzed with a LSR 2 flow cytometer. No EGFP positive population could be identified. **(B)** Embryonic neuroepithelial cells of E10.5 *Shh*$^{EGFPcre/+}$ embryos were isolated, stained for EGFP and analyzed with a LSR 2 flow cytometer. An EGFP positive population could clearly be identified.

3.2.2 Expression profiling of wild type and LRP2 deficient midline cells

To identify the cause for the holoprosencephalic phenotype of LRP2 deficient mice, our lab has previously analyzed the expression of several key players in forebrain patterning. In this target based approach, alterations in the SHH, BMP4 and FGF8 pathways (Spoelgen et al., 2005) were found. However, I wanted to characterize changes in gene expression on a more global level, anticipating that I could identify changes in additional important pathways or even find factors that have not yet been described to play a role in forebrain development.

Dissection of defined LRP2 expressing cell populations for expression profiling

During development, subtle changes in gene expression level can elicit major phenotypes. By comparing whole embryos or brains one might easily miss these changes. Since I knew from my analysis of the *Lrp2*$^{tm(EGFPcre)}$ mouse line that *Lrp2* promoter activity in the neuroepithelium is highest in the ventral and dorsal forebrain midline (Figure 30), I decided to use these tissues for expression profiling. With regard to the appropriate time during embryonic development I chose E9.5, since this is the timepoint when morphological manifestation of the phenotype starts. At later stages, changes in gene expression might also be secondary effects and would therefore be more difficult to interpret. A very important prerequisite was to find an appropriate method to dissect E9.5 embryos in a way that would lead to a pure preparation of midline neuroepithelium. I chose two alternative methods: laser capture microdissection (LCM) and manual dissection from whole-mounts.

LCM is a technique by which defined tissue samples can be excised from a histological section using a microscope equipped with a special laser. Since this method had to be newly established in the lab, I will shortly summarize the workflow. Exact experimental procedures are described in the methods section.

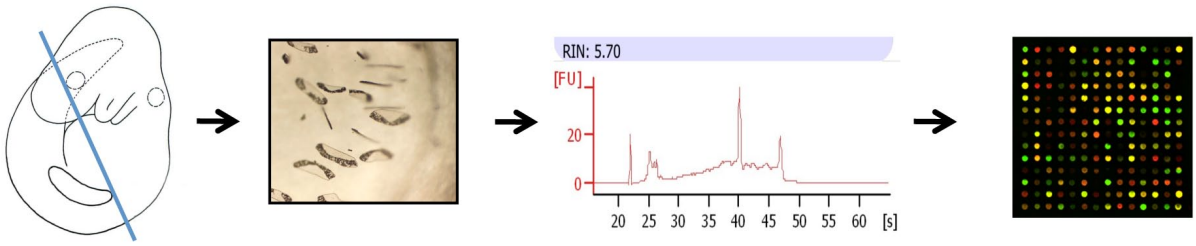

Figure 33. Preparation of samples for gene expression profiling by laser capture microdissection. Coronal sections of E9.5 embryos were prepared. Midline tissue was dissected and collected by laser capture microdissection. Medium quality RNA was isolated from tissue samples. Amplified and labeled cDNA was hybridized to an Illumina Microarray.

First, cryosections of shortly fixed E9.5 embryos (24-26 somite stage) were produced. The ventral and dorsal midline was excised from the sections by LCM. Tissue samples were collected and RNA was extracted. Due to low concentration and medium integrity of the LCM RNA samples, they were amplified using the Ovation PicoSL WTA System (Nugen). In this system, double stranded cDNA is generated from the total RNA samples using a mix of polyT and random primers to ensure efficient reverse transcription of the partially degraded RNA. Subsequently, the cDNA is amplified in a linear amplification

procedure using DNA/RNA hybrid primers. Subsequently, samples were labeled and hybridized to a MouseWG-6 v2.0 Expression BeadChip (Illumina). The obvious advantage of this approach was the high precision in dissection of tissue samples. Disadvantages were the time-consuming and expensive procedure, the medium quality of the RNA due to the fixation step, and the need to perform an amplification step because of the low RNA recovery.

As an alternative method to obtain RNA from midline tissue, I manually dissected the ventral and dorsal midline from whole-mount preparations. The workflow is illustrated in figure 34. From heads of E9.5 embryos (22-24 somite stage), the dorsal forebrain midline was cut off using a fine scalpel. The tissue was trimmed by removing lateral tissue and midbrain tissue and shock-frozen in liquid nitrogen. The remaining head was opened along the entire dorsal midline and mounted flat. Subsequently the ventral forebrain midline was excised with a fine scalpel and shock-frozen. RNA was prepared, labeled and hybridized to a MouseWG-6 v2.0 Expression BeadChip (Illumina). The advantages of this method were the relatively easy and fast preparation, the high quality of the obtained RNA as well as the high RNA yields. Certainly the dissection of the midline tissue by this method was less precise compared to the LCM approach.

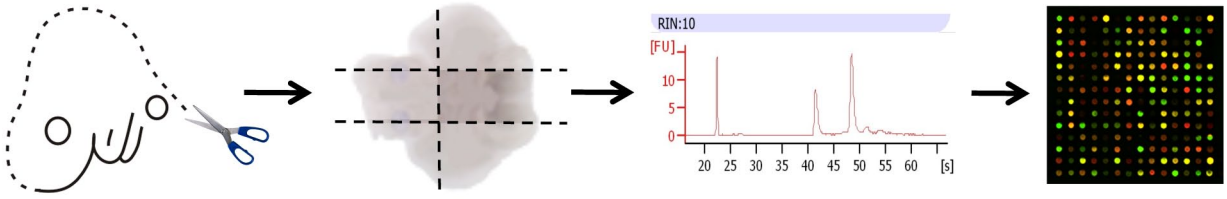

Figure 34. Preparation of samples for gene expression profiling by manual tissue dissection.
Midline tissue was dissected from heads of E9.5 embryos using a fine scalpel. High quality RNA was isolated from tissue samples. Labeled cRNA was hybridized to an Illumina Microarray.

Expression profiling reveals changes in gene expression in LRP2 deficient embryos compared to controls

Hybridization of labeled samples to Illumina microarrays was performed by Gabriele Born (Hübner lab, MDC Berlin). Statistical evaluation of the data by multivariate analysis of variance (ANOVA) was done by Herbert Schulz (Hübner lab, MDC Berlin). Since heterozygous embryos (*Lrp2*$^{EGFPcre/+}$) exhibited an expression pattern undistinguishable

from wild type embryos (*Lrp2*$^{+/+}$), these two genotypes were combined in the analysis and compared to LRP2 deficient embryos (*Lrp2*$^{EGFPcre/-}$). Analysis of the ventral midline samples was more yielding than analysis of the dorsal midline samples. Probably this was due to the thinner nature of the dorsal neuroepithelium, which resulted in lower RNA yields. First, data from the two different preparation methods were analyzed separately (see appendix, tables 4 and 5). In addition, the data of both experiments were combined and analyzed together, by this means significantly increasing n (the number of samples). Clustering of differentially expressed genes is shown in figure 35. Table 2 and 3 show genes differentially expressed in the ventral and dorsal neuroepithelium of control and LRP2 deficient embryos.

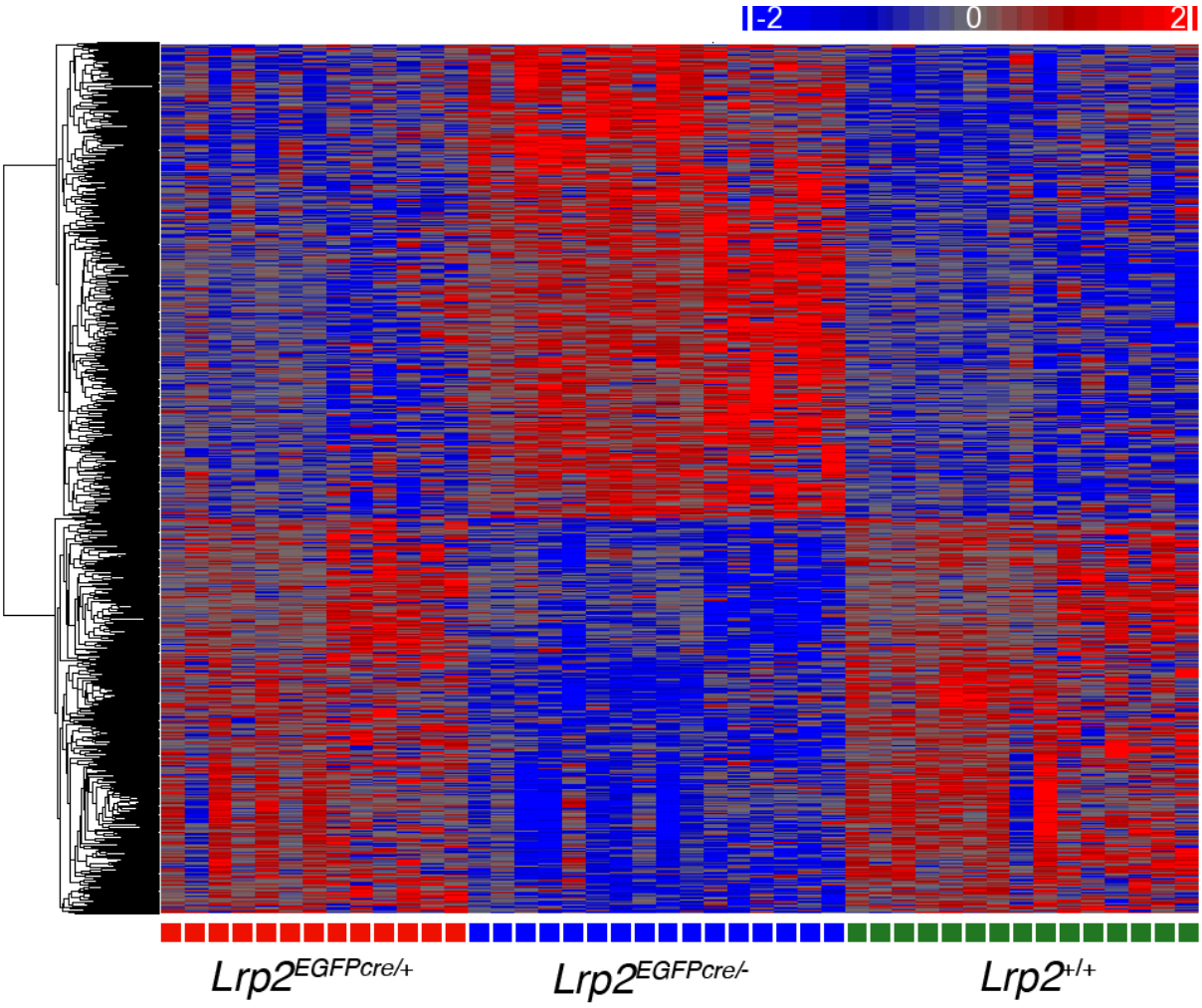

Figure 35. Genes differentially expressed in *Lrp2*$^{+/+}$, *Lrp2*$^{EGFPcre/+}$ and *Lrp2*$^{EGFPcre/-}$ embryos.
Hierarchical clustering of 991 probes significantly regulated by genotype (*Lrp2*$^{+/+}$ and *Lrp2*$^{EGFPcre/+}$ vs. *Lrp2*$^{EGFPcre/-}$). The cluster dendrogram represents the cluster node similarity matrix of samples (bottom) and probes (left). The heatmap represents the expression differences between samples in a color scale ranging from red (up-regulated) to blue (down-regulated).

Table 2. Genes differentially expressed in the ventral midline of *Lrp2*$^{EGFPcre/-}$ embryos.
Cut-off: false discovery rate (FDR) 5%, Fold-Change (FC): 1.5x

SYMBOL	DEFINITION	FDR	p-value	Fold-Change
Foxg1	forkhead box G1	0.0014	1.39E-07	-6.47
Lrp2	low density lipoprotein receptor-related protein 2	0.0000	2.18E-09	-3.86
Zic1	zinc finger protein of the cerebellum 1	0.0014	7.15E-08	-3.32
Dlk1	delta-like 1 homolog	0.0017	4.72E-08	-3.14
Sepp1	selenoprotein P, plasma, 1	0.0253	4.98E-06	-2.94
Igfbp5	insulin-like growthfactor binding protein 5	0.0151	4.00E-04	-2.87
Sox21	SRY-box containing gene 21	0.0354	3.87E-06	-2.29
Stmn2	stathmin-like 2	0.0370	1.02E-05	-2.28
Shisa 2	transmembrane protein 46	0.0061	4.77E-07	-2.25
Sox9	SRY-box containing gene 9	0.0127	7.34E-04	-2.22
Zic4	zinc finger protein of the cerebellum 4	0.0254	3.75E-04	-2.20
Six2	sine oculis-related homeobox 2 homolog	0.0239	7.26E-05	-2.17
Vax1	ventral anterior homeobox containing gene 1	0.0035	4.90E-09	-2.06
Id4	inhibitor of DNA binding 4	0.0039	3.04E-05	-1.99
Nrarp	Notch regulated ankyrin repeat protein	0.0014	5.28E-06	-1.98
Syt11	synaptotagmin XI	0.0004	8.53E-06	-1.98
Tubb2b	tubulin, beta 2b	0.0298	1.53E-03	-1.97
Tcf7l2	transcription factor 7-like 2	0.0015	5.41E-05	-1.78
Zic4	zinc finger protein of the cerebellum 4	0.0216	3.07E-03	-1.53
Dlx3	distal-less homeobox 3	0.0191	9.67E-03	1.51
Jag1	jagged 1	0.0248	1.27E-03	1.54
Frzb	frizzled-related protein	0.0004	3.17E-06	1.58
Snai1	snail homolog 1	0.0226	7.01E-05	1.61
Nkx6-1	NK6 homeobox 1	0.0243	1.15E-02	1.61
Twist1	Twist homolog 1	0.0344	6.10E-04	1.61
Dlx2	distal-less homeobox 2	0.0008	1.20E-06	2.09
Id2	inhibitor of DNA binding 2	0.0131	1.05E-04	2.16
Id1	inhibitor of DNA binding 1	0.0000	1.71E-08	2.43
Lmo2	LIM domain only 2	0.0035	1.28E-07	2.54
Fst	follistatin	0.0017	1.40E-04	2.75
Foxd1	forkhead box D1	0.0106	2.99E-05	3.28
Fgf10	fibroblast growth factor 10	0.0039	7.03E-07	3.35
Car4	carbonic anhydrase 4	0.0002	1.64E-08	3.82

Table 3. Genes differentially expressed in the dorsal midline of *Lrp2*$^{EGFPcre/-}$ embryos.
Cut-off: false discovery rate (FDR) 5%, Fold-Change (FC): 1.5x

SYMBOL	DEFINITION	FDR	p-value	Fold-Change
Lrrn1	leucine rich repeat protein 1, neuronal	0.0241	7.70E-06	-2.70
Nfatc4	nuclear factor of activated T-cells 4	0.0248	2.90E-04	-2.62
Rspo2	R-spondin 2 homolog	0.0105	1.41E-06	-2.51
Lrp2	low density lipoprotein receptor-related protein 2	0.0000	3.29E-06	-2.43
Nnat	neuronatin	0.0477	3.66E-03	-2.41
Phf6	PHD finger protein 6	0.0219	1.09E-04	-2.29
Wnt8b	wingless related MMTV integration site 8b	0.0492	3.78E-06	-2.25
Ypel5	yippee-like 5	0.0049	2.50E-05	-2.05
Raet1b	retinoic acid early transcript beta	0.0459	5.57E-05	-1.98
Tubb2b	tubulin, beta 2b	0.0353	2.90E-03	-1.97
Cdon	cell adhesion molecule-related/down-regulated by oncogenes	0.0209	4.64E-06	-1.92
Nrxn2	neurexin II	0.0426	1.01E-03	-1.86
Igfbp5	insulin-like growthfactor binding protein 5	0.0127	1.10E-02	-1.85
Syt11	synaptotagmin XI	0.0004	9.29E-05	-1.73
Sox9	SRY-box containing gene 9	0.0127	1.51E-02	-1.69
Tcf7l2	transcription factor 7-like 2, T-cell specific, HMG-box	0.0015	8.50E-04	-1.55
Nrp1	neuropilin 1	0.0010	6.71E-04	1.55
Dlx3	distal-less homeobox 3	0.0191	3.45E-03	1.57
Fgf18	fibroblast growth factor 18	0.0015	2.66E-05	1.62
Nkx6-1	NK6 homeobox 1	0.0243	5.14E-03	1.67
Nomo1	nodal modulator 1	0.0055	2.74E-04	1.76
Spon1	spondin 1 (f-spondin)	0.0150	2.18E-04	1.83
Id1	inhibitor of DNA binding 1	0.0000	3.69E-06	1.89
Ckn1	Cockayne syndrome 1 homolog	0.0055	1.98E-05	1.95
Sox10	SRY-box containing gene 10	0.0102	1.48E-04	1.96
Ptch1	patched homolog 1	0.0451	4.61E-05	1.98
Chst2	carbohydrate sulfotransferase 2	0.0000	3.43E-07	2.03
Tpst2	protein-tyrosine sulfotransferase 2	0.0061	4.64E-04	2.03
Trh	thyrotropin releasing hormone	0.0343	1.65E-04	2.19
Cdk6	cyclin-dependent kinase 6	0.0009	4.63E-06	2.20
Fst	follistatin	0.0017	5.01E-04	2.38
Grrp1	glycine/arginine rich protein 1	0.0042	3.26E-05	2.42
En1	engrailed 1	0.0150	2.96E-06	3.17

All major signaling centers in the developing forebrain are disturbed in LRP2-deficient embryos

In order to verify the data obtained from the microarray analysis, I performed ISH on wholemount embryos. First I analyzed the FGF and WNT signaling pathways, since the microarray data showed that components of both pathways exhibited changes in expression level. Of the many known FGFs, FGF8 and 17 are expressed in the ANR and constitute the anterior patterning center of the forebrain. ISH showed that in LRP2-deficient embryos, the expression domains of *Fgf8* and *Fgf17* mRNA were substantially shifted to dorsal regions in comparison to the control embryos (Figure 36 B, C). In addition, *Fgf8* and *Fgf17* were expressed in the midline cells of LRP2 deficient embryos, while in controls the immediate midline was devoid of *Fgf* mRNA expression (Figure 36D, E).

In combination with BMPs, WNTs constitute the dorsal patterning center of the developing forebrain. ISH revealed that the expression domain of *Wnt3a* mRNA in the dorsal diencephalon was considerably extended anteriorly in $Lrp2^{EGFPcre/-}$ embryos compared to controls (Figure 37 B). Expression of *Wnt8b* mRNA in the telencephalon was reduced dorsally and slightly shifted anteriorly (Figure 37 D). Expression of *Tcf7l2*, a transcription factor downstream of WNT signaling was reduced in the dorsal as well as the ventral

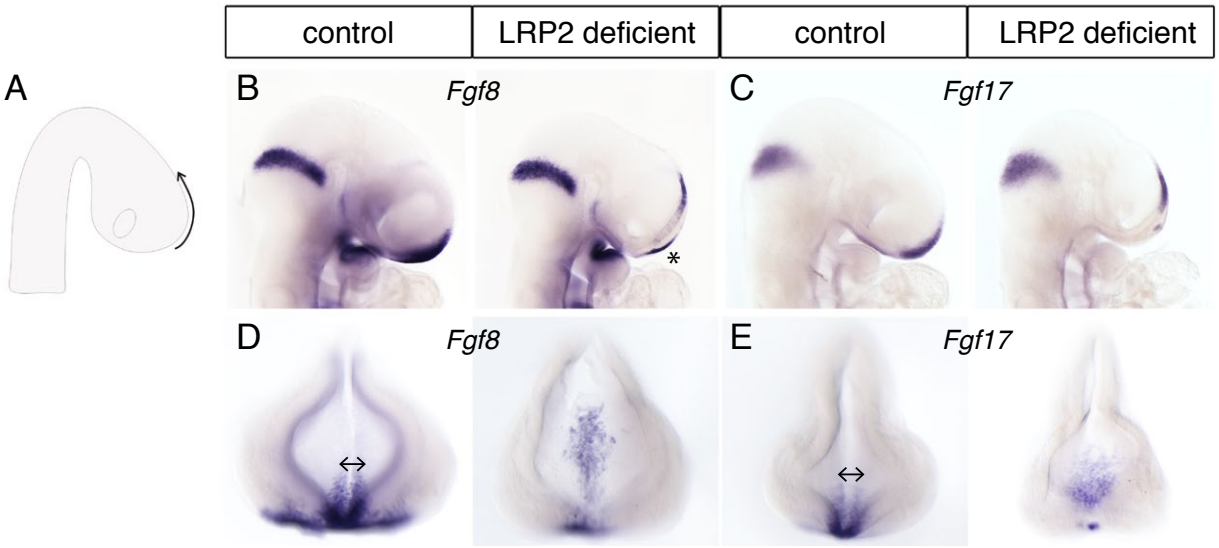

Figure 36. Expression pattern of components of the FGF signaling pathway is altered in LRP2 deficient embryos.

(A) Scheme of the mouse brain at embryonic day (E) 9.5. The arrow indicates the shift of the *fibroblast growth factor (Fgf) 8* and *Fgf17* expression domains seen in LRP2 deficient embryos. **(B-E)** Expression of *Fgf8* (B, D) and *Fgf17* (C, E) in control and LRP2 deficient embryos in lateral (B, C) and frontal (D, E) views. In LRP2 deficient embryos, *Fgf8* and *Fgf17* expression in the anterior neural ridge (ANR) is shifted dorsally (B, C) and is no longer excluded from the immediate midline (double arrow in D, E). Expression of *Fgf8* in the facial ectoderm is not affected (asterisk in B).

diencephalon (Figure 37 E). Expression of *Wnt1* mRNA was not affected (Figure 37 C).
I also tested expression of *Shh* in *Lrp2*$^{EGFPcre/+}$ and *Lrp2*$^{EGFPcre/-}$ embryos. While in lateral aspects, no discernable differences were visible (Figure 38 B), coronal vibratome sections revealed that *Shh* mRNA expression was excluded from the immediate midline in LRP2 deficient embryos (Figure 38 C).

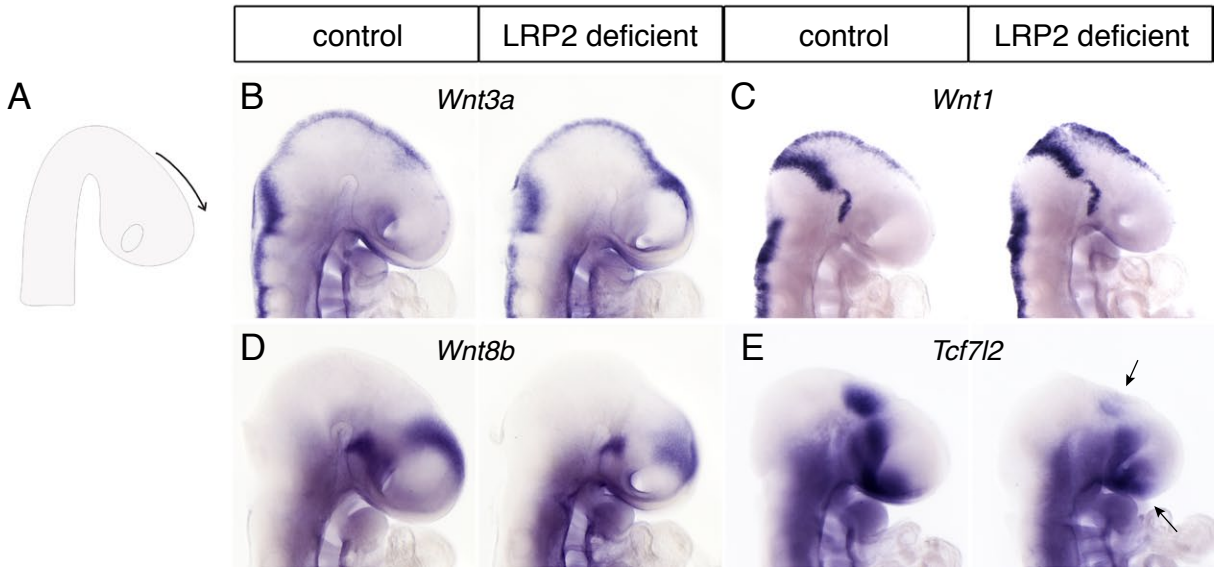

Figure 37. Expression pattern of components of the WNT signaling pathway is altered in LRP2 deficient embryos.
(A) Scheme of the mouse brain at embryonic day (E) 9.5. The arrow indicates the extension of the *wingless/int (Wnt) 3a* expression domain seen in LRP2 deficient embryos. **(B)** The expression domain of *Wnt3a* mRNA is extended anteriorly into the telencephalon in LRP2 deficient embryos. **(C)** Expression of *Wnt1* is unchanged in LRP2 deficient embryos compared to controls. **(D)** Expression of *Wnt8b* mRNA is reduced dorsally and slightly shifted anteriorly in LRP2 deficient embryos. **(E)** Expression of *T-cell factor 7 like 2* (*Tcf7l2)* is reduced in the ventral and dorsal diencephalon of LRP2 deficient embryos (arrows).

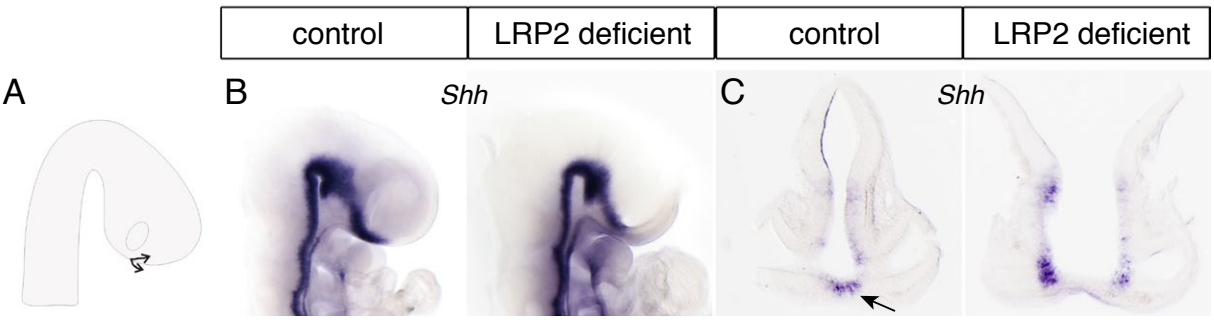

Figure 38. Expression pattern of SHH is altered in LRP2 deficient embryos.
(A) Scheme of the mouse brain at embryonic day (E) 9.5. The arrows indicate the loss of *Shh* expression in the immediate ventral midline of LRP2 deficient embryos. **(B, C)** Expression of *Shh* mRNA in control and LRP2 deficient embryos in lateral views (B) and on coronal vibratome sections (C). Note the loss of *Shh* mRNA expression in the immediate ventral midline of LRP2 deficient embryos (arrow in C).

The telencephalon is not correctly specified in LRP2 deficient embryos

Expression of many other genes was differentially regulated in LRP2 deficient and control embryos according to the microarray data (Tables 2-4). By ISH I could illustrate the changes in a three dimensional way. Many genes with a telencephalic expression domain showed a similar change in expression pattern in LRP2 deficient embryos compared to controls (Figures 39 A and 40 A). Broad and robust telencephalic expression domains in controls were either condensed, like *forkhead box 1 (Foxg1), aristaless 3* and *4 (Alx3, Alx4)* (Figure 39 B, D, E), reduced, like *hairy and enhancer of split 5 (Hes5)* and *delta1* (Figure 39 F, G) or completely absent, like *ventral anterior homoeobox 1 (Vax1)* (Figure 39 C) in $Lrp2^{EGFPcre/-}$ embryos, indicating a loss of telencephalic structures. On the other hand, genes expressed in the ventral telencephalon showed a shift of expression from the posterior towards the anterior diencephalon, like *Foxa2* (Figure 40 F) or from the anterior diencephalon towards the telencephalon, like *neuregulin1 (Nrg1), Foxd1, Fgf18, paired homeodomain transcription factor 2 (Pitx2)* and *lymphoid enhancer binding factor 1 (Lef1)* (Figure 40 B-E, G) in $Lrp2^{EGFPcre/-}$ embryos, indicating an expansion of anterior structures.

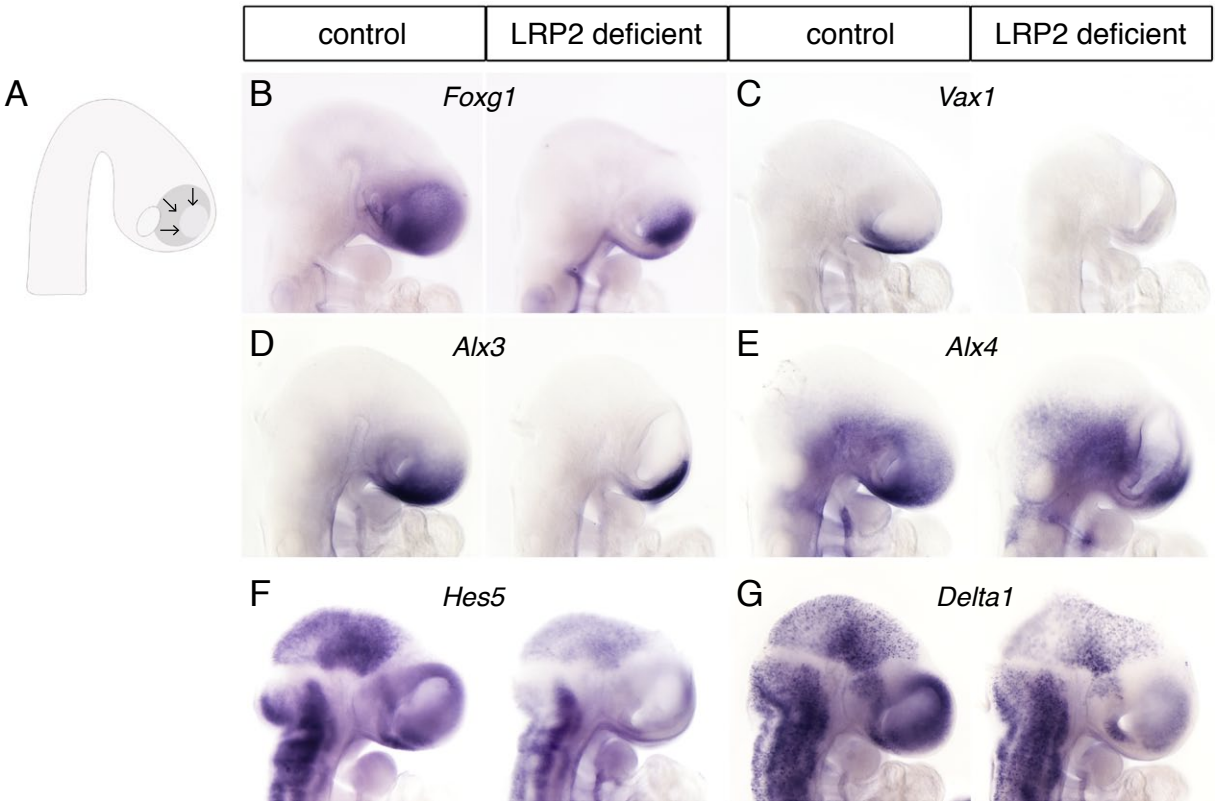

Figure 39. Expression of telencephalic markers is reduced in LRP2 deficient embryos.
(A) Scheme of the mouse brain at embryonic day 9.5, indicating the reduced expression of telencephalic markers seen in LRP2 deficient embryos. **(B-G)** Expression of telencephalic markers is reduced in the telencephalon of LRP2 deficient embryos.

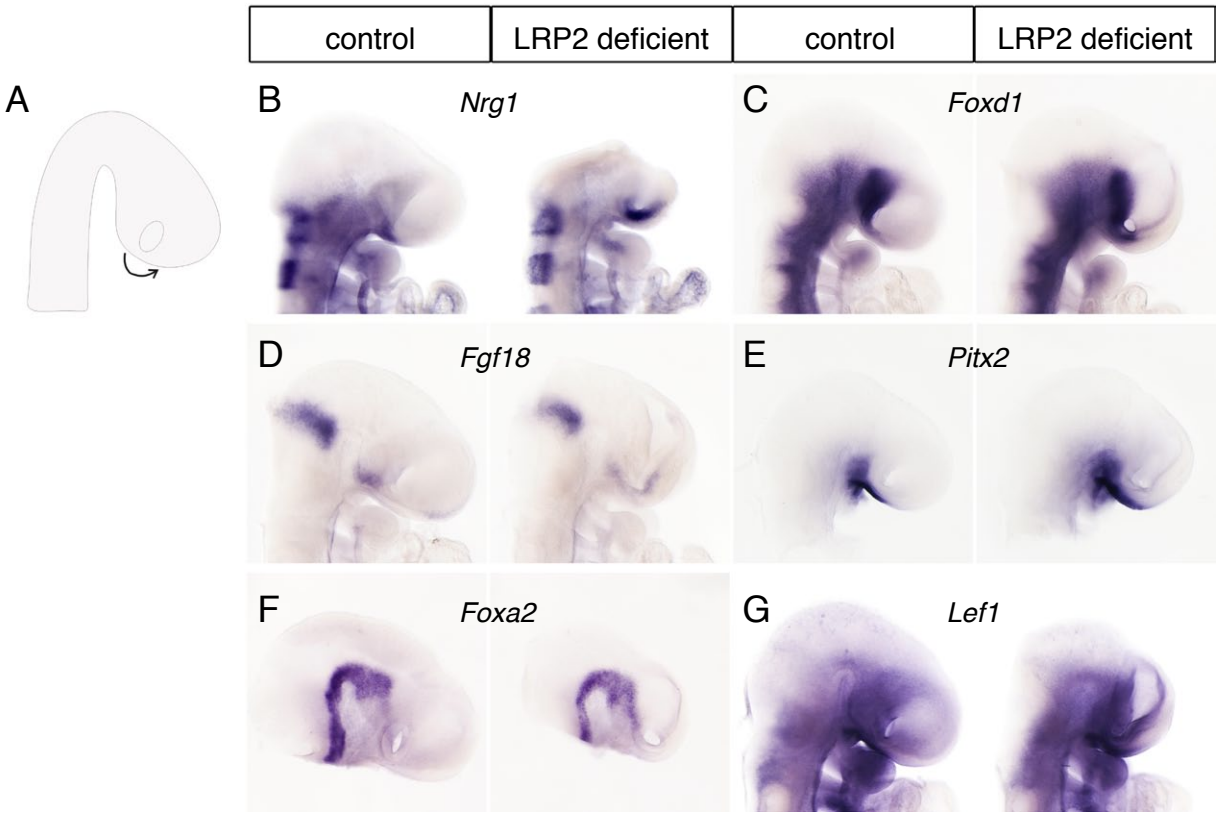

Figure 40. Diencephalic domain is extended anteriorly in LRP2 deficient embryos.
(A) Scheme of the mouse brain at embryonic day 9.5, indicating the anterior expansion of expression domains of diencephalic markers seen in LRP2 deficient embryos. **(B-G)** Expression of diencephalic markers is expanded anteriorly in LRP2 deficient embryos.

4. DISCUSSION

4.1 LRP2 IN ZEBRAFISH DEVELOPMENT

In the first part of my thesis, I have analyzed the role of Lrp2 during embryonic development of the zebrafish. My studies have revealed that the function of the receptor in renal tubular clearance pathways is conserved between mammals and fish, but not its function in brain development.

4.1.1 Lrp2 is the main endocytosis receptor in the zebrafish pronephros

In the ontogeny of mammals, three different kidneys with increasing complexity form: the pro-, meso- and metanephros. Of these, the pro- and mesonephros are degraded and just the metanephros, the development of which is completed at late embryonic stages, is functional. In fish, only two successive kidneys, the pro- and mesonephros, form. While the mesonephros is the kidney in the adult organism, the pronephros is used as the functional kidney of free-swimming larvae to maintain proper osmoregulation during early life. Without a functional pronephros, larvae die of edema because they have salty blood and yet live in a very dilute environment. For studies on kidney function and disease, the zebrafish pronephros is a suitable model because its architecture is simple (only 2 bilateral nephrons compared to a million nephrons in the mammalian metanephros), but it contains all the functional units (Drummond, 2003).

In the proximal tubule cells of the adult mammalian kidney, LRP2 acts as a low-affinity but high-capacity scavenger receptor for retrieval of numerous plasma proteins filtered through the glomerulus, such as DBP and RBP, transporters for vitamin D and A metabolites, respectively. LRP2 deficient mice exhibit proteinuria (Willnow et al., 1996) and a dramatic breakdown of the endocytic machinery in proximal tubule cells (Nykjaer et al., 1999). Similarly, in the pronephros of zebrafish embryos deficient for Lrp2, I detected complete absence of fluid phase uptake (Figure 10) as well as a loss of endocytic structures (Figure 11) that looks identical to what has been observed in mammals. These findings argue that in zebrafish, the receptor plays a similarly important role in the renal retrieval pathway as it does in mammals.

The observations made in mammals and zebrafish deficient for LRP2 imply that other endocytic receptors contribute only insignificantly to renal clearance processes, since

endocytosis is completely shut down upon loss of LRP2. An alternative explanation could be that LRP2 is directly required for the establishment of a functional endocytic apparatus in kidney proximal tubule cells, so that in the absence of LRP2, endocytosis mediated by other receptors is also impaired.
In mammals, lack of LRP2 results in uncontrolled renal loss of essential metabolites and deregulation of systemic vitamin homeostasis (Christensen and Birn, 2001). In zebrafish, the nature of ligands internalized by Lrp2 in the pronephros is unclear at present. Vitamin carriers such as DBP and RBP are expressed in zebrafish as well (Abe et al., 1975) (Tingaud-Sequeira et al., 2006), suggesting a conserved function for this receptor pathway in vitamin handling in mammalian metanephros and zebrafish pronephros. However, the main function of the zebrafish pronephros is osmoregulation (Drummond, 2005) and little is known about the relevance of proteinuria in fish. Still, the functional similarities between zebrafish pronephros and mammalian metanephros recommend LRP2 deficient zebrafish as a potential model for proteinuria studies.

4.1.2 Lrp2 is not crucial for forebrain development of the zebrafish

We have previously reported the impact of splice morpholino-mediated knock-down of Lrp2 in zebrafish larvae (Anzenberger et al., 2006). However, expression of the receptor from maternal transcripts precluded analysis of receptor defects at early embryonic stages, including patterning of the forebrain. The availability of the zebrafish *lrp2* mutants *bugeye* and *5cben* has now enabled me to address these issues. The finding that I could not detect a distinct brain phenotype in Lrp2 deficient zebrafish embryos came unexpected, since the distinct expression pattern of Lrp2 in the zebrafish brain suggested a function similar as in mammals. Conceptually, there are two main explanations why loss of Lrp2 does not result in an overt forebrain phenotype. Either loss of Lrp2 function in Lrp2 deficient embryos is compensated by other LRP family members, or different mechanisms in forebrain induction in mammals and fish overcome the need for Lrp2 in zebrafish.

Is loss of Lrp2 function compensated by other LDLR family members?
An obvious candidate for taking over the function of Lrp2 in Lrp2 deficient zebrafish is its paralog Lrp2b. Following a whole-genome duplication in the teleost fish lineage, many genes – including *lrp2* – exist in two paralogous forms (Jaillon et al., 2004). There are several alternatives of what can happen to these two copies. In some cases, one copy is

lost or inactivated by accumulating mutations. If both genes are expressed, one possibility is that the two proteins share the same function, but their expression domains have diverged. Another possibility is that the two proteins are expressed in the same tissues, but their function has been divided, with both proteins taking over part of the original protein activity. A third possibility is that both proteins are expressed in the same domains and still carry out the same function.

Lrp2b mRNA is present at very low levels (Figure 21) and was not detectable by ISH. Therefore, I cannot conclude whether Lrp2b is expressed in a similar pattern as Lrp2. Theoretically, it might also be expressed in different tissues. In addition, it is justified to ask whether the protein is expressed at all. As described in the results section (3.1.3), several observations indicate that this is the case, such as existence of ESTs from different libraries and the absence of stop codons in the large open reading frame. However, not knowing in which tissue Lrp2b is expressed renders it hard to analyze the potential relevance of this protein. At least, reabsorption processes in the kidney are not affected by loss of Lrp2b as shown by morpholino knock-down and dextran uptake experiments (Figure 23).

To test the possibility that Lrp2b compensates for loss of Lrp2 during development of the forebrain, I knocked down Lrp2b expression in Lrp2 mutant fish. Inspection of the double deficient embryos at 24 hpf did not reveal any noticeable differences compared to *bugeye* embryos (Figure 24). Thus, it does not seem likely that Lrp2b compensates for loss of Lrp2 function.

Another possibility how loss of Lrp2 might be compensated in Lrp2 deficient embryos is that other members of the LRP family take over Lrp2 function. Besides *lrp2* and *lrp2b*, also *ldlr* (NC_007114.5), *lrp1* (NC_007122.5), *lrp1b* (NC_007133.5), *lrp4* (NC_007118.5), *lrp5* (NC_007136.5), *lrp6* (NC_007130.5) and *lrp8* (NC_007117.5) have been described. The most closely related LRP to Lrp2 and Lrp2b is Lrp1. It is conceivable that one of these receptors compensates for loss of Lrp2 in Lrp2 deficient embryos.

Different key aspects in ventral midline induction in zebrafish and mammals

A second reason why loss of Lrp2 does not result in a forebrain phenotype in zebrafish may be mechanistic differences in forebrain development of mammals and fish. Although the basic principles are conserved across vertebrate species, there are some important aspects distinguishing brain development of zebrafish from brain development of mammals. In this regard, the most crucial issue concerns ventral midline induction. In mammals, SHH

protein synthesized in the PCP is transported to the overlying neuroepithelium where it specifies the ventral midline, one of the main organizer centers of the developing forebrain (Roelink et al., 1995). Loss of SHH in mice results in dramatic defects in midline structures (Chiang et al., 1996). In contrast, ventral midline induction in zebrafish proceeds at earlier stages, before the PCP has even formed (Etheridge et al., 2001) (Tian et al., 2003). Furthermore, induction of the immediate midline is dependent on nodal signaling (Shinya et al., 1999) (Muller et al., 2000), while Shh signaling is dispensable. Shh is only needed to specify the lateral part of the ventral midline. Consequently, Shh deficient zebrafish display only mild phenotypes with subtle midline defects compared to SHH deficient mice, indicating that this morphogen is less crucial for brain development in zebrafish than it is in mice (Schauerte et al., 1998).

In parallel to my studies, new insights into the role of LRP2 during forebrain development of the mouse were gained in our lab. These findings indicate that the first function of LRP2 during forebrain development is to ensure that the ventral midline cells receive PCP-derived SHH early and at high concentration. Here, LRP2 may function as a co-receptor for SHH. In LRP2 deficient mice, induction of SHH target genes in the ventral midline is delayed. This initial delay results in a defect in midline specification which cannot be recovered at later stages (Christ et al., in revision). In zebrafish, the need to tightly regulate the availability of Shh to the midline cells is obviously less crucial than it is in mice. Probably, this renders Lrp2 function dispensable for zebrafish midline induction. This hypothesis is supported by the late onset of Lrp2 expression in the zebrafish forebrain and by the lack of a forebrain midline phenotype in *bugeye* and *5cben* embryos as shown in this study.

Interestingly, a forebrain phenotype is described for zebrafish deficient for Brother of Cdo (Boc), another co-receptor required for SHH signaling (Izzi et al., 2011) (Allen et al., 2011). Boc is expressed in the zebrafish brain and spinal cord as early as 10 hpf (Thisse et al., 2004), and *boc* mutants display reduced Shh signaling, defects in axon guidance, disturbed formation of the optic chiasm as well as forebrain patterning defects (Bergeron et al., 2011).

From 36 hpf to 96 hpf, Lrp2 displays a very specific and robust expression pattern in the developing zebrafish brain (Figure 6). It is therefore hard to envision that the receptor does not fulfill a distinct function. For instance, Lrp2 might be involved in Shh-dependent patterning of the zebrafish eye at later stages (Stenkamp et al., 2002). Until now, it cannot formally be excluded that the large eye phenotype observed in *bugeye* and *5cben*

mutants (Veth et al., 2011) is at least partly due to a developmental defect. The detailed investigation of the reasons underlying this phenotype is an ongoing collaboration with the lab of Brian Link (Medical College of Wisconsin, USA).
In addition, although Lrp2 expression decreases at 96 hpf, it might be interesting to investigate expression and function of Lrp2 in the adult zebrafish brain. In the mouse, a function for LRP2 in promoting neurogenesis in the subventricular zone, one of the neurogenic niches in the adult mammalian brain, has been described (Gajera et al., 2010). Likely, this is achieved by downregulation of anti-proliferative signals provided by BMP4. In the zebrafish brain, adult neurogenesis occurs at multiple neurogenic sites including the ventricular zone (Byrd and Brunjes, 2001) (Adolf et al., 2006). Since the role of BMP in controlling self-renewal of stem cells is conserved between species (Li and Xie, 2005), a function for Lrp2 in adult neurogenesis may also be relevant for zebrafish.

4.2 LRP2 IN MOUSE DEVELOPMENT

In the second part of my thesis, I have analyzed the role of LRP2 in forebrain development of the mouse. Towards this aim I have generated and analyzed a new reporter mouse model, *Lrp2*$^{tm(EGFPcre)}$. In addition, I have performed expression analysis of forebrain midline cells in control and LRP2 deficient embryos and I have identified interesting changes in gene expression in the main patterning centers of the mouse forebrain, which are related to the defects seen in LRP2 deficient embryos.

4.2.1 New insights into LRP2 expression and its regulation

The data obtained with the *Lrp2*$^{tm(EGFPcre)}$ mouse model gave interesting insights into transcriptional regulation of the *Lrp2* gene and prompted us to revise previous assumptions about onset and extent of LRP2 expression. On the one hand, LRP2 expression starts way earlier during mouse embryonic development than anticipated. On the other hand, Lrp2 promoter activity is much weaker than expected from the robust signal observed by immunohistochemical detection of LRP2 protein.

Early onset of LRP2 expression in mice

So far, it was unclear from published data at which timepoint expression of LRP2 in the mouse embryo starts. Drake et al. describe the first expression of LRP2 in the developing

neuroectoderm of the E6.0 embryo (Drake et al., 2004). Gerbe et al. describe expression of LRP2 in single cells of the inner cell mass (ICM) at E3.5. Since these cells are still unpolarized, LRP2 is not expressed apically, but stored in intracellular compartments. The authors claim that the LRP2 expressing ICM cells give rise exclusively to extraembryonic tissues such as the yolk sac, but not to the embryo proper (Gerbe et al., 2008).

In contrast to this, Assemat et al. describe expression of LRP2 in all cells of the 8-cell morula (E2.5) (Assemat et al., 2005), meaning that every cell in the future embryo is descendant from a cell that has previously expressed LRP2. This data is in agreement with what I have seen in my lineage tracing experiments using the *Lrp2*$^{tm(EGFPcre)}$ line. Here, lacZ staining of E8.0 embryos from *Lrp2*$^{tm(EGFPcre)}$ x *Gt(ROSA)26Sor*^{tm1Sor} matings showed that embryos positive for EGFPcre expressed lacZ in all embryonic tissues (Figure 27).

So far, most studies focus on the role of LRP2 in polarized epithelial cells, such as the embryonic neuroepithelium, the yolk sac, the epithelia lining the reproductive organs or the proximal tubules of the kidney. Thus, analysis of LRP2 expression and function in the unpolarized, stem-cell like cells of the early embryo would be an interesting project, possibly addressing novel functions of LRP2.

On the other hand, to be able to analyze the progeny of LRP2 expressing neuroepithelial cells by lineage tracing, one could generate an alternative mouse model. One way to address this would be a system in which the *Lrp2* promoter drives expression of an inducible form of the cre recombinase, which is activated by administration of 4-hydroxytamoxifen (*Lrp2*$^{tm(ERT2creERT2)}$). This way, both the spatial and the temporal activity of cre can be controlled (Matsuda and Cepko, 2007). Using such a mouse model, one could activate cre in the LRP2 expressing cell population at E10.0 and analyze the progeny of these cells at postnatal day 1 or at even later stages.

The ventral midline is the major expression domain of LRP2 in the forebrain

One major advantage of the *Lrp2*$^{tm(EGFPcre)}$ model is that it can be used as a reporter for *Lrp2* promoter activity. However, there is one caveat when comparing LRP2 and EGFP expression: due to technical difficulties during the cloning of the *Lrp2*$^{tm(EGFPcre)}$ targeting vector, a strategy was chosen in which 3,5 kb of the first intron of the Lrp2 gene were lost after homologous recombination (Figure 25). In general, most gene regulatory elements lie within the upstream genomic sequence, but some are also present in intronic sequences. Thus, the removal of 3,5 kb from the first intron might potentially affect the expression of EGFP in comparison to LRP2. However, expression of EGFP in the kidney and the

developing forebrain recapitulates the major sites of LRP2 expression. It is therefore very unlikely that important regulatory sequences are missing in the *Lrp2*$^{tm(EGFPcre)}$ reporter mouse.

A more probable explanation for the low EGFP expression level is a weak *Lrp2* promoter activity. This notion is supported by the fact that we were so far not able to detect *Lrp2* mRNA in the CNS by conventional ISH with digoxigenin labeled probes, but only by radioactive ISH. The observation that this low transcription rate obviously still results in robust LRP2 protein levels may be explained by a long half-life of LRP2 (approximately 48 hours, our unpublished data). Therefore, in contrary to LRP2 expression, EGFP expression marks the sites of current high transcriptional activity. Thus, the concentration of LRP2 expression in the ventral midline of the neuroepithelium can be appreciated earlier and more decidedly by analysis of EGFP expression than by analysis of LRP2 expression (Figure 29).

The finding that LRP2 expression is highest in the ventral midline cells, less high in dorsal midline cells, and even lower in lateral cells, is interesting because it indicates that LRP2 function is most important in the ventral midline cells. This can give a lead when trying to decode the hierachy of the changes in gene expression caused by LRP2 deficiency. A model in which the first defects in the LRP2 deficient forebrain occur in the ventral midline cells is in agreement with other recent findings from our lab suggesting a role of LRP2 as a co-receptor for SHH (Christ et al., in revision).

Regulation of LRP2 expression

Little is known about regulation of LRP2 expression in the forebrain. However, factors that regulate LRP2 expression in other tissues have been described. In the mouse uterus, for instance, LRP2 expression is regulated by the progesterone receptor. Other known regulators of LRP2 expression are RA and vitamin D. In several cell lines it was shown that expression of LRP2 is upregulated by treatment with retinoids or vitamin D (Liu et al., 1998) (Chlon et al., 2008).

Since my *Lrp2*$^{tm(EGFPcre)}$ reporter mouse enables me to analyze *Lrp2* promoter activity in LRP2 deficient embryos, I could show that in the absence of LRP2 protein, the *Lrp2* promoter is not active at E9.5 (Figure 30 B). This finding indicates that LRP2 expression is needed for activation of *Lrp2* transcription in the developing forebrain. Several scenarios could be envisioned for this positive feedback loop. It has been suggested that LRP2 undergoes RIP and that subsequently its ICD is translocated to the nucleus where it regulates expression

of target genes, including *Lrp2* itself (Li et al., 2008). However, by mating *Lrp2*$^{tm(EGFPcre)}$ mice with *Lrp2*$^{tm(ICD)}$ mice expressing the soluble LRP2 ICD instead of full length LRP2 (Christ et al., 2010), I could show that the ICD alone is not sufficient to induce *Lrp2* transcription at E9.5 (Figure 30 C). For the interpretation of this result, one has to keep in mind that potentially the actual cleavage of full length LRP2 by RIP is important for the activity of the ICD. This cannot be modeled using the *Lrp2*$^{tm(ICD)}$ mouse, since this model expresses the soluble LRP2 ICD and RIP does not occur. Therefore, one cannot formally exclude that the LRP2 ICD generated by RIP is needed for regulation of *Lrp2* promoter activity.

Alternatively, full length LRP2 may influence its own expression by direct regulation of signaling pathways and thereby affecting gene transcription. Finally, there is also the possibility that the effect of LRP2 deficiency on *Lrp2* promoter activity is rather indirect and that due to a defect or delay in tissue specification in LRP2 deficient embryos, the neuroepithelium is simply not competent to initiate expression of certain genes, including the *Lrp2* gene itself.

Interestingly, also in Lrp2 deficient zebrafish, *lrp2* mRNA levels are drastically reduced (Figure 9). Since this observation does not necessarily have to be caused by decreased RNA stability due the point mutation, it can also be seen as another hint that the functional receptor is needed to induce its own transcription.

To gain additional insight which factors might regulate LRP2 expression, the *Lrp2* promoter was analyzed in silico in collaboration with Marie Gebhardt and Miguel Andrade (Computational Biology and Data Mining, MDC). By two complementary approaches (see methods section for details), transcription factor binding sites were identified in evolutionary conserved regions flanking the *Lrp2* transcription start site. The results of both approaches are presented in figure 41. Among the identified transcription factors are known regulators of LRP2 expression like the progesterone receptor and the RA receptor. Interestingly, there are also binding sites for transcription factors that were identified as differentially regulated in LRP2 deficient embryos in my microarray analysis, e.g. lim domain only protein 2 (LMO2), SOX9, NKX6.1, ALX4, zinc finger of the cerebellum 1 (ZIC1), FOXD1 and PITX2. This result may suggest the presence of regulatory feedback loops by which the organism tries to overcome the lack of LRP2 protein.

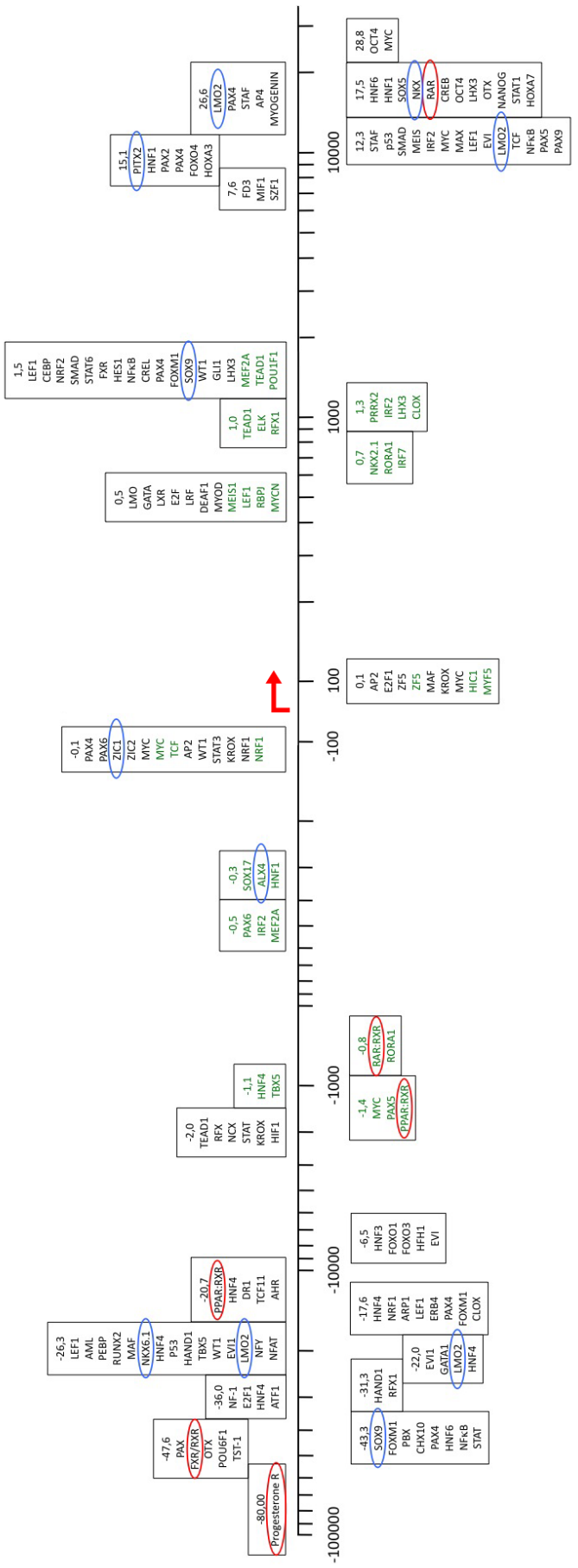

Figure 41. Transcription factor binding sites (TFBS) in the Lrp2 genomic region.
Orthologous conserved regions containing TFBS have been identified either using the ECR Browser (black) or ClustalW multiple sequence alignment (green). The red arrow indicates the transcription start site (TSS). Transcription factors encircled in red are known regulators of LRP2 expression. Transcription factors encircled in blue are differentially regulated in LRP2 deficient embryos. For better visualization, the genomic region upstream and downstream of the TSS is displayed on a logarithmic scale.

4.2.2 A role for LRP2 in controlling the morphology of ventral midline cells

My analysis of the morphology of ventral midline cells in the E9.5 neuroepithelium revealed apparent morphological defects in this cell type (Figure 31). In comparison to wild type cells, the LRP2 deficient cells look columnar and immature instead of wedge-shaped. Their apical constriction is defective leading to an impairment of MHP formation and subsequent bending of the ventral neuroepithelium. Ultimately, this results in the delayed neural tube closure observed in LRP2 deficient mice (Willnow et al., 1996). Obviously, the ventral midline cells belong to the structures very early affected by LRP2 deficiency. This observation is in agreement with expression of LRP2 being strongest in the ventral midline cells.

It is known that one prerequisite for apical constriction is the correct formation of apicobasal cell polarity (Sawyer et al., 2010). To investigate whether apicobasal polarity is disturbed upon loss of LRP2, I analysed the expression of cell polarity markers. No differences were detectable in control and LRP2 deficient embryos (Figure 31), demonstrating that initial formation of apicobasal polarity is not affected.

In the vertebrate neural tube, the cytoplasmic protein shroom3 functions as an apical determinant and regulates the architecture of actin filaments and microtubules within the cells undergoing apical constriction (Lee et al., 2007). Interestingly, there is evidence that LRP2 is induced by shroom3. One hypothesis is that the function of LRP2 during apical constriction is to reduce apical cell membrane via increased endocytosis rate (John Wallingford, personal communication). Another possibility how LRP2 may contribute to MHP formation is via the inhibition of BMP4 activity. Recently, it has been shown that blockade of BMP signaling is crucial for apical constriction and neural tube closure (Eom et al., 2011). In LRP2 deficient mice, SHH, which is a negative regulator of BMP4 expression, is excluded from the immediate ventral midline (Figure 38). Instead, ectopic ventral *Bmp4* mRNA expression can be detected as shown by ISH (Christ et al., in revision) and microarray analysis (this study, see appendix table 5). Together, these findings suggest that lack of SHH expression in the ventral midline of LRP2 deficient mice results in ectopic expression of BMP4, which in turn leads to impaired MHP formation and delayed or impaired neural tube closure.

4.2.3 A detailed account of the gene expression defects in the LRP2 deficient forebrain

Expression of all four key morphogens is altered in LRP2 deficient embryos at E9.5

As part of my thesis project, I performed gene expression profiling of ventral and dorsal midline cells from control and LRP2 deficient embryos. This was the first time that a defined forebrain cell population was analyzed for changes in gene expression caused by LRP2 deficiency. Inspection of the results obtained from my microarray analysis as well as validation of these results by ISH provided substantial extension of our knowledge on the defective specification of the major signaling centers in the developing forebrain.

Our lab has described earlier a dorsal shift of *Fgf8* mRNA expression and a dorsal increase of *Bmp4* mRNA expression in LRP2 deficient embryos at E9.5, as well as reduced *Shh* mRNA expression in the AEP at E10.5 (Spoelgen et al., 2005). More recent findings indicate that establishment of SHH expression in the ventral midline is impaired already at E9.5 (Figure 38 and Christ et al., in revision). In addition, I showed that not only *Fgf8*, but also *Fgf17* mRNA expression is shifted dorsally and that both genes are expressed in the immediate midline in LRP2 deficient embryos, while in control embryos expression is excluded from the midline (Figure 36). Furthermore, I found the expression domains of *Fgf18* mRNA in the ventral diencephalon to be extended anteriorly (Figure 40). We previously reported that *Wnt1* mRNA expression is unchanged in LRP2 deficient embryos (Spoelgen et al., 2005). I could confirm this finding, but my analysis of other additional WNT signaling molecules revealed that dorsal expression of *Wnt3a* mRNA is distinctly extended anteriorly in LRP2 deficient embryos compared to controls (Figure 37). Interestingly, also mRNA expression of *Tcf7l2*, a key transcription factor downstream of WNT signaling, is downregulated in the mutants. Thus, signaling by all four major morphogen pathways – SHH, BMP, FGF, WNT – is defective upon loss of LRP2. The resulting situation in the LRP2 deficient embryo is illustrated in figure 42.

All described changes in the patterning centers are in agreement with a model in which initial defects in the establishment of SHH expression in the ventral midline causes miss-patterning of the entire forebrain (Christ et al., in revision). A delicate balance exists between the patterning centers of the forebrain. SHH is needed for maintenance of FGF8 expression in the ANR. In turn, FGF8 activates SHH expression in the rostral ventral telencephalon via NKX2.1 (Ohkubo et al., 2002) (Storm et al., 2006). FGF8 also regulates WNT8b and BMP4 expression in the dorsal midline in a dose-dependent manner (Storm

et al., 2003). WNT signaling maintains FGF8 expression and thereby counteracts BMP4 signaling (Paek et al., 2011) (Wang et al., 2011). Finally, BMP activity restricts FGF8 and SHH expression to the ventral forebrain (Ohkubo et al., 2002) (Liu and Niswander, 2005). Thus, initial defects in SHH signaling can lead to a deregulation of the whole morphogen network. However, I cannot formally exclude that LRP2 also exerts a direct effect on the other signaling pathways. For instance, binding of LRP2 to BMP4 has been described (Spoelgen et al., 2005). To dissect these complicated hierachies, we will employ conditional *Lrp2* mutants which are deficient for LRP2 in a certain region of the forebrain or starting from a specific developmental time point.

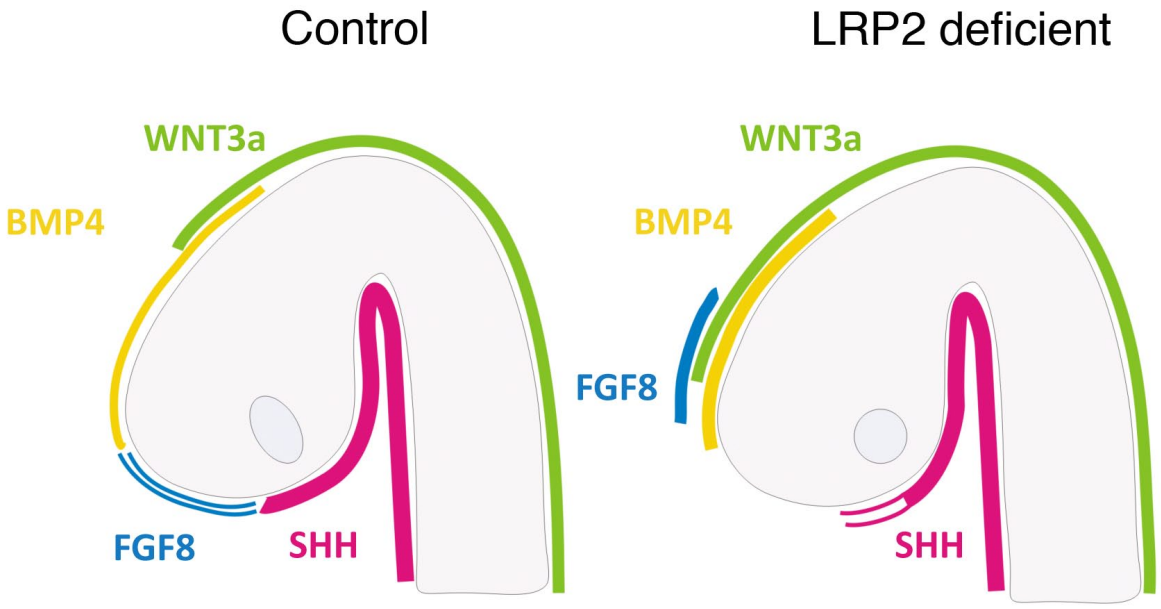

Figure 42. Deregulation of patterning centers in the forebrain of LRP2 deficient mice at embryonic day 9.5.
In mice deficient for LRP2, FGF8 (+FGF17) expression is shifted dorsally and is no longer excluded from the immediate midline. Dorsal BMP4 expression is increased and dorsal WNT3A expression is extended anteriorly. Ventral SHH expression fails to be established in the immediate midline.

Dorsalization and expansion of diencephalic identity lead to impaired induction of the telencephalon in LRP2 deficient embryos

The LRP2 deficient forebrain receives enhanced dorsal signals (BMP, WNT), while at the same time ventral/anterior signals (SHH, FGF) are missing or reduced (Figure 42). In combination, this leads to a dorsalization of the forebrain, meaning that dorsal identity is expanded and ventral identity is reduced. Additionally, my analysis of forebrain markers showed that mRNA expression of many diencephalic genes (*Nrg1, Foxd1, Foxa2, Fgf18*,

Pitx2, Lef1) extends anteriorly (Figure 40), while mRNA expression of telencephalic genes (*Sox21, Foxg1, Alx3, Alx4, Hes5, Delta1* and *Vax1*) is reduced (Figure 39). This can either be interpreted as a posteriorization of the forebrain or alternatively as a defect in forebrain maturation. At earlier stages (16 somite stage, E9.0), many diencephalic genes are expressed more anteriorly also in wild types, while at later stages (25 somite stage, E9.5), their expression domain is restricted to posterior regions. In LRP2 deficient embryos, the early expression pattern persists, suggesting that these embryos are detained in an immature state in some developmental aspects. A model of how these changes in forebrain gene expression (dorsalization and posteriorization) could lead to a decreased induction of telencephalic identity is depicted in figure 43.

A closer look at some of the differentially expressed genes that were identified in my microarray experiments may to some extend explain the emergence of the complex *Lrp2* mutant phenotype. Many of the genes that are downregulated in the telencephalon of LRP2 deficient mice (Figure 40) are known to elicit forebrain defects when mutated in mouse models. For instance, mice mutant for *Vax1* display dysgenesis of the optic nerve, coloboma, defects in the basal telencephalon and mild lobar HPE (Hallonet et al., 1999). Similarly, *Alx3* mutant mice show craniofacial midline defects and increased failure of neural

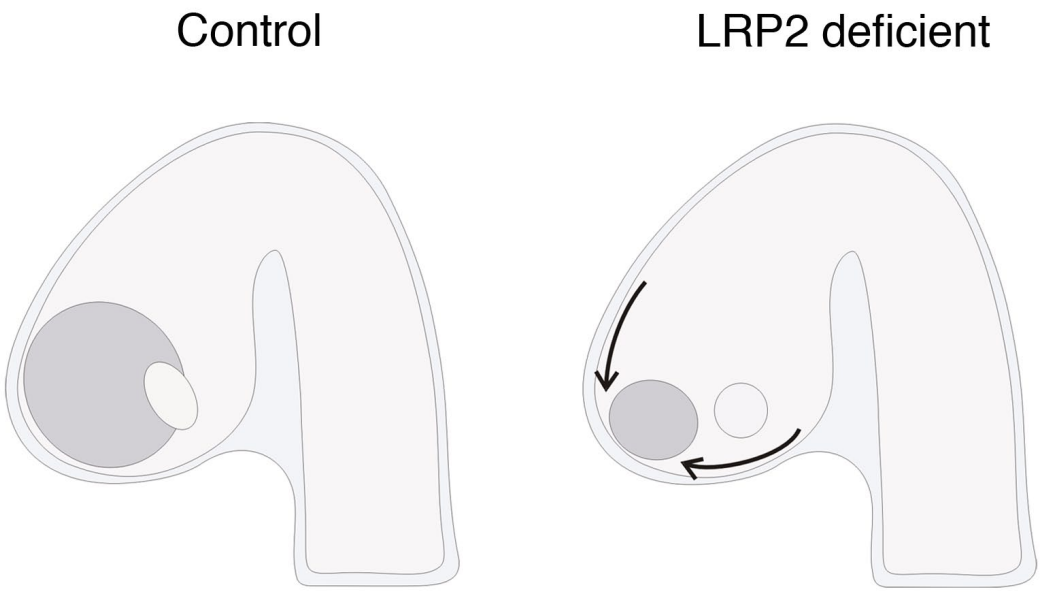

Figure 43. Defective induction of the telencephalon in LRP2 deficient mice.
In mice deficient for LRP2, the expression of dorsal morphogens is increased and the expression of diencephalic markers is extended anteriorly. Together, this leads to a limited specification of anterior telencephalic identity.

tube closure (Lakhwani et al., 2010). Thus, both mutants recapitulate aspects of the LRP2 deficient phenotype (Willnow et al., 1996). Another study showed that in *Tcf7l2*$^{-/-}$ mice, ventral diencephalon signaling is expanded, leading to increased induction of pituitary progenitors (Brinkmeier et al., 2007). This is in agreement with the finding that ventral diencephalic signaling is also expanded LRP2 deficient mice, which show reduced *Tcf7l2* mRNA expression. Furthermore, SOX21, which has been reported to promote neuronal differentiation by counteracting SOX1-3 (Sandberg et al., 2005), is downregulated in LRP2 deficient embryos. Interestingly, impaired neuronal differentiation has been described in LRP2 deficient embryos, leading to a complete absence of interneurons in the ventral forebrain (Spoelgen et al., 2005).

Taken together, my findings provide an explanatory model for the consequences of LRP2 deficiency in mouse forebrain development. Thus, they will help to guide further studies aiming at unraveling the molecular mechanism of this critical receptor pathway.

3. MATERIAL & METHODS

3.1 MATERIAL

3.1.1 Oligonucleotides

Mouse specific primer sequences

Primer	Sequence (5'-3')
BPA	GATTGGGAAGACAATAGCAGGCATGC
G20	GACCATTTGGCCAGCCAAGG
G21	CATATCTTGGAAATAAAGCGAC
PspOMI_EGFPcre_f	GGGCCCATGGTGAGCAAGGGCGAGG
EGFPcre_PstI_r	CTGCAGCTAATCGCCATCTTCCAGCAG
SondeSouthern_forw	GCTTGGTCCACAGAACCCAC
SondeSouthern_rev	CCACTATCCCATCGCAATCCC
neocheckLAr2	CTTAAGGTGCTTGTCTAGAGAC
MegWT_f2	GAAATCCGCCTGCCTCTGC
SV40_pA_for	CCGTAACCTGGATAGTGAAAC

Zebrafish specific primer sequences

Primer	Sequence (5'-3')
F_qPCR_lrp2A_1	GAACACACCAAATGCCAGTC
R_qPCR_lrp2A_1	GTGGGAGCATGTAGATGTGC
F_qPCR_lrp2B_3	CTGAGAATGACAGCAATAGCC
R_qPCR_lrp2B_3	CCTTCCTATTTTCTCCACTTCC
F_qPCR_bactin_1	TCCTTCCACCATGAAGATCA
R_qPCR_bactin_1	CTTGCTGATCCACATCTGCT
2bMo_test_for	AAGCTTTGTGCACGTCAGTGCATGAGTGGTGAGTTCCAGTGTAG-CAAAGTGGTGAGCAAGGGCGAGG
2bMo_test_rev	GGATCCTTACTTGTACAGCTCGTC

Morpholino sequences

Morpholino	Sequence (5'-3')
lrp2bATG_E	TGCTACACTGGAACTCACCACTCAT
lrp2bATG_K	CACCACTCATGCACTGACCTGCACA

qPCR probe sequences

5'-modification: FAM, 3'-modification: TAMRA

qPCR probe	Sequence (5'-3')
P_qPCR_lrp2A_1	TGCATCCCGCGCTCGTATCT
P_qPCR_lrp2B_3	CCCAAAGAGGAATCCAGCACGTCA
P_qPCR_bactin_1	CGGTGGCTCCATCTTGGCCT

3.1.2 ISH probes

Mouse specific ISH probes

ISH probe	Linearize with	Promotor	ISH probe	Linearize with	Promotor
Alx3	*Not*I	T3	*Hes5*	*Hind*III	T3
Alx4	*Kpn*I	T7	*Lef1*	*Bgl*II	T7
Delta1	*Sal*I	T3	*Pitx2*	*Xba*I	T7
Fgf8	*BamH*I	T7	*Shh*	*Hind*III	T3
Fgf10	*Pst*I	T7	*Sox21*	*BamH*I	SP6
Fgf17	*Nhe*I	T7	*Tcf7l2*	*Xho*I	T7
Fgf18	*Nco*I	SP6	*Vax1*	*Xba*I	SP6
Foxa2	*Xmn*I	T7	*Wnt1*	*Sal*I	T7
Foxd1	*EcoR*I	T7	*Wnt3a*	*EcoR*I	T3
Foxg1	*Sal*I	T7	*Wnt8b*	*BamH*I	T7
Nrg1	*BamH*I	T7			

The probes for *Nrg1*, *Sox21* and *Foxd1* were a gift from C. Birchmeier (MDC Berlin), the probe for *Fgf10* was a gift from A. Neubüser (Unversität Freiburg).

Zebrafish specific ISH probes

ISH probe	Linearize with	Promotor	ISH probe	Linearize with	Promotor
axial	*Dra*I	T3	*nkx2.1b*	*Apa*I	SP6
dab2	*Apa*I	SP6	*oep*	*Hind*III	T3
emx3	*BamH*I	T3	*pax6a*	*Xho*I	T3
fgf8	*Apa*I	SP6	*pax6b*	*EcoR*I	T7
foxa1	*Xho*I	T3	*shha*	*Hind*II	T7
lrp2	*Sal*I	T7	*shhb*	*Apa*I	SP6
netrin	*EcoR*I	T7	*wt1a*	*Apa*I	T7

The probes for *oep*, *pax6a*, *pax6b*, *emx3*, *foxa1*, *shha*, *netrin* and *axial* were a gift from U. Strähle (FZK Karlsruhe) and the probe for *wt1a* was a gift from N. Hasty (MRC Edinburgh).

3.1.3 Antibodies

Antigen	Raised in	Dilution	Provided by
LRP2 (rabbit)	rabbit	1:500	T. Willnow
LRP2 (rabbit)	sheep	1:10.000	R. Kosyraki
GFP	rabbit	1:500	abcam
Zn-5	mouse	1:500	S. Seyfried
BLBP	rabbit	1:500	Chemicon
Laminin	rabbit	1:500	Sigma
Prominin	rat	1:500	eBioscience
phospho-histone	rabbit	1:800	Millipore

3.1.4 Media

Medium	Composition
LB medium	bacto-tryptone 10 g/l, bacto-yeast extract 5 g/l, NaCl 10 g/l; pH 7.2
SOC medium	bacto-peptone 20 g/l, bacto-yeast extract 5 g/l, NaCl 0.5 g/l, KCl 0.17 g/l, MgCl2 0.95 g/l, glucose 3.6 g/l; pH 7.0
LB agar	LB-medium, agar 15 g/l
ES cell medium	DMEM 5.58 g, $NaHCO_3$ 1.0 g, ES-FCS 82.5 ml, penicillin/streptomycin 5.5 ml, L-glutamine 5.5 ml, non essential amino acids 5.5 ml, 2-mercaptoethanol 3.8 µl, murine LIF 55 µl
ES cell freezing medium	ES cell medium 60 ml, ES-FCS 20 ml, ES-FCS 82.5 ml, 20% DMSO 20 ml

3.1.5 Buffers and solutions

Buffer/Solution	
DNA-loading buffer (10x)	bromphenol blue 0.25% (w/v), xylencyanol 0.25% (w/v), glycerol 30% (w/v)
Eosin staining solution	eosin 0.1% (w/v), ethanol 90%
Hämatoxylin staining solution	aluminium potassium sulfate 5% (w/v), hematoxylin 0.1% (w/v), sodium iodate 0.02% (w/v), glacial acetic acid 2% (v/v)
Hot Shot base buffer	NaOH 1.25 M, EDTA 1mM
Hot Shot neutralization buffer	TrisHCl 2M; pH 5

Low TE buffer	Tris-HCl 10 mM, EDTA 1 mM; pH 8.0
Lysis buffer (Mini Prep)	NaOH 200 mM, SDS 1%
Neutralization buffer (Mini Prep)	potassium acetate 3.0 M; pH 5.5
NTMT	NaCl 100mM, TrisHCl pH 9,5 100mM, $MgCl_2$ 50mM, Tween-20 0,1%
Orange G staining solution	Orange G 0.5% in ethanol 10%
PBS	NaCl 1.5 M, Na_2HPO_4 80 mM, NaH_2PO_4 20 mM
PBST	PBS, 0.1% Tween-20
PBDT	PBS, 1% DMSO, 0,1% Tween-20
PFA 4%	paraformaldehyde 4% (w/v) in PBS
Prehybridization buffer	formamide 50%, SSC pH4.5 5x, heparin 50 µg/ml, tRNA 100 µg/ml, Triton X-100 0.1%
Resuspension buffer (Mini Prep)	Tris-HCl 50 mM, EDTA 10 mM, RNase A 100 µg/ml; pH 8.0
SSC 20x	NaCl 3M, Na_3Citrat 0,3M, pH 4.5 or 7,0
SSCT 2x	2x SSC pH 7,0, 0,1% Tween-20
SSCT 0,2x	0,2x SSC pH 7,0, 0,1% Tween-20
SSC washing solution I (ISH)	formamide 50%, SSC pH4.5 4x, SDS 1%
SSC washing solution II (ISH)	formamide 50%, SSC pH4.5 2x
SSC washing buffer I (Southern Blot)	2x SSC, 0.1% SDS
SSC washing buffer II (Southern Blot)	0.1 x SSC, 0.5% SDS
TAE buffer	TrisHCl 40 mM, EDTA 1 mM, glacial acetic acid 20 mM; pH 8.0
TBS	Tris-HCl 50 mM, NaCl 150 mM; pH 7.4
TBST	TBS, 0,1% Tween2
Tail buffer	Tris-HCl 10 mM, Na-Acetate 0.3 M, EDTA 0.1 mM, SDS 1%; pH 7.0

3.1.6 Kits

Prime-It II Random Primer Labelling Kit (Stratagene)
BigDye Terminator v3.1 Cycle Sequencing Kit (Applied Biosystems)
Bioanalyzer RNA 6000 Pico/Nano Assay (Agilent)
pGEM-T Easy Vector (Promega)
DNA isolation Kit (Qiagen)
High Pure PCR Product Purification Kit (Roche)
RNeasy Mini Kit (Qiagen)
RNeasy Micro Kit (Qiagen)
RNeasy FFPE Kit (Qiagen)

First-Strand cDNA Synthesis SuperScript II RT Kit (Invitrogen)
qPCR Mastermix (Eurogentec)
Neural Tissue Dissociation Kit (Miltenyi Biotec)
Ovation PicoSL WTA System (Nugen)
Encore Biotin IL Module (Nugen)
Illumina TotalPrep RNA Amplification Kit (Ambion)

3.1.7 Technical equipment

FLA 3000-2R Radioluminographie Scanner (Fuji)
MPPI-2 microinjector (Applied Scientific Instrumentation)
Stereomicroscope MZ16F (Leica)
377 DNA Sequencer (ABI PRISM)
NanoDrop ND-1000 spectrophotometer (Thermo Fisher Scientific)
7000 Sequence Detection System (ABI PRISM)
Rotary microtome HM355S (Microm)
Cryostat HM 560M (Microm)
2100 Bioanalyzer (Agilent)
LSR 2 flow cytometer (BD Biosciences)
VT 1200S vibratome (Leica)
SPE Laser Scanning Microscope (Leica)

3.1.8 Chemicals

Chemicals were purchased from Sigma or Roth if not stated otherwise.

3.2 ANIMAL EXPERIMENTS

3.2.1 Mouse husbandry

Mice were kept at standard conditions according to the German animal protection act. The generation of $Lrp2^{tm(EGFPcre)}$ mice is described in a separate methods section (3.6) and in the result part (4.2.1) of this study. The mouse line was backcrossed on a pure C57BL/6 background. The generation of $Lrp2^{-/-}$ mice has been described before (Willnow et al.,

1996).

Matings between heterozygous $Lrp2^{+/-}$ animals and heterozygous $Lrp2^{EGFPcre/+}$ animals (both lines on C57BL/6 background) resulted in embryos of the following genotypes: 25% $Lrp2^{EGFPcre/-}$ (receptor-deficient), 25% $Lrp2^{EGFPcre/+}$, 25% $Lrp2^{+/+}$ and 25% $Lrp2^{+/-}$. All analyzed embryos were compared to somite-matched control littermates. Polymerase chain reaction (PCR) was used to genotype the $Lrp2^{+/-}$ animals, the $Lrp2^{EGFPcre/+}$ animals and the embryos obtained from matings of those lines (see 3.3.2).

Timed matings were set up in the evening to obtain embryos at defined stages of development. The presence of a vaginal plug in the morning was considered as day E0.5 (embryonic day 0.5). Embryos were harvested by sacrificing pregnant mice according to the German animal protection act, staged by counting the somites and further processed.

3.2.2 Zebrafish husbandry

Zebrafish were maintained and raised at 28.5°C under standard conditions according to the German animal protection act. Embryos were kept in egg water (60 µg/ml Instant Ocean Sea Salts, Aquarium Systems Inc, USA) with or without 0,003% PTU (1-Phenyl-2-thiourea, Sigma, USA) to suppress pigmentation and were staged by hours post fertilization (hpf) at 28.5°C or by counting somites (Kimmel et al., 1995)

Zebrafish lines bugeye ($lrp2^{mw1}$) and 5cben ($lrp2^{p5bnc}$) with non-sense mutations in lrp2 were described before (Veth et al., 2011). Mutants were compared to wild type controls matched for genetic background and age.

3.2.3 Morpholino injections

Morpholino antisense oligonucleotides were purchased from GENE TOOLS (USA). Sequences were chosen to target the ATG region of *lrp2b* (see material section 3.1.1 for sequences). All morpholinos were injected at a final concentration of 100 µM in ddH_2O using a MPPI-2 microinjector (Applied Scientific Instrumentation). The effects of the morpholinos were verified by co-injection of a test RNA consisting of the *mCherry* coding sequence fused to the *lrp2b* ATG region (-15 to +25).

3.2.4 Dye filtration and uptake experiments

Lysine-fixable fluorescein dextran (70 kDa; Molecular Probes) was prepared in PBS (1 mg/ml). Using a MPPI-2 microinjector (Applied Scientific Instrumentation) the tracer was injected into the common cardinal vein of embryos anaesthetized with 0.2 mg/ml tricaine in egg water. Uptake of tracer dye by duct cells was evaluated 1 hr after injection on whole mount preparations using a fluorescent dissecting stereomicroscope.

3.3 MOLECULAR BIOLOGY METHODS

3.3.1 Cloning

Enzymatic digest of DNA

The appropriate amount of DNA was incubated with the corresponding restriction enzyme(s) and buffer at a ratio of 0.5 U enzyme/µg DNA (37°C; 2 hrs to overnight). All restriction enzymes were obtained from New England Biolabs, USA.

Amplification of DNA fragments by PCR

For cloning, PCR was carried out using the Phusion polymerase and 5x buffer (Finnzymes). The reaction was set up according to manufacturer's instructions. The following cycling conditions were used: intial denaturation (3 min, 98°C), denaturation (30 sec, 98°C), annealing (30 sec, 65-69°C), elongation (1 min/kb, 72°C), 30-35 cycles, final elongation (7 min, 72°C).

Agarose gel electrophoresis of DNA and RNA

DNA and RNA fragments were separated according to their molecular weight on 0.8-2.0% agarose gels in TAE buffer. Ethidium bromide was added to the gel at a final concentration of 0.5 µg/ml to enable visualization of the DNA or RNA fragments.

Isolation of DNA from agarose gels

PCR products or DNA digests were separated by length on 0.8-1.2% agarose gels containing ethidium bromide. By exposing the agarose gel to UV-light, the DNA was visualized and bands of interest were cut from the gel. The DNA was extracted using the High Pure PCR Product Purification Kit (Roche) according to manufacturer's instructions.

Determination DNA and RNA concentration

DNA and RNA samples were measured using the NanoDrop ND-1000 spectrophotometer. For gene expression profiling, RNA concentration and integrity were determined using the Bioanalyzer RNA 6000 Pico or Nano Assay (Agilent) according to manufacturer's instructions.

Ligation of DNA fragments

Ligation of PCR products into the pGEM-T Easy Vector (Promega) was done according to manufacturer's instructions.

For ligation of DNA fragments into other target vectors, insert and vector DNA were cut with the appropriate restriction enzymes and subsequently purified. For a 10 µl ligation reaction, 50 ng of vector DNA was mixed with the appropriate amount of insert DNA according to the equation:

$mass_{insert}(ng) = 5 \times mass_{vector}(ng) \times length_{insert}(bp)/length_{vector}(bp)$

After addition of ligation buffer (2 µl, Fermentas), T4 DNA ligase (1 U, Fermentas) and water the mixture was incubated at 16°C overnight. 2 µl of the ligation reaction were used to transform electro-competent E. coli (XL1Blue or DH5α).

Transformation of bacteria with DNA

Electro-competent E. coli XL1Blue or DH5a cells were transformed with purified plasmid DNA or directly with DNA-ligation reactions. An aliquot of electro-competent XL1Blue or DH5a cells was thawed on ice. 10 ng of plasmid DNA (or 2 µl of the ligation reaction) were mixed with 40 µl of electro-competent XL1Blue or DH5a cell suspension and electroporated at 1.8 kV.

The cell suspension was transferred from the cuvette to a 2.0 ml tube, mixed with 1 ml of SOC medium and incubated at 37°C for 30 min. Cells were collected (2500x g; 5 min; RT), re-suspended in 100 µl of LB medium and plated on an LB agar plate containing the appropriate selective agent.

Cryopreservation of bacteria

1 ml of an overnight culture of E. coli XL1Blue or DH5a was mixed with 1 ml of 100% glycerol and immediately frozen at -80°C.

Isolation of plasmid DNA from bacteria

For screening of bacteria colonies, 5 ml of LB medium were inoculated with a single colony of E. coli XL1Blue or DH5a picked from an LB agar plate containing the appropriate selective agent. The LB culture was grown overnight at 37°C with vigorous shaking. The next day the cells were harvested by centrifugation (14000x g; 5 min; RT). The pellet was resuspended in resuspension buffer and subsequently lysed by adding an equal volume of lysis buffer. The solution was mixed cautiously with an equal volume of neutralization buffer and incubated on ice for 15 min. Cellular debris and genomic DNA were removed by centrifugation of the solution (14000x g; 20 min; 4°C). The supernatant containing the plasmid DNA was transferred to a new reaction tube and the DNA was collected by adding LiCl (3 M, 0.1x volume) and 100% isopropanol (2.5x volume) followed by centrifugation (14000x g, 30 min, 4°C). The pellet was washed with 70% ethanol and resuspended in sterile water. The purified plasmid DNA was stored at -20°C.

For Isolation of larger amounts of plasmid DNA, the DNA isolation Kit (Qiagen) was used according to manufacturer's instructions.

Sequencing of DNA

DNA sequencing was performed using the BigDye Terminator v3.1 Cycle Sequencing Kit (Applied Biosystems), according to manufacturer's instructions. Amplification was performed as follows: initial denaturation (96°C, 1 min), denaturation (96°C, 10 sec), annealing (55°C, 5 sec), elongation (60°C, 4 min), 30 cycles. After amplification, the DNA was purified with Sephadex G-50 (Amersham), sequenced with an ABI PRISM 377 DNA Sequencer and analyzed with Lasergene DNA Star SeqMan Version 7.0.0.

3.3.2 Genotyping

Isolation of genomic DNA for Southern Blot

For genotyping of adult mice, tissue was obtained by subjecting mice to a tail biopsy. For genotyping of ES cell clones, ES cells were grown and harvested in gelatine coated 96 well plates. In order to isolate genomic DNA, the tissue/cells were incubated with proteinase K (0.5 mg/ml) in tail buffer (52°C; overnight). Proteins were removed by extracting with an equal volume of phenol/chloroform/isoamylalcohol (25:24:1) followed by centrifugation (14000x g; 5 min; RT) to separate the phases. The DNA containing phase was mixed with 100% ethanol (2.5 volumes). The precipitate was collected by centrifugation (14000x g,

10 min, 4°C) washed with 70% ethanol and redissolved in low TE buffer. Isolated genomic DNA was stored at 4°C.

Isolation of genomic DNA for PCR (Hot Shot)

For genotyping of adult mice, tissue was obtained by subjecting mice to an ear punch biopsy. For genotyping of mouse embryos, embryonic tail tissue was used. The tissue was incubated in Base buffer (75 µl; 95°C; 30 min). After cooling to RT, Neutralization buffer (75 µl) was added. Isolated genomic DNA was stored at 4°C.

Genotyping by PCR

For genotyping, PCR was carried out using the Taq polymerase and 10x buffer (New England Biolabs). The following cycling conditions were used: intial denaturation (3 min, 94°C), denaturation (15 sec, 94°C), annealing (15 sec, 54-56°C), elongation (15 sec, 72°C), 38 cycles.

PCR was used to genotype the $Lrp2^{+/-}$ animals, the $Lrp2^{EGFPcre/+}$ animals and the embryos obtained from timed matings of those lines. The primer pairs BPA/G21 and SV40_pA_for/neocheckLAr2 amplify fragments that are specific for the knockout allele and the knock-in allele, respectively. The primer pairs G20/G21 and MegWT_f2/neocheckLAr2 amplify fragments that are specific for the wildtype allele (for primer sequences see 3.1.1).

Genotyping by Southern Blot

Genomic DNA was digested with 20 U of restriction enzyme HindIII or BglII overnight at 37°C. DNA was loaded on a 1% agarose gel and resolved at 80 V for approximately 6 hrs in TAE buffer. Following, the gel was transferred to NaOH (0.4 M, 30 min, RT) to denature the double stranded DNA. The transfer of the DNA to a nylon membrane was performed in 0.4 M NaOH overnight using capillary action. To this end the following stack was assembled: 2 sheets of Whatman paper reaching a reservoir with 0.4 M NaOH, agarose gel containing the DNA fragments, nylon membrane, 2 sheets of Whatman paper and a pack of paper cloths. After the transfer the membrane was baked at 80°C for 10 min and the DNA was permanently attached to the membrane by exposure to ultraviolet radiation (0.010 Joule, Crosslinker, Bio-Link). The membrane was pre-hybridized in rapid-hyb buffer (GE Healthcare, UK) (1 hr, 65°C). The DNA probe was labelled using the Prime-It II Random Primer Labelling Kit (Stratagene) according to manufacturer's instructions and subsequently added to the membrane. Hybridization was performed overnight. The next day the mem-

brane was washed (4 x 5 min SSC washing buffer I, 2 x 5 min SSC washing buffer II, 65°C). To visualize the DNA fragments the membrane was exposed to an imaging plate (Fuji) for 12 hrs and analyzed using the FLA 3000-2R Radioluminographie Scanner (Fuji).

Isolation of total RNA from tissue samples

For isolation of total RNA from frozen samples, the RNeasy Mini or RNeasy Micro Kits (Qiagen) were used according to manufacturer's instructions.
For isolation of RNA from LCM tissue, the RNeasy FFPE Kit (Qiagen) was used according to manufacturer's instructions with a prolonged proteinase K digestion step (12-16 hrs, 55°C).

First strand cDNA synthesis

Generation of cDNA from RNA was done using the First-Strand cDNA Synthesis Super-Script II RT Kit with random hexamer primers (Invitrogen) according to manufacturer's instructions.

Quantitative RT PCR (qPCR)

qPCR was performed using the qPCR Mastermix (Eurogentec) according to manufacturer's instructions and a 7000 Sequence Detection System (ABI PRISM).
The following cycling program was used:
Primer/probe sets used for qPCR are listed in the material section (3.1). All PCR products were sequenced to confirm primer specificity. Expression levels of lrp2 and lrp2b were normalized to beta actin expression levels.

3.3.6 Flow cytometry

For flow cytometry, embryonic heads were prepared in PBS. Cells were isolated using the Neural Tissue Dissociation Kit (Miltenyi Biotec) according to manufacturer's instructions. Isolated cells were stained with an A488-conjugated α-GFP antibody (Invitrogen) using the Foxp3 staining buffer set (eBioscience) according to manufacturer's instructions. Flow cytometric experiments were carried out in the MDC flow cytometry core facility headed by Dr. H.-P. Rahn using an LSR 2 flow cytometer (BD). Excitation of potential GFP containing cells was carried out using a 488nm argon laser line. Analyzed cells were gated by a dotplot FSC (forward scatter) vs. SSC (side scatter).

3.3.7 Laser capture microdissection

For LCM, mouse embryos were prepared in PBS (4°C), shortly fixed in PFA (2%, 25 min, RT), washed (PBS, 2 x 5 min, 4°C), and embedded in Tissue-Tek OCT (Sakura) on dry ice. Subsequently, cryosctions were produced using a HM 560M cryostat (Microm) (knife: -35°C, specimen: -18 to-13 °C, 12 µm) and collected on Membrane Slides (Molecular Machines). Slides were washed (DEPC-H_2O, 3 x 1-2 min), dehydrated (EtOH 70%, 2.5 min, EtOH 100%, 10 sec) and dried on drying agent in a speed vac (1 hr, RT). LCM was performed on a Axio Observer Z1 (Zeiss) equipped with a PALM MicroBeam (Zeiss) using the PALM Robo Software.

3.3.8 Gene expression profiling

Preparation of labeled cDNA/cRNA

RNA was prepared as described in 3.3.5. Labeled cDNA was generated from RNA samples obtained by LCM using the Ovation PicoSL WTA System (Nugen) and the Encore Biotin IL Module (Nugen) according to manufacturer's instructions. Labeled cRNA was generated from RNA samples obtained by manual dissection using the Illumina TotalPrep RNA Amplification Kit (Ambion) according to manufacturer's instructions.

Microarray

Gene expression profiling of E9.5 forebrain midline tissue (3-5 samples per genotype and RNA preparation method) was performed by G. Born (Hübner Lab, MDC) using the MouseWG-6 v2.0 Expression BeadChip (Illumina) according to the manufacturer's protocols.

Statistics

Statistical evaluation was performed by Dr. H. Schulz (Hübner Lab, MDC). Array data have been quantile normalized on probe level without background correction using the Illumina BeadStudio 1.0.2.20706 Platform. Data have been log(2) transformed after an offset addition (8). After the removal of consistently low expressed transcripts (minimum detection p-value > 0.05) the differential expression has been ascertained using two way (dorsal vs. ventral; $Lrp2^{+/+}$ and $Lrp2^{EGFPcre/+}$ vs. $Lrp2^{EGFPcre/-}$), respectively three way ANOVA statistic (LCM vs. manual dissection; dorsal vs. ventral; $Lrp2^{+/+}$ and $Lrp2^{EGFPcre/+}$ vs.

Lrp2$^{EGFPcre/-}$) followed by a FDR (Benjamini and Hochberg, 1995) multiple testing correction. Only probes showing a significant genotype effect have been selected for further investigations. The resulting set of probes which undergo 5% FDR have been average linkage clustered using a Euclidean dissimilarity matrix on rows and columns after normalization of probes to a mean of zero and a standard deviation of one.

3.4 Histology and Stainings

3.4.1 Tissue sections

Paraffin sections

For paraffin sections embryos were fixed in 4% PFA (4°C, overnight), washed (PBS, 3 x 5 min), dehydrated through a series of graded methanol solutions (25%, 50%, 75%, and 100%, 5 min each) and stored at -20°C. The samples were transferred to 100% ethanol for 30 min at room temperature. Following, the samples were incubated in Roti-Histol (Roth) (2 x 2 hrs), and infiltrated with paraffin (67°C, 2 x 2 hrs, 1 x overnight). The next day, the samples were embedded in paraffin and stored at RT until use. Sectioning was done at 10 µm on a rotary microtome (Leica RM 2155, Leica). Slides were stored at RT until further processing.

Plastic sections

For plastic sections, specimens were embedded in Technovit 7100 (Heraeus Kulzer) according to manufacturer's instructions. Samples were cut at 10 µm on a HM355S rotary microtome (Microm).

Cryosections

For cryosections, embryos were fixed in 4% PFA (4°C, overnight), washed (PBS, 3 x 5 min), and incubated in 30% sucrose/PBS overnight. The embryos were embedded in Tissue-Tek OCT (Sakura) on dry ice. Samples were cut at 10 µm on a HM 560M cryostat (Microm).

Vibratome sections

For vibratome sections, stained mouse embryos were embedded in low melt agarose (10% in PBS) and cut at 50 µm on a VT 1200S vibratome (Leica).

3.4.2 Histological stainings

Orange G staining

Plastic sections were counterstained using orange G (Sigma-Aldrich), staining the cytoplasm of tissues. The sections were incubated for 30 sec in orange G staining solution, rinsed with tap water for 2 min, dried and mounted with Histo-kitt (Roth).

H&E staining

For H&E staining, paraffin sections were incubated at 60°C for 10 min. Subsequently, they were incubated in Roti-Histol (3 x 2 min), ethanol (3 x 100%, 80%, 70%, 50%, 30%, 2 min each) and H_2O (2 min). Sections were stained in Hematoxylin solution (90 sec), washed with tap water (5 min), stained in Eosin solution (45 sec), washed with H_2O (10 sec) and 70% ethanol (10 sec). Subsequently, sections were dehydrated in ethanol (90%, 100%, 2 min each), dried and mounted with Histo-kitt (Roth).

3.4.3 Immunohistochemistry

Fluorescent immunohistochemistry on cryosections

The slides were removed from the -80°C freezer and allowed to equilibrate at RT for 10 min. After equilibration, the slides were washed (TBS, 5 min) and blocked for 1 hr at RT with (TBS containing 10% donkey serum and 1% BSA, 1 hr, RT). After blocking the slides were incubated with the primary antibody (in TBS containing 1% BSA, 4°C, overnight). The next day, the slides were washed (TBS, TBST, TBS, 5 min each, RT). Sections were incubated with Alexa488- and Alexa555-conjugated secondary antibodies raised in donkey (1:500 in TBS containing 1% BSA, 2 hrs, RT). The slides were washed (TBS, TBST, TBS, 5 min each, RT) and then incubated for 10 min with DAPI staining solution. Afterwards the sections were washed (TBS, 5 min) and mounted with Fluorescent Mounting Medium (Dako).

DAB immunohistochemistry on paraffin sections

Paraffin sections were incubated at 60°C for 10 min. Subsequently, they were incubated in Roti-Histol (3 x 3 min), ethanol (99%, 95%, 80%, 70%, 50%, 1 min each), H_2O (1 min) and PBS containing 3% H_2O_2 and 10% MeOH (3 min). Sections were washed (PBS, 2 x 10 min), blocked (PBS containing 10% NGS, 10% NDS, 0,1% Triton, 0,05% Tween-20, 2hrs)

and incubated with the first antibody (in blocking solution, 4°C, o/n). The next day, sections were washed (PBS, 3 x 10 min) incubated with the secondary antibody (in blocking solution, RT, 2 hrs) and washed again PBS, 3 x 10 min). Subsequently, sections were incubated in peroxidase anti-peroxidase (PAP) solution (1:200 in blocking solution, RT, 2 hrs), washed (0,1 M TrisHCl pH7,5, 3x 10 min) and stained with DAB staining solution. The staining reaction was stopped by washing the sections in H_2O. Sectiones were dehydrated in ethanol (50%, 70%, 80%, 95%, 99%, 1 min each), dried and mounted with Histo-kitt (Roth).

Immunohistochemistry on whole-mount zebrafish embryos

Embryos were fixed (4% PFA, 1h, RT), washed (PBS, 2 x 5 min, RT), incubated in H_2O (5 min, RT), Aceton (20 min, -20°C) and again H_2O (5 min, RT). Subsequently they were blocked (5% NGS in PBDT, 1hr, RT) and incubated with the first antibody (1:500 in PBDT, 4°C, o/n). The next day, embryos were washed (PBDT, 8 x 1 hr) and incubated with the secondary antibody (1:200 in PBDT, 4°C, o/n). The next day, embryos were washed (PBDT, 6 x 10 min) and embedded in slow fade fluorescent mounting medium (Invitrogen).

3.4.4 In situ hybridization

Generation of digoxigenin-labelled RNA probes

Digoxigenin (DIG)-labelled probes for in situ hybridization were generated using the DIG labeling Kit (Roche) according to manufacturer's instructions. The RNA was purified using the RNeasy Mini Kit (Qiagen).

Whole-mount ISH on mouse embryos

Mouse embryos were dissected in PBS and fixed overnight in 4% paraformaldehyde (PFA) in PBS. After washing (PBST, 3 x 5 min) the embryos were dehydrated through a series of graded methanol solutions (25%, 50%, 75% 100%, 5 min each) and stored at -20°C until use. For ISH, embryos were punctured (eyes, hindbrain, heart) to facilitate penetration of solutions, rehydrated through a series of graded methanol solutions (reverse of above) and washed (PBST, 2 x 5 min). Specimen were bleached in PBST containing 6% H_2O_2 (4°C, 1hr). After washing (PBST, 2 x 5 min), the embryos were permeabilized (10 µg/ml proteinase K in PBST, RT, 10 min). The proteinase K digest was stopped by washing (PBST, 1 min). Next, the embryos were re-fixed with 4% PFA (RT, 20 min) then washed (PBST, 2 x

5 min). The embryos were then incubated with pre-hybridization solution (65°C, 3hrs). After pre-hybridization the embryos were incubated with the DIG-labelled RNA probe in fresh pre-hybridization buffer (1 µg/ml, 65°C, overnight). The next day, the embryos were washed extensively in SSC washing solution I (65°C, 2 x 30 min), SSC washing solution II (65°C, 2 x 30 min), and PBST (RT, 3 x 10 min). After washing, the embryos were blocked (PBST with 10% sheep serum and 1% BSA, RT, 3 hrs) and were finally incubated with an anti-digoxigenin-alkaline-phosphatase conjugate (anti-DIG-AP, Fab fragments, Roche) at a dilution of 1:5000 overnight. Un-specifically bound antibody was removed the next day by washing (PBST, RT, 3 x 5 min, 10 x 20 min). Next, embryos were washed in NTMT buffer (RT, 2 x 5 min) before they were incubated with NTMT containing 1.88 mg/ml nitro blue tetrazolium chloride (NBT) and 0.94 mg/ml 5-Bromo-4-chloro-3-indolyl phosphate (BCIP) for 30 min to 5 hrs. The staining reaction was stopped by washing (NTMT, 3 x 5 min). The embryos were incubated in low pH PBST (pH5.3, RT, 4 hrs), then re-fixed (4% PFA, RT, 20 min). To decrease background the stained embryos were dehydrated and rehydrated through a series of graded methanol solutions (25%, 50%, 75% and 100%, 5 min each) and cleared by incubation in glycerol (25%, 50% and 80% in PBS, RT, 5 min each). The embryos were stored at 4°C in the dark.

Whole-mount ISH on zebrafish embryos

Whole-mount in situ hybridization on zebrafish embryos was carried out as described above for mouse embryos with the following modifications: Embryos were neither punctured nor bleached. Proteinase K digestion was 10 min for 20 hpf embryos, 18 min for 30hpf embryos, 30 min for 48 hpf embryos and 40 min for 72 hpf embryos. After hybridization, embryos were washed with the following solutions: 50% formamide in SSCT (3x 20 min, 65°C), 2x SSCT (1x 15 min, 65°C), 0,2x SSCT (3x 20 min, 65°C). For blocking, PBST containing 2% sheep serum and 0,2% BSA was used.

3.5 MICROSCOPY

3.5.1 Confocal microscopy

Confocal microscopy was performed in the MDC imaging core faclility headed by Dr. A. Sporbert using a SPE Laser Scanning Microscope (Leica) was used. For all scans, a pinhole of one airy unit was chosen.

3.5.2 Electron microscopy

Electron microscopy analysis was performed by Fr. Schrade (Bachmann Lab, Charite Berlin). Zebrafish embryos were fixed (glutaraldehyde 2.5% in Sorensen's phosphate buffer, 12 hrs), postfixed (osmium tetroxide 2%), dehydrated in ethanol, and embedded in Epon 812. Ultrathin sections were contrasted with uranyl acetate and lead citrate. Sections were viewed on a Zeiss EM.

3.6 GENERATION OF KNOCK-IN MOUSE MUTANTS

3.6.1 Knock-in vector construction

The sequences homologous to the endogenous Lrp2 gene locus (long arm and short arm), were amplified from bacterial artificial chromosome (BAC) DNA by A. Christ. The EGFPcre coding sequence was amplified from a plasmid obtained from Addgene (plasmid 11921: pBS592 promoterless EGFPcre). The EGFP moiety of this fusion gene carries the S65T mutation for enhanced fluorescence and is codon-optimised for higher level expression.
The vector pBSSK neoA (provided by Dr. M. Gotthard) was slightly modified by replacing its neomycin resitance cassette, which contained a single LoxP site (FRT-neo-LoxP-FRT) with another neomycin resistance cassette (FRT-neo-FRT). The resulting vector was named pBSSK neoA3.
The different fragments of the knock-in vector (long arm and short arm, EGFPcre mini gene, DTA cassette) were cloned into pBSSK neoA3, which was used for targeting of embryonic stem cells (Figure 44).

3.6.2 ES cell culture

Cultivation of ES cells

ES cells were grown in petri dishes coated with 0.1% gelatine in PBS and inactivated feeder cells (neomycin resistant mouse fibroblasts, inactivated with mitomycin at 5% CO_2 and 37°C). To split the cells, they were washed once in PBS and then treated with 0.25% trypsin/EDTA (Invitrogen, UK) for 5 min at 37°C. The reaction was stopped by adding the double amount of ES cell medium. The cells were separated by pipetting up and down and were split until the desired cell density was reached.

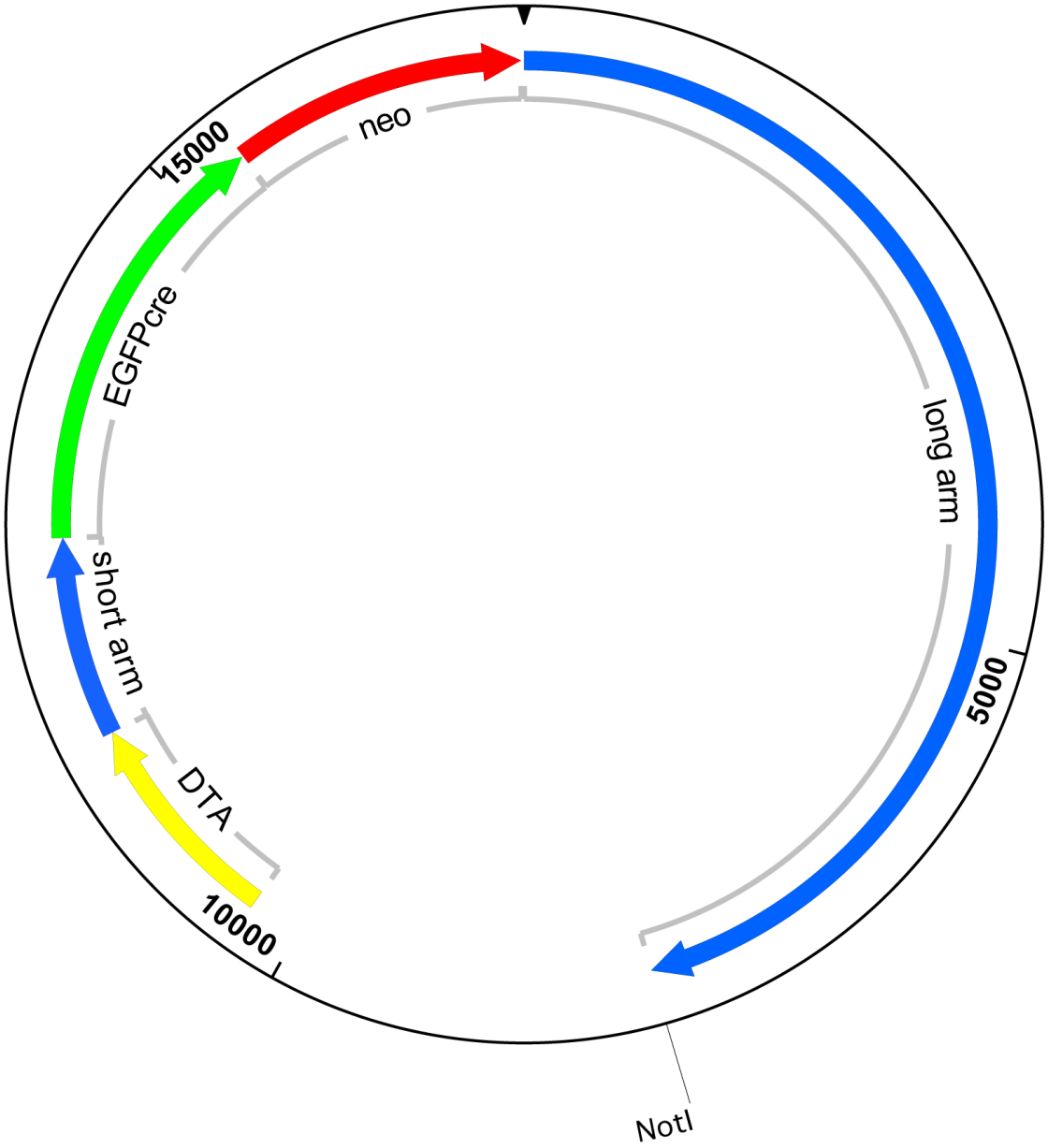

Figure 44. Construction of the knock-in targeting vector.
The arrows indicate the different fragments inserted into the pBSSK neoA vector. Diphtheria toxin A (DTA, yellow arrow) was inserted to ensure homologous recombination in the embryonic stem cells. Non-homologous recombination results in the production of the toxin and in the death of the cell producing it. The green arrow indicates the mini gene consisting of an intron of the rabbit ß-globin gene followed by the EGFPcre coding sequence and a translation stop codon. The neomycin resistance cassette (neo, red arow) serves as a marker to select for murine embryonic stem cells carrying the mini gene. The sequences homologous to the endogenous Lrp2 gene locus (short and long arm) are indicated in blue.

Electroporation of ES cells

800 µl (1 half of a 10 cm petri dish) ICp4 ES cells (inner cell mass, passage 4) derived from mice from AB2.1 ES cells were electroporated with 50 µg linearized knock-in construct vector DNA. The cells were electroporated with a pulse of 250 V and 5 µF. After electroporation the cells were seeded on a 10 cm petri dish coated with gelatine and feeder cells.

Isolation of ES cell clones

To select for positive ES cell clones 0.18 mg/ml geneticin (G418 = neomycin, Gibco) was added to the ES cell culture medium 2 days after electroporation. After 6-8 days cell clones were picked, transferred into a 96 well plate and incubated with trypsin/EDTA (Invitrogen) (30 µl, 37°C, 3 min). To stop the reaction, ES cell medium (70 µl) was added into each well. By pipetting up and down cell clones were separated. 100 µl of the ES cell clones were transferred into a 96 well plate coated with gelatine and feeder cells. After 2–3 days, cells were split 1:4 onto two 96 well plates coated with gelatine and feeder cells and wo 96 well plates coated only with gelatine. ES cell clones grown in gelatine coated 96 well plates were used to isolate genomic DNA for Southern blot analysis. ES cell clones grown on feeder coated 96 well plates were frozen to use for expanding of positive cell clones after Southern blot analysis.

Freezing of ES cell clones

The ES cell clones in the 96 well plates were frozen at -80°C until positive ES cell clones were identified and used for injection into blastocysts. To freeze the ES cells they were washed once in PBS and then treated with trypsin/EDTA (Invitrogen, UK) (30 µl, 7 min, 37°C) to ensure separating into single cells. To stop the reaction ES cell medium (70 µl) was added in each well and the cells were separated by pipetting up and down. Finally, of ES cell freezing medium (100 µl) was added and cells were slowly frozen at -80°C.

3.6.3 Injection of embryonic stem cell clones into blastocysts

ES cell clones, which were tested positive in Southern blot analysis were thawed at 37°C and transferred into 24 well plates coated with gelatine and feeder cells with fresh ES cell medium. After 2 days the positive ES cell clones were expanded into 6 well plates. Before the injection the cells were trypsinized and washed 2 times with PBS. Finally, the cells were suspended in ES cell medium (250 µl) and injected into blastocysts from C57BL6

mice. The injected blastocysts were transferred into the uterus of a pseudo pregnant foster mother to obtain chimeras. Germ line transmission of the modified gene was confirmed in the offspring of the chimeras by Southern blot analysis.

3.7 IN SILICO ANALYSES

3.7.1 Phylogenetic tree

The Phylogenetic tree was created by Dr. M. Andrade (MDC Berlin). Representative amino acid sequences from Lrp2 and Lrp2b proteins were collected from NCBI databases GenBank and GenPept and aligned using MUSCLE (Edgar et al., 2004). A phylogenetic tree of the multiple sequence alignment was produced using ClustalW (Thompson et al., 1994) and displayed with NJPLot (Perrière et al., 1996).

3.7.2 Identification of transcription factor binding sites

Evolutionary conserved regions (ECRs) within 1 Mb around the *Lrp2* transcription start site were identified using the ECR Browser (Ovcharenko et al., 2004). Included in this tool was the subsequent search for transcription factor binding sites (TFBS) in the ECRs. In a second approach, the extent of orthologous conservation of the non-coding Lrp2 gene region was measured using the ClustalW2 multiple sequence alignment program from EMBL-EBI (Larkin et al., 2007). Conservation levels were used to score the MotifViz predicted binding sites. A global score (the sum of the scores assigned to its TFBS) was assigned to each transcription factor. This global score was combined with a score measuring the possible relevance of the factor to the regulation of *Lrp2* as extracted from bibliography and from the ENCODE project data available on the UCSC Genome Browser (Gelineau-van Waes et al., 2008) (Rosenbloom et al., 2010). Binding sites for the about 30 factors were predicted in the *Lrp2* gene sequence between -1500 and +1500 bp from the transcription start site.

6. APPENDIX

Table 4. Genes differentially expressed in the ventral midline of *Lrp2*$^{EGFPcre/-}$ embryos (Array: LCM only). Differential expression of probes was ascertained using two way ANOVA. Cut-off: false discovery rate (FDR) 30%, Fold-Change (FC): 1.5x

SYMBOL	DEFINITION	p-value	FDR	FC
Foxg1	Mus musculus forkhead box G1 (Foxg1), mRNA.	5.23E-04	0.17	-4.24
Igfbp5	insulin-like growth factor binding protein 5	3.19E-05	0.08	-4.12
Igfbp5	insulin-like growth factor binding protein 5	1.49E-05	0.08	-3.75
Sepp1	Mus musculus selenoprotein P, plasma, 1 (Sepp1), transcript variant 1, mRNA.	5.98E-05	0.10	-3.24
Sox9		9.43E-04	0.18	-3.15
A230057G18Rik		3.89E-05	0.08	-3.06
Sepp1	Mus musculus selenoprotein P, plasma, 1 (Sepp1), transcript variant 1, mRNA.	2.29E-03	0.24	-3.01
Ckb	creatin kinase, brain	9.62E-04	0.18	-3.01
Igfbp5	Mus musculus insulin-like growth factor binding protein 5 (Igfbp5), mRNA.	2.52E-05	0.08	-2.65
Ddit4	Mus musculus DNA-damage-inducible transcript 4 (Ddit4), mRNA.	3.59E-03	0.28	-2.63
B230207O03Rik		9.10E-04	0.17	-2.60
LOC381813	Mus musculus protein arginine N-methyltransferase 8 (Prmt8), mRNA.	4.91E-04	0.16	-2.38
E030033D05Rik		4.70E-04	0.16	-2.19
D130026O08Rik		9.09E-04	0.17	-2.15
scl000530.1_2		4.08E-04	0.16	-2.14
Tcf7l2	Mus musculus transcription factor 7-like 2, T-cell specific, HMG-box (Tcf7l2), mRNA.	8.59E-04	0.17	-2.11
Rasl11b		1.84E-04	0.13	-2.11
A230057G18Rik		1.72E-03	0.23	-2.09
Rasl11b	Mus musculus RAS-like, family 11, member B (Rasl11b), mRNA.	4.84E-04	0.16	-2.07
Tcf7l2	Mus musculus transcription factor 7-like 2, T-cell specific, HMG-box (Tcf7l2), mRNA.	4.11E-04	0.16	-2.05
Shfdg1	Mus musculus split hand/foot malformation (ectrodactyly) type 1 (Shfm1), mRNA.	3.92E-04	0.16	-2.02
Foxg1		1.00E-04	0.11	-1.98
A330080J22Rik		1.83E-04	0.13	-1.97
Gpc4	glypican proteoglycan 4	1.26E-04	0.12	-1.95
D130007C19Rik		2.95E-03	0.26	-1.95
Dlk1	delta-like 1 homolog	2.07E-04	0.13	-1.93
Kif1b	kinesin family member 1B	7.22E-04	0.17	-1.80
Tubb2b	Mus musculus tubulin, beta 2b (Tubb2b), mRNA.	1.97E-03	0.23	-1.77
Tmem46	Mus musculus transmembrane protein 46 (Tmem46), mRNA.	2.61E-04	0.14	-1.74
Tmem46	Mus musculus transmembrane protein 46 (Tmem46), mRNA.	6.22E-04	0.17	-1.73
Plekhk1	rhotekin 2, pleckstrin homology domain containing, family K member 1	3.36E-03	0.27	-1.71
A330080J22Rik		2.22E-03	0.24	-1.70
D0H4S114	Mus musculus DNA segment, human D4S114 (D0H4S114), mRNA.	2.14E-03	0.24	-1.67

Gp38		2.93E-03	0.26	-1.64
Tmsb4x	Mus musculus thymosin, beta 4, X chromosome (Tmsb4x), mRNA.	5.36E-04	0.17	-1.61
Tmsb4x	Mus musculus thymosin, beta 4, X chromosome (Tmsb4x), mRNA.	4.64E-04	0.16	-1.61
BC017133	Mus musculus poly(A) binding protein interacting protein 2B (Paip2b), mRNA.	1.92E-03	0.23	-1.60
4732462B05Rik		3.73E-03	0.29	-1.60
Dpysl2	Mus musculus dihydropyrimidinase-like 2 (Dpysl2), mRNA.	4.35E-04	0.16	-1.58
Gng2	Mus musculus guanine nucleotide binding protein (G protein), gamma 2 subunit (Gng2), transcript variant 2, mRNA.	3.55E-05	0.08	-1.57
scl000528.1_16		3.38E-05	0.08	-1.57
1810013L24Rik		1.36E-03	0.21	-1.57
Dag1	Mus musculus dystroglycan 1 (Dag1), mRNA.	8.80E-04	0.17	-1.56
Marcks	myristoylated alanine rich protein kinase C substrate	1.05E-03	0.19	-1.56
Arrb1	arrestin, beta 1	2.44E-03	0.25	-1.55
Ptn	pleiotrophin, other names: HARP, HB-GAM, HBBN, HBGF-8, HBNF, OSF, Osf-1, Osf1	2.13E-04	0.13	-1.55
AW555464		1.93E-03	0.23	-1.55
Lrp2	Mus musculus low density lipoprotein 2, mRNA.	2.19E-03	0.24	-1.55
2700063G02Rik		7.12E-04	0.17	-1.54
Ddah2	dimethylarginine dimethylaminohydrolase 1	1.50E-03	0.22	-1.53
Cox6b	Mus musculus cytochrome c oxidase, subunit VIb polypeptide 1 (Cox6b1), mRNA.	3.40E-04	0.15	-1.53
5830471E12Rik		8.24E-04	0.17	1.50
Rbbp6	retinoblastoma binding protein 6	1.93E-03	0.23	1.50
2610019E17Rik		3.14E-03	0.27	1.51
C80879		1.53E-03	0.22	1.51
Thoc4	Mus musculus THO complex 4 (Thoc4), mRNA.	1.57E-03	0.22	1.52
Ubqln1	Mus musculus ubiquilin 1 (Ubqln1), transcript variant 1, mRNA.	1.67E-03	0.22	1.53
Tex292	Mus musculus cirrhosis, autosomal recessive 1A (human) (Cirh1a), mRNA.	3.87E-03	0.29	1.53
Pa2g4		9.74E-04	0.18	1.54
Slitrk2	SLIT and NTRK-like family, member 2	9.25E-05	0.11	1.54
Heatr3	Mus musculus HEAT repeat containing 3 (Heatr3), mRNA.	7.02E-04	0.17	1.55
Abcf2	Mus musculus ATP-binding cassette, sub-family F (GCN20), member 2 (Abcf2), mRNA.	2.37E-03	0.24	1.55
1110001A05Rik		2.83E-03	0.26	1.55
Bing4	Mus musculus WD repeat domain 46 (Wdr46), mRNA.	2.60E-03	0.26	1.56
Prmt5	Mus musculus protein arginine N-methyltransferase 5 (Prmt5), mRNA.	5.95E-04	0.17	1.56
Tpst2	Mus musculus protein-tyrosine sulfotransferase 2 (Tpst2), mRNA.	3.16E-03	0.27	1.56
2210015D19Rik		4.01E-03	0.30	1.56
Rbm28	RNA binding motif protein 28	8.94E-04	0.17	1.57
Sssca1	Sjogren's syndrome/scleroderma autoantigen 1	2.45E-04	0.14	1.57
LOC217431		2.25E-03	0.24	1.58
Lix1	limb expression 1 homolog	6.45E-04	0.17	1.60
Ppan	peter pan homolog	3.38E-03	0.27	1.61
Homer3	Mus musculus homer homolog 3 (Drosophila) (Homer3), mRNA.	3.52E-03	0.28	1.63
Dnajc13		3.53E-03	0.28	1.63

Nrg1	Mus musculus neuregulin 1 (Nrg1), mRNA. XM_900811 XM_900817	2.78E-04	0.14	1.63
Mrpl22	Mus musculus mitochondrial ribosomal protein L22 (Mrpl22), mRNA.	8.25E-04	0.17	1.64
Tgif	Mus musculus TG interacting factor 1 (Tgif1), mRNA.	1.24E-03	0.21	1.65
3110040D16Rik		8.65E-04	0.17	1.65
BC031781	Mus musculus cDNA sequence BC031781 (BC031781), mRNA.	3.94E-03	0.30	1.66
Surf2	surfeit gene 2	3.00E-03	0.26	1.67
2410019A14Rik	Mus musculus RIKEN cDNA 2410019A14 gene (2410019A14Rik), mRNA.	2.33E-03	0.24	1.68
2810475A17Rik		2.92E-03	0.26	1.70
Lyar	Mus musculus Ly1 antibody reactive clone (Lyar), mRNA.	7.64E-04	0.17	1.71
3110050K21Rik		3.79E-05	0.08	1.72
Lix1	limb expression1 homolog	6.91E-04	0.17	1.74
1700012G19Rik		2.26E-03	0.24	1.75
Wfikkn1	WAP, FS, Ig, KU, and NTR-containing protein 1	2.78E-03	0.26	1.78
A630012P03Rik		4.00E-03	0.30	1.78
Id2	Mus musculus inhibitor of DNA binding 2 (Id2), mRNA.	2.64E-03	0.26	1.79
Pcdh18	Mus musculus protocadherin 18 (Pcdh18), mRNA.	1.24E-03	0.21	1.81
Chst2	Mus musculus carbohydrate sulfotransferase 2 (Chst2), mRNA.	1.91E-03	0.23	1.83
Lmo2	Mus musculus LIM domain only 2 (Lmo2), mRNA.	1.79E-03	0.23	1.85
Lef1	lymphoid enhancer binding factor 1, Wnt signaling	2.12E-03	0.24	1.89
Rbm13	Mus musculus RNA binding motif protein 13 (Rbm13), mRNA.	4.02E-03	0.30	1.98
Nrg1	Mus musculus neuregulin 1 (Nrg1), mRNA. XM_900811 XM_900817	2.65E-04	0.14	2.02
Fst	follistatin	1.43E-03	0.21	2.04
D530050H15Rik		3.51E-04	0.15	2.11
2700033K02Rik		2.04E-03	0.23	2.19
Car4	Mus musculus carbonic anhydrase 4 (Car4), mRNA.	7.07E-07	0.02	2.62
Foxd1	Mus musculus forkhead box D1 (Foxd1), mRNA.	3.96E-05	0.08	3.46

Table 5. Genes differentially expressed in the ventral midline of *Lrp2*$^{EGFPcre/-}$ embryos (Array: manual dissection only).

Differential expression of probes was ascertained using two way ANOVA. Cut-off: false discovery rate (FDR) 20%, Fold-Change (FC): 1.5x

SYMBOL	DEFINITION	p-value	FDR	FC
Lrp2	Mus musculus low density lipoprotein 2, mRNA.	1.12E-05	0.04	-4.23
Matr3	Mus musculus matrin 3 (Matr3), mRNA.	4.73E-03	0.19	-2.93
Alx4	aristaless-like homeobox 4	2.84E-04	0.08	-2.69
Fgf17	Mus musculus fibroblast growth factor 17 (Fgf17), mRNA.	8.42E-04	0.12	-2.65
Zic1	zinc finger protein of the cerebellum	1.46E-04	0.08	-2.59
LOC269859		7.17E-03	0.20	-2.51
Htr3b	Mus musculus 5-hydroxytryptamine (serotonin) receptor 3B (Htr3b), mRNA.	1.30E-05	0.04	-2.38
Stmn2	stathmin-like 2	2.14E-04	0.08	-2.35

Vax1	Mus musculus ventral anterior homeobox containing gene 1 (Vax1), mRNA.	2.51E-05	0.05	-2.35
Foxg1	Mus musculus forkhead box G1 (Foxg1), mRNA.	5.38E-06	0.04	-2.33
Tubb2b	Mus musculus tubulin, beta 2b (Tubb2b), mRNA.	4.46E-03	0.18	-2.24
Ldh2	Mus musculus lactate dehydrogenase B (Ldhb), mRNA.	3.61E-05	0.06	-2.14
Sox21	Mus musculus SRY-box containing gene 21 (Sox21), mRNA.	2.31E-03	0.15	-1.99
Tubb2b	Mus musculus tubulin, beta 2b (Tubb2b), mRNA.	7.77E-04	0.11	-1.97
Neurog3	Mus musculus neurogenin 3 (Neurog3), mRNA.	1.26E-05	0.04	-1.89
D130059O18Rik		5.23E-03	0.19	-1.88
Dlk1	delta-like 1 homolog	1.03E-03	0.13	-1.87
Smoc1	Mus musculus SPARC related modular calcium binding 1 (Smoc1), mRNA.	1.12E-04	0.08	-1.86
Gdi3		7.35E-03	0.20	-1.84
Ncoa4	Mus musculus nuclear receptor coactivator 4 (Ncoa4), transcript variant 2, mRNA.	4.84E-03	0.19	-1.83
LOC383411		1.19E-05	0.04	-1.81
LOC226017		8.63E-04	0.12	-1.81
Hes5	Mus musculus hairy and enhancer of split 5 (Drosophila) (Hes5), mRNA.	6.94E-03	0.20	-1.80
2610036C07Rik		3.92E-03	0.18	-1.78
F830029L24Rik		5.33E-03	0.19	-1.75
LOC383295		5.94E-03	0.20	-1.75
2310047C04Rik	Mus musculus RIKEN cDNA 2310047C04 gene (2310047C04Rik), mRNA.	2.02E-03	0.15	-1.75
Syt11	synaptotagmin XI	2.20E-03	0.15	-1.71
Atp6ap2	Mus musculus ATPase, H+ transporting, lysosomal accessory protein 2 (Atp6ap2), mRNA.	1.37E-03	0.13	-1.71
Etfa	Mus musculus electron transferring flavoprotein, alpha polypeptide (Etfa), nuclear gene encoding mitochondrial protein, mRNA.	7.30E-03	0.20	-1.71
Hap1	huntingtin-associated protein 1	6.05E-03	0.20	-1.71
BC034507		7.93E-03	0.20	-1.71
Alx3	Mus musculus aristaless 3 (Alx3), mRNA.	7.30E-04	0.11	-1.70
Msi2h	Musashi homolog 2	7.44E-03	0.20	-1.70
Ptn	pleiotrophin, other names: HARP, HB-GAM, HBBN, HBGF-8, HBNF, OSF, Osf-1, Osf1	8.12E-04	0.11	-1.70
2010001H16Rik		3.42E-03	0.17	-1.70
Cldn10		4.63E-04	0.10	-1.70
Acaa2	acetyl-CoA acyltransferase 1	7.51E-03	0.20	-1.69
Mylk	myosin light chain kinase	4.73E-04	0.10	-1.69
Igfbpl1	Mus musculus insulin-like growth factor binding protein-like 1 (Igfbpl1), mRNA.	1.50E-04	0.08	-1.68
Syt11	Mus musculus synaptotagmin XI (Syt11), mRNA.	5.87E-03	0.20	-1.68
Car10		1.14E-05	0.04	-1.67
Snx2	sorting nexin 2	4.70E-03	0.19	-1.67
2400003C14Rik	Mus musculus RIKEN cDNA 2400003C14 gene (2400003C14Rik), mRNA.	6.48E-04	0.11	-1.65
Igsf1	Mus musculus immunoglobulin superfamily, member 1 (Igsf1), transcript variant 4, mRNA.	1.10E-04	0.08	-1.65
Sox21	Mus musculus SRY-box containing gene 21 (Sox21), mRNA.	4.05E-03	0.18	-1.65
LOC232532		5.19E-03	0.19	-1.65
Asah1	Mus musculus N-acylsphingosine amidohydrolase 1 (Asah1), mRNA.	2.88E-03	0.17	-1.64

Atp6v0d1	Mus musculus ATPase, H+ transporting, lysosomal V0 subunit D1 (Atp6v0d1), mRNA.	7.69E-03	0.20	-1.61
4833426H15Rik		7.72E-03	0.20	-1.61
Zic4	Mus musculus zinc finger protein of the cerebellum 4 (Zic4), mRNA.	1.14E-03	0.13	-1.61
Igsf1	Mus musculus immunoglobulin superfamily, member 1 (Igsf1), transcript variant 4, mRNA.	6.21E-04	0.11	-1.59
E130201N16Rik	Mus musculus proline rich 15 (Prr15), mRNA.	3.09E-03	0.17	-1.59
Khdrbs1		7.49E-03	0.20	-1.59
Drg1	Mus musculus developmentally regulated GTP binding protein 1 (Drg1), mRNA.	7.93E-03	0.20	-1.58
Rab6b		8.06E-04	0.11	-1.58
1190002H23Rik		2.47E-04	0.08	-1.58
Acas2	Mus musculus acyl-CoA synthetase short-chain family member 2 (Acss2), mRNA.	1.29E-03	0.13	-1.57
AW413632		1.34E-03	0.13	-1.57
4931406I20Rik	Mus musculus RIKEN cDNA 4931406I20 gene (4931406I20Rik), mRNA.	7.23E-03	0.20	-1.57
LOC56628		1.22E-03	0.13	-1.57
Ube2e3	Mus musculus ubiquitin-conjugating enzyme E2E 3, UBC4/5 homolog (yeast) (Ube2e3), mRNA.	4.08E-03	0.18	-1.56
Zic3		7.21E-03	0.20	-1.56
BC030477	Mus musculus WSC domain containing 1 (Wscd1), mRNA.	6.73E-04	0.11	-1.56
Tox	Mus musculus thymocyte selection-associated HMG box gene (Tox), mRNA. XM_919293 XM_919306	2.16E-03	0.15	-1.56
Lrig1		5.54E-03	0.20	-1.56
Tmem46	Mus musculus transmembrane protein 46 (Tmem46), mRNA.	4.44E-05	0.06	-1.56
Cyp27a1	Mus musculus cytochrome P450, family 27, subfamily a, polypeptide 1 (Cyp27a1), mRNA.	1.99E-03	0.15	-1.55
Grina	glutamate receptor, ionotropic, N-methyl D-aspartate-associated protein 1	3.40E-04	0.09	-1.55
Dlk1	delta-like 1 homolog	1.07E-03	0.13	-1.55
Zfp238	zinc finger protein 238	5.33E-03	0.19	-1.55
Atp11c	Mus musculus Atpase, class VI, type 11C (Atp11c), transcript variant 1, mRNA.	5.19E-03	0.19	-1.55
LOC269529		8.78E-04	0.12	-1.54
Fusip1		7.46E-03	0.20	-1.52
Hmgb1	high mobility group box 1	6.64E-03	0.20	-1.52
Lancl2		5.12E-03	0.19	-1.52
Tinag	Mus musculus tubulointerstitial nephritis antigen (Tinag), mRNA.	4.34E-04	0.10	-1.52
Idb4		5.52E-03	0.20	-1.51
2310033F14Rik		2.20E-03	0.15	-1.51
Fblim1	Mus musculus filamin binding LIM protein 1 (Fblim1), mRNA.	7.93E-03	0.20	1.50
Paqr9	Mus musculus progestin and adipoQ receptor family member IX (Paqr9), mRNA.	6.34E-03	0.20	1.50
Slc7a11	Mus musculus solute carrier family 7 (cationic amino acid transporter, y+ system), member 11 (Slc7a11), mRNA.	3.98E-03	0.18	1.51
4833414E09Rik		6.03E-03	0.20	1.52
Srm	Mus musculus spermidine synthase (Srm), mRNA.	5.02E-04	0.10	1.52
Itga3	Mus musculus integrin alpha 3 (Itga3), mRNA.	7.93E-03	0.20	1.52
Pcdha1	Mus musculus protocadherin alpha 1 (Pcdha1), mRNA.	1.48E-05	0.04	1.52

Nrp	Mus musculus neuropilin 1 (Nrp1), mRNA.	1.27E-03	0.13	1.52
B130065G19Rik		1.20E-03	0.13	1.52
Tcf12		5.25E-03	0.19	1.53
Snai1	Mus musculus snail homolog 1 (Drosophila) (Snai1), mRNA.	7.88E-03	0.20	1.53
Lmo2	Mus musculus LIM domain only 2 (Lmo2), mRNA.	4.44E-03	0.18	1.53
Nrp		2.60E-04	0.08	1.53
Stard8	Mus musculus START domain containing 8 (Stard8), mRNA.	4.82E-03	0.19	1.54
Ccnd2		1.97E-03	0.15	1.54
Stx3	Mus musculus syntaxin 3 (Stx3), transcript variant A, mRNA.	7.49E-05	0.07	1.54
2810022L02Rik	Mus musculus RIKEN cDNA 2810022L02 gene (2810022L02Rik), mRNA.	3.96E-04	0.10	1.55
Pitx2	Mus musculus paired-like homeodomain transcription factor 2 (Pitx2), transcript variant 3, mRNA.	2.42E-03	0.16	1.55
E130308A19Rik		1.84E-03	0.14	1.55
Arid3b	AT rich interactive domain 3B	1.10E-03	0.13	1.56
Lmo2	Mus musculus LIM domain only 2 (Lmo2), mRNA.	1.62E-05	0.04	1.56
Rab38	Mus musculus Rab38, member of RAS oncogene family (Rab38), mRNA.	6.21E-05	0.07	1.56
2700023E23Rik		2.35E-03	0.15	1.56
5330439J01Rik		5.86E-03	0.20	1.57
Dkk1	dickkopf homolog 1, Wnt signaling	6.31E-04	0.11	1.57
Has2	Mus musculus hyaluronan synthase 2 (Has2), mRNA.	7.10E-04	0.11	1.57
Tbx1	T-box 1	2.34E-03	0.15	1.58
Prkx	Mus musculus protein kinase, X-linked (Prkx), mRNA.	1.82E-03	0.14	1.60
B230386D16Rik		7.12E-03	0.20	1.60
Sema3a	Mus musculus sema domain, immunoglobulin domain (Ig), short basic domain, secreted, (semaphorin) 3A (Sema3a), mRNA.	4.86E-04	0.10	1.60
Dcn	decorin (proteoglycan)	6.04E-04	0.11	1.61
9430001M03Rik		2.28E-03	0.15	1.61
Nol5	nucleolar protein 5	2.22E-03	0.15	1.61
Lss	lanosterol synthase	7.00E-04	0.11	1.61
Bmp4		2.07E-03	0.15	1.61
Figf	Mus musculus c-fos induced growth factor (Figf), mRNA.	6.29E-04	0.11	1.62
Leprel1	leprecan-like 1	3.39E-05	0.06	1.63
D030015G18Rik		6.90E-03	0.20	1.63
Peg3	paternally expressed 3	7.21E-03	0.20	1.64
Idb3	Mus musculus inhibitor of DNA binding 3 (Id3), mRNA.	1.70E-04	0.08	1.64
9630032J03Rik		4.60E-04	0.10	1.64
9130206I24Rik		3.30E-03	0.17	1.65
Msx2	homeobox, msh-like 2	4.00E-05	0.06	1.65
Copeb	Kruppel-like factor 6	7.39E-03	0.20	1.65
5830411I20		1.68E-03	0.14	1.66
Stk40	Mus musculus serine/threonine kinase 40 (Stk40), mRNA.	8.80E-04	0.12	1.66
Dgkk	Mus musculus diacylglycerol kinase kappa (Dgkk), mRNA.	2.92E-03	0.17	1.66
3632451O06Rik		7.22E-03	0.20	1.67
Pitx2	paired-like homeodomain transcription factor 2	2.51E-03	0.16	1.67
2310045A20Rik		2.60E-03	0.16	1.68

Bcl9l	BCL9-related beta-catenin-binding protein; nuclear co-factor of beta-catenin signalling	5.73E-03	0.20	1.68
Pcolce2	procollagen C-endopeptidase enhancer 2	1.59E-03	0.14	1.68
Ccnd2	cyclin D2	4.40E-03	0.18	1.69
E230020D15Rik		2.44E-03	0.16	1.69
Chst2	Mus musculus carbohydrate sulfotransferase 2 (Chst2), mRNA.	7.12E-03	0.20	1.70
Gata3	Mus musculus GATA binding protein 3 (Gata3), mRNA.	1.56E-03	0.14	1.70
Gdnf	glial cell derived neurotrophic factor	1.53E-04	0.08	1.71
5430433G21Rik		2.26E-04	0.08	1.72
Fgf18	Mus musculus fibroblast growth factor 18 (Fgf18), mRNA.	5.13E-04	0.10	1.73
4933407C03Rik		3.11E-03	0.17	1.75
Sp5	Mus musculus trans-acting transcription factor 5 (Sp5), mRNA.	5.43E-03	0.19	1.76
Unc5c	netrin receptor UNC5C	3.18E-04	0.09	1.78
Zdhhc21	Mus musculus zinc finger, DHHC domain containing 21 (Zdhhc21), mRNA.	6.08E-03	0.20	1.79
Fgf10	Mus musculus fibroblast growth factor 10 (Fgf10), mRNA.	6.82E-03	0.20	1.82
Plp	proteolipid protein (myelin) 1	5.67E-03	0.20	1.83
Idb1	inhibitor of DNA binding 1	7.76E-04	0.11	1.84
Car4	Mus musculus carbonic anhydrase 4 (Car4), mRNA.	2.47E-03	0.16	1.86
Dlx3	Mus musculus distal-less homeobox 3 (Dlx3), mRNA.	3.82E-03	0.18	1.87
Wfikkn1	WAP, FS, Ig, KU, and NTR-containing protein 1	1.43E-04	0.08	1.87
Bbx	bobby sox homolog	5.22E-03	0.19	1.88
Vgll2	Mus musculus vestigial like 2 homolog (Drosophila) (Vgll2), mRNA.	1.28E-03	0.13	1.92
Fgf10	Mus musculus fibroblast growth factor 10 (Fgf10), mRNA.	6.52E-03	0.20	1.94
Itga6	integrin alpha 6	2.04E-03	0.15	2.06
Vgll2	Mus musculus vestigial like 2 homolog (Drosophila) (Vgll2), mRNA.	4.44E-03	0.18	2.13
Dgkk	Mus musculus diacylglycerol kinase kappa (Dgkk), mRNA.	2.88E-03	0.17	2.45

7. BIBLIOGRAPHY

Abe, T., Muto, Y. and Hosoya, N. (1975) 'Vitamin A transport in chicken plasma: isolation and characterization of retinol-binding protein (RBP), prealbumin (PA), and RBP--PA complex', *J Lipid Res* 16(3): 200-10.

Adolf, B., Chapouton, P., Lam, C. S., Topp, S., Tannhauser, B., Strahle, U., Gotz, M. and Bally-Cuif, L. (2006) 'Conserved and acquired features of adult neurogenesis in the zebrafish telencephalon', *Dev Biol* 295(1): 278-93.

Allen, B. L., Song, J. Y., Izzi, L., Althaus, I. W., Kang, J. S., Charron, F., Krauss, R. S. and McMahon, A. P. (2011) 'Overlapping Roles and Collective Requirement for the Coreceptors GAS1, CDO, and BOC in SHH Pathway Function', *Dev Cell* 20(6): 775-87.

Andersen, O. M., Reiche, J., Schmidt, V., Gotthardt, M., Spoelgen, R., Behlke, J., von Arnim, C. A., Breiderhoff, T., Jansen, P., Wu, X. et al. (2005) 'Neuronal sorting protein-related receptor sorLA/LR11 regulates processing of the amyloid precursor protein', *Proc Natl Acad Sci U S A* 102(38): 13461-6.

Anzenberger, U., Bit-Avragim, N., Rohr, S., Rudolph, F., Dehmel, B., Willnow, T. E. and Abdelilah-Seyfried, S. (2006) 'Elucidation of megalin/LRP2-dependent endocytic transport processes in the larval zebrafish pronephros', *J Cell Sci* 119(Pt 10): 2127-37.

Assemat, E., Chatelet, F., Chandellier, J., Commo, F., Cases, O., Verroust, P. and Kozyraki, R. (2005) 'Overlapping expression patterns of the multiligand endocytic receptors cubilin and megalin in the CNS, sensory organs and developing epithelia of the rodent embryo', *Gene Expr Patterns* 6(1): 69-78.

Bergeron, S. A., Tyurina, O. V., Miller, E., Bagas, A. and Karlstrom, R. O. (2011) 'Brother of cdo (umleitung) is cell-autonomously required for Hedgehog-mediated ventral CNS patterning in the zebrafish', *Development* 138(1): 75-85.

Boycott, K. M., Flavelle, S., Bureau, A., Glass, H. C., Fujiwara, T. M., Wirrell, E., Davey, K., Chudley, A. E., Scott, J. N., McLeod, D. R. et al. (2005) 'Homozygous deletion of the very low density lipoprotein receptor gene causes autosomal recessive cerebellar hypoplasia with cerebral gyral simplification', *Am J Hum Genet* 77(3): 477-83.

Brinkmeier, M. L., Potok, M. A., Davis, S. W. and Camper, S. A. (2007) 'TCF4 deficiency expands ventral diencephalon signaling and increases induction of pituitary progenitors', *Dev Biol* 311(2): 396-407.

Brown, A. J., Sun, L., Feramisco, J. D., Brown, M. S. and Goldstein, J. L. (2002) 'Cholesterol addition to ER membranes alters conformation of SCAP, the SREBP escort protein that regulates cholesterol metabolism', *Mol Cell* 10(2): 237-45.

Brown, S. A., Warburton, D., Brown, L. Y., Yu, C. Y., Roeder, E. R., Stengel-Rutkowski, S., Hennekam, R. C. and Muenke, M. (1998) 'Holoprosencephaly due to mutations in ZIC2, a homologue of Drosophila odd-paired', *Nat Genet* 20(2): 180-3.

Bujo, H., Yamamoto, T., Hayashi, K., Hermann, M., Nimpf, J. and Schneider, W. J. (1995) 'Mutant oocytic low density lipoprotein receptor gene family member causes atherosclerosis and female sterility', Proc Natl Acad Sci U S A 92(21): 9905-9.

Byrd, C. A. and Brunjes, P. C. (2001) 'Neurogenesis in the olfactory bulb of adult zebrafish',

Neuroscience 105(4): 793-801.

Chassaing, N., Lacombe, D., Carles, D., Calvas, P., Saura, R. and Bieth, E. (2003) 'Donnai-Barrow syndrome: four additional patients', *Am J Med Genet A* 121A(3): 258-62.

Chen, W. J., Goldstein, J. L. and Brown, M. S. (1990) 'NPXY, a sequence often found in cytoplasmic tails, is required for coated pit-mediated internalization of the low density lipoprotein receptor', *J Biol Chem* 265(6): 3116-23.

Chiang, C., Litingtung, Y., Lee, E., Young, K. E., Corden, J. L., Westphal, H. and Beachy, P. A. (1996) 'Cyclopia and defective axial patterning in mice lacking Sonic hedgehog gene function', *Nature* 383(6599): 407-13.

Chlon, T. M., Taffany, D. A., Welsh, J. and Rowling, M. J. (2008) 'Retinoids modulate expression of the endocytic partners megalin, cubilin, and disabled-2 and uptake of vitamin D-binding protein in human mammary cells', *J Nutr* 138(7): 1323-8.

Christ, A., Terryn, S., Schmidt, V., Christensen, E. I., Huska, M. R., Andrade-Navarro, M. A., Hubner, N., Devuyst, O., Hammes, A. and Willnow, T. E. (2010) 'The soluble intracellular domain of megalin does not affect renal proximal tubular function in vivo', *Kidney Int* 78(5): 473-7.

Christensen, E. I. and Birn, H. (2001) 'Megalin and cubilin: synergistic endocytic receptors in renal proximal tubule', *Am J Physiol Renal Physiol* 280(4): F562-73.

Christensen, E. I. and Verroust, P. J. (2002) 'Megalin and cubilin, role in proximal tubule function and during development', *Pediatr Nephrol* 17(12): 993-9.

Cohen, M. M., Jr. (2006) 'Holoprosencephaly: clinical, anatomic, and molecular dimensions', *Birth Defects Res A Clin Mol Teratol* 76(9): 658-73.

Cohen, M. M., Jr. and Shiota, K. (2002) 'Teratogenesis of holoprosencephaly', *Am J Med Genet* 109(1): 1-15.

Copp, A. J., Greene, N. D. and Murdoch, J. N. (2003) 'The genetic basis of mammalian neurulation', *Nat Rev Genet* 4(10): 784-93.

Creuzet, S., Schuler, B., Couly, G. and Le Douarin, N. M. (2004) 'Reciprocal relationships between Fgf8 and neural crest cells in facial and forebrain development', *Proc Natl Acad Sci U S A* 101(14): 4843-7.

Crossley, P. H., Martinez, S., Ohkubo, Y. and Rubenstein, J. L. (2001) 'Coordinate expression of Fgf8, Otx2, Bmp4, and Shh in the rostral prosencephalon during development of the telencephalic and optic vesicles', *Neuroscience* 108(2): 183-206.

Curran, T. and D'Arcangelo, G. (1998) 'Role of reelin in the control of brain development', *Brain Res Brain Res Rev* 26(2-3): 285-94.

D'Arcangelo, G., Homayouni, R., Keshvara, L., Rice, D. S., Sheldon, M. and Curran, T. (1999) 'Reelin is a ligand for lipoprotein receptors', *Neuron* 24(2): 471-9.

Davidson, G., Wu, W., Shen, J., Bilic, J., Fenger, U., Stannek, P., Glinka, A. and Niehrs, C. (2005) 'Casein kinase 1 gamma couples Wnt receptor activation to cytoplasmic signal transduction', *Nature* 438(7069): 867-72.

Detrick, R. J., Dickey, D. and Kintner, C. R. (1990) 'The effects of N-cadherin misexpression

on morphogenesis in Xenopus embryos', *Neuron* 4(4): 493-506.

Donnai, D. (1996) 'Pitt-Rogers-Danks syndrome and Wolf-Hirschhorn syndrome', *Am J Med Genet* 66(1): 101-3.

Doyon, Y., McCammon, J. M., Miller, J. C., Faraji, F., Ngo, C., Katibah, G. E., Amora, R., Hocking, T. D., Zhang, L., Rebar, E. J. et al. (2008) 'Heritable targeted gene disruption in zebrafish using designed zinc-finger nucleases', *Nat Biotechnol* 26(6): 702-8.

Drake, C. J., Fleming, P. A., Larue, A. C., Barth, J. L., Chintalapudi, M. R. and Argraves, W. S. (2004) 'Differential distribution of cubilin and megalin expression in the mouse embryo', *Anat Rec A Discov Mol Cell Evol Biol* 277(1): 163-70.

Drummond, I. (2003) 'Making a zebrafish kidney: a tale of two tubes', *Trends Cell Biol* 13(7): 357-65.

Drummond, I. A. (2005) 'Kidney development and disease in the zebrafish', *J Am Soc Nephrol* 16(2): 299-304.

Drummond, I. A., Majumdar, A., Hentschel, H., Elger, M., Solnica-Krezel, L., Schier, A. F., Neuhauss, S. C., Stemple, D. L., Zwartkruis, F., Rangini, Z. et al. (1998) 'Early development of the zebrafish pronephros and analysis of mutations affecting pronephric function', *Development* 125(23): 4655-67.

Duchesne, A., Gautier, M., Chadi, S., Grohs, C., Floriot, S., Gallard, Y., Caste, G., Ducos, A. and Eggen, A. (2006) 'Identification of a doublet missense substitution in the bovine LRP4 gene as a candidate causal mutation for syndactyly in Holstein cattle', *Genomics* 88(5): 610-21.

Edgar, R. C. (2004) 'MUSCLE: multiple sequence alignment with high accuracy and high throughput', *Nucleic Acids Res* 32(5): 1792-7.

Eom, D. S., Amarnath, S., Fogel, J. L. and Agarwala, S. (2011) 'Bone morphogenetic proteins regulate neural tube closure by interacting with the apicobasal polarity pathway', *Development* 138(15): 3179-88.

Etheridge, L. A., Wu, T., Liang, J. O., Ekker, S. C. and Halpern, M. E. (2001) 'Floor plate develops upon depletion of tiggy-winkle and sonic hedgehog', *Genesis* 30(3): 164-9.

Fernandes, M., Gutin, G., Alcorn, H., McConnell, S. K. and Hebert, J. M. (2007) 'Mutations in the BMP pathway in mice support the existence of two molecular classes of holoprosencephaly', *Development* 134(21): 3789-94.

Fernandes, M. and Hebert, J. M. (2008) 'The ups and downs of holoprosencephaly: dorsal versus ventral patterning forces', *Clin Genet* 73(5): 413-23.

FitzPatrick, D. R., Keeling, J. W., Evans, M. J., Kan, A. E., Bell, J. E., Porteous, M. E., Mills, K., Winter, R. M. and Clayton, P. T. (1998) 'Clinical phenotype of desmosterolosis', *Am J Med Genet* 75(2): 145-52.

Frade, J. M. (2002) 'Interkinetic nuclear movement in the vertebrate neuroepithelium: encounters with an old acquaintance', *Prog Brain Res* 136: 67-71.

Fuccillo, M., Joyner, A. L. and Fishell, G. (2006) 'Morphogen to mitogen: the multiple roles of hedgehog signalling in vertebrate neural development', *Nat Rev Neurosci* 7(10): 772-83.

Fujino, T., Asaba, H., Kang, M. J., Ikeda, Y., Sone, H., Takada, S., Kim, D. H., Ioka, R. X., Ono, M., Tomoyori, H. et al. (2003) 'Low-density lipoprotein receptor-related protein 5 (LRP5) is essential for normal cholesterol metabolism and glucose-induced insulin secretion', *Proc Natl Acad Sci U S A* 100(1): 229-34.

Gajera, C. R., Emich, H., Lioubinski, O., Christ, A., Beckervordersandforth-Bonk, R., Yoshikawa, K., Bachmann, S., Christensen, E. I., Gotz, M., Kempermann, G. et al. (2010) 'LRP2 in ependymal cells regulates BMP signaling in the adult neurogenic niche', *J Cell Sci* 123(Pt 11): 1922-30.

Gelineau-van Waes, J., Maddox, J. R., Smith, L. M., van Waes, M., Wilberding, J., Eudy, J. D., Bauer, L. K. and Finnell, R. H. (2008) 'Microarray analysis of E9.5 reduced folate carrier (RFC1; Slc19a1) knockout embryos reveals altered expression of genes in the cubilin-megalin multiligand endocytic receptor complex', *BMC Genomics* 9: 156.

Geng, X. and Oliver, G. (2009) 'Pathogenesis of holoprosencephaly', *J Clin Invest* 119(6): 1403-13.

Gerbe, F., Cox, B., Rossant, J. and Chazaud, C. (2008) 'Dynamic expression of Lrp2 pathway members reveals progressive epithelial differentiation of primitive endoderm in mouse blastocyst', *Dev Biol* 313(2): 594-602.

Goldstein, J. L. and Brown, M. S. (1979) 'The LDL receptor locus and the genetics of familial hypercholesterolemia', *Annu Rev Genet* 13: 259-89.

Goldstein, J. L. and Brown, M. S. (1986) 'Atherosclerosis and its complications: contributions from the Association of American Physicians, 1886-1986', *Trans Assoc Am Physicians* 99: ccxxxi-ccxlvii.

Goldstein, J. L., Hobbs, H. H. and Brown, M. S. (2001) Familial hypercholesterolemia. in B. A. Scriver CR, Sly WS, Valle D, Childs B, Kinzler KW, Vogelstein B (ed.) *The Metabolic and Molecular Basis of Inherited disease.* New York: McGraw-Hill.

Gotthardt, M., Trommsdorff, M., Nevitt, M. F., Shelton, J., Richardson, J. A., Stockinger, W., Nimpf, J. and Herz, J. (2000) 'Interactions of the low density lipoprotein receptor gene family with cytosolic adaptor and scaffold proteins suggest diverse biological functions in cellular communication and signal transduction', *J Biol Chem* 275(33): 25616-24.

Grant, B. and Hirsh, D. (1999) 'Receptor-mediated endocytosis in the Caenorhabditis elegans oocyte', *Mol Biol Cell* 10(12): 4311-26.

Grigorenko, A. P., Moliaka, Y. K., Soto, M. C., Mello, C. C. and Rogaev, E. I. (2004) 'The Caenorhabditis elegans IMPAS gene, imp-2, is essential for development and is functionally distinct from related presenilins', *Proc Natl Acad Sci U S A* 101(41): 14955-60.

Gutin, G., Fernandes, M., Palazzolo, L., Paek, H., Yu, K., Ornitz, D. M., McConnell, S. K. and Hebert, J. M. (2006) 'FGF signalling generates ventral telencephalic cells independently of SHH', *Development* 133(15): 2937-46.

Hallonet, M., Hollemann, T., Pieler, T. and Gruss, P. (1999) 'Vax1, a novel homeobox-containing gene, directs development of the basal forebrain and visual system', *Genes Dev* 13(23): 3106-14.

Hammes, A., Andreassen, T. K., Spoelgen, R., Raila, J., Hubner, N., Schulz, H., Metzger, J., Schweigert, F. J., Luppa, P. B., Nykjaer, A. et al. (2005) 'Role of endocytosis in cellular uptake of

sex steroids', *Cell* 122(5): 751-62.

Harfe, B. D., Scherz, P. J., Nissim, S., Tian, H., McMahon, A. P. and Tabin, C. J. (2004) 'Evidence for an expansion-based temporal Shh gradient in specifying vertebrate digit identities', *Cell* 118(4): 517-28.

Herz, J. and Bock, H. H. (2002) 'Lipoprotein receptors in the nervous system', *Annu Rev Biochem* 71: 405-34.

Herz, J., Clouthier, D. E. and Hammer, R. E. (1992) 'LDL receptor-related protein internalizes and degrades uPA-PAI-1 complexes and is essential for embryo implantation', *Cell* 71(3): 411-21.

Herz, J., Couthier, D. E. and Hammer, R. E. (1993) 'Correction: LDL receptor-related protein internalizes and degrades uPA-PAI-1 complexes and is essential for embryo implantation', *Cell* 73(3): 428.

Hiesberger, T., Trommsdorff, M., Howell, B. W., Goffinet, A., Mumby, M. C., Cooper, J. A. and Herz, J. (1999) 'Direct binding of Reelin to VLDL receptor and ApoE receptor 2 induces tyrosine phosphorylation of disabled-1 and modulates tau phosphorylation', *Neuron* 24(2): 481-9.

Hoch, R. V., Rubenstein, J. L. and Pleasure, S. (2009) 'Genes and signaling events that establish regional patterning of the mammalian forebrain', *Semin Cell Dev Biol* 20(4): 378-86.

Irons, M., Elias, E. R., Salen, G., Tint, G. S. and Batta, A. K. (1993) 'Defective cholesterol biosynthesis in Smith-Lemli-Opitz syndrome', *Lancet* 341(8857): 1414.

Ishibashi, S., Brown, M. S., Goldstein, J. L., Gerard, R. D., Hammer, R. E. and Herz, J. (1993) 'Hypercholesterolemia in low density lipoprotein receptor knockout mice and its reversal by adenovirus-mediated gene delivery', *J Clin Invest* 92(2): 883-93.

Izzi, L., Levesque, M., Morin, S., Laniel, D., Wilkes, B. C., Mille, F., Krauss, R. S., McMahon, A. P., Allen, B. L. and Charron, F. (2011) 'Boc and gas1 each form distinct shh receptor complexes with ptch1 and are required for shh-mediated cell proliferation', *Dev Cell* 20(6): 788-801.

Jaillon, O., Aury, J. M., Brunet, F., Petit, J. L., Stange-Thomann, N., Mauceli, E., Bouneau, L., Fischer, C., Ozouf-Costaz, C., Bernot, A. et al. (2004) 'Genome duplication in the teleost fish Tetraodon nigroviridis reveals the early vertebrate proto-karyotype', *Nature* 431(7011): 946-57.

Johnson, E. B., Hammer, R. E. and Herz, J. (2005) 'Abnormal development of the apical ectodermal ridge and polysyndactyly in Megf7-deficient mice', *Hum Mol Genet* 14(22): 3523-38.

Kadowaki, H., Nishitoh, H., Urano, F., Sadamitsu, C., Matsuzawa, A., Takeda, K., Masutani, H., Yodoi, J., Urano, Y., Nagano, T. et al. (2005) 'Amyloid beta induces neuronal cell death through ROS-mediated ASK1 activation', *Cell Death Differ* 12(1): 19-24.

Kantarci, S., Al-Gazali, L., Hill, R. S., Donnai, D., Black, G. C., Bieth, E., Chassaing, N., Lacombe, D., Devriendt, K., Teebi, A. et al. (2007) 'Mutations in LRP2, which encodes the multiligand receptor megalin, cause Donnai-Barrow and facio-oculo-acoustico-renal syndromes', *Nat Genet* 39(8): 957-9.

Kato, M., Patel, M. S., Levasseur, R., Lobov, I., Chang, B. H., Glass, D. A., 2nd, Hartmann, C., Li, L., Hwang, T. H., Brayton, C. F. et al. (2002) 'Cbfa1-independent decrease in osteoblast proliferation, osteopenia, and persistent embryonic eye vascularization in mice deficient in Lrp5, a Wnt coreceptor', *J Cell Biol* 157(2): 303-14.

Kazanskaya, O., Glinka, A. and Niehrs, C. (2000) 'The role of Xenopus dickkopf1 in prechordal plate specification and neural patterning', *Development* 127(22): 4981-92.

Kelley, R. I. (2000) 'Inborn errors of cholesterol biosynthesis', *Adv Pediatr* 47: 1-53.

Khaliullina, H., Panakova, D., Eugster, C., Riedel, F., Carvalho, M. and Eaton, S. (2009) 'Patched regulates Smoothened trafficking using lipoprotein-derived lipids', *Development* 136(24): 4111-21.

Kim, N., Stiegler, A. L., Cameron, T. O., Hallock, P. T., Gomez, A. M., Huang, J. H., Hubbard, S. R., Dustin, M. L. and Burden, S. J. (2008) 'Lrp4 is a receptor for Agrin and forms a complex with MuSK', *Cell* 135(2): 334-42.

Krauss, R. S. (2007) 'Holoprosencephaly: new models, new insights', *Expert Rev Mol Med* 9(26): 1-17.

Kur, E., Christa, A., Veth, K. N., Gajera, C. R., Andrade-Navarro, M. A., Zhang, J., Willer, J. R., Gregg, R. G., Abdelilah-Seyfried, S., Bachmann, S. et al. (2011) 'Loss of Lrp2 in zebrafish disrupts pronephric tubular clearance but not forebrain development', *Dev Dyn* 240(6): 1567-77.

Lakhwani, S., Garcia-Sanz, P. and Vallejo, M. (2010) 'Alx3-deficient mice exhibit folic acid-resistant craniofacial midline and neural tube closure defects', *Dev Biol* 344(2): 869-80.

Langbein, S., Szakacs, O., Wilhelm, M., Sukosd, F., Weber, S., Jauch, A., Lopez Beltran, A., Alken, P., Kalble, T. and Kovacs, G. (2002) 'Alteration of the LRP1B gene region is associated with high grade of urothelial cancer', *Lab Invest* 82(5): 639-43.

Lee, C., Scherr, H. M. and Wallingford, J. B. (2007) 'Shroom family proteins regulate gamma-tubulin distribution and microtubule architecture during epithelial cell shape change', *Development* 134(7): 1431-41.

Li, L. and Xie, T. (2005) 'Stem cell niche: structure and function', *Annu Rev Cell Dev Biol* 21: 605-31.

Li, Y., Cam, J. and Bu, G. (2001a) 'Low-density lipoprotein receptor family: endocytosis and signal transduction', *Mol Neurobiol* 23(1): 53-67.

Li, Y., Cong, R. and Biemesderfer, D. (2008) 'The COOH terminus of megalin regulates gene expression in opossum kidney proximal tubule cells', *Am J Physiol Cell Physiol* 295(2): C529-37.

Li, Y., van Kerkhof, P., Marzolo, M. P., Strous, G. J. and Bu, G. (2001b) 'Identification of a major cyclic AMP-dependent protein kinase A phosphorylation site within the cytoplasmic tail of the low-density lipoprotein receptor-related protein: implication for receptor-mediated endocytosis', *Mol Cell Biol* 21(4): 1185-95.

Liu, A. and Niswander, L. A. (2005) 'Bone morphogenetic protein signalling and vertebrate nervous system development', *Nat Rev Neurosci* 6(12): 945-54.

Liu, C. X., Musco, S., Lisitsina, N. M., Yaklichkin, S. Y. and Lisitsyn, N. A. (2000) 'Genomic

organization of a new candidate tumor suppressor gene, LRP1B', *Genomics* 69(2): 271-4.

Liu, W., Yu, W. R., Carling, T., Juhlin, C., Rastad, J., Ridefelt, P., Akerstrom, G. and Hellman, P. (1998) 'Regulation of gp330/megalin expression by vitamins A and D', *Eur J Clin Invest* 28(2): 100-7.

Marschang, P., Brich, J., Weeber, E. J., Sweatt, J. D., Shelton, J. M., Richardson, J. A., Hammer, R. E. and Herz, J. (2004) 'Normal development and fertility of knockout mice lacking the tumor suppressor gene LRP1b suggest functional compensation by LRP1', *Mol Cell Biol* 24(9): 3782-93.

Matsuda, T. and Cepko, C. L. (2007) 'Controlled expression of transgenes introduced by in vivo electroporation', *Proc Natl Acad Sci U S A* 104(3): 1027-32.

May, P., Bock, H. H. and Herz, J. (2003) 'Integration of endocytosis and signal transduction by lipoprotein receptors', *Sci STKE* 2003(176): PE12.

May, P., Herz, J. and Bock, H. H. (2005) 'Molecular mechanisms of lipoprotein receptor signalling', *Cell Mol Life Sci* 62(19-20): 2325-38.

Muenke, M. and Beachy, P. A. (2000) 'Genetics of ventral forebrain development and holoprosencephaly', *Curr Opin Genet Dev* 10(3): 262-9.

Muller, F., Albert, S., Blader, P., Fischer, N., Hallonet, M. and Strahle, U. (2000) 'Direct action of the nodal-related signal cyclops in induction of sonic hedgehog in the ventral midline of the CNS', *Development* 127(18): 3889-97.

Nagy, A., Moens, C., Ivanyi, E., Pawling, J., Gertsenstein, M., Hadjantonakis, A. K., Pirity, M. and Rossant, J. (1998) 'Dissecting the role of N-myc in development using a single targeting vector to generate a series of alleles', *Curr Biol* 8(11): 661-4.

Nykjaer, A., Dragun, D., Walther, D., Vorum, H., Jacobsen, C., Herz, J., Melsen, F., Christensen, E. I. and Willnow, T. E. (1999) 'An endocytic pathway essential for renal uptake and activation of the steroid 25-(OH) vitamin D3', *Cell* 96(4): 507-15.

Ohkubo, Y., Chiang, C. and Rubenstein, J. L. (2002) 'Coordinate regulation and synergistic actions of BMP4, SHH and FGF8 in the rostral prosencephalon regulate morphogenesis of the telencephalic and optic vesicles', *Neuroscience* 111(1): 1-17.

Okada, T., Okumura, Y., Motoyama, J. and Ogawa, M. (2008) 'FGF8 signaling patterns the telencephalic midline by regulating putative key factors of midline development', *Dev Biol* 320(1): 92-101.

Paek, H., Hwang, J. Y., Zukin, R. S. and Hebert, J. M. (2011) 'beta-Catenin-dependent FGF signaling sustains cell survival in the anterior embryonic head by countering Smad4', *Dev Cell* 20(5): 689-99.

Perriere, G. and Gouy, M. (1996) 'WWW-query: an on-line retrieval system for biological sequence banks', *Biochimie* 78(5): 364-9.

Pinson, K. I., Brennan, J., Monkley, S., Avery, B. J. and Skarnes, W. C. (2000) 'An LDL-receptor-related protein mediates Wnt signalling in mice', *Nature* 407(6803): 535-8.

Raychowdhury, R., Niles, J. L., McCluskey, R. T. and Smith, J. A. (1989) 'Autoimmune target in Heymann nephritis is a glycoprotein with homology to the LDL receptor', *Science* 244(4909): 1163-5.

Ribes, V. and Briscoe, J. (2009) 'Establishing and interpreting graded Sonic Hedgehog signaling during vertebrate neural tube patterning: the role of negative feedback', *Cold Spring Harb Perspect Biol* 1(2): a002014.

Riedel, F., Vorkel, D. and Eaton, S. (2011) 'Megalin-dependent yellow endocytosis restricts melanization in the Drosophila cuticle', *Development* 138(1): 149-58.

Roach, E., Demyer, W., Conneally, P. M., Palmer, C. and Merritt, A. D. (1975) 'Holoprosencephaly: birth data, benetic and demographic analyses of 30 families', *Birth Defects Orig Artic Ser* 11(2): 294-313.

Roebroek, A. J., Reekmans, S., Lauwers, A., Feyaerts, N., Smeijers, L. and Hartmann, D. (2006) 'Mutant Lrp1 knock-in mice generated by recombinase-mediated cassette exchange reveal differential importance of the NPXY motifs in the intracellular domain of LRP1 for normal fetal development', *Mol Cell Biol* 26(2): 605-16.

Roelink, H., Porter, J. A., Chiang, C., Tanabe, Y., Chang, D. T., Beachy, P. A. and Jessell, T. M. (1995) 'Floor plate and motor neuron induction by different concentrations of the amino-terminal cleavage product of sonic hedgehog autoproteolysis', *Cell* 81(3): 445-55.

Rosenfeld, J. A., Ballif, B. C., Martin, D. M., Aylsworth, A. S., Bejjani, B. A., Torchia, B. S. and Shaffer, L. G. (2010) 'Clinical characterization of individuals with deletions of genes in holoprosencephaly pathways by aCGH refines the phenotypic spectrum of HPE', *Hum Genet.*

Sandberg, M., Kallstrom, M. and Muhr, J. (2005) 'Sox21 promotes the progression of vertebrate neurogenesis', *Nat Neurosci* 8(8): 995-1001.

Sawyer, J. M., Harrell, J. R., Shemer, G., Sullivan-Brown, J., Roh-Johnson, M. and Goldstein, B. (2010) 'Apical constriction: a cell shape change that can drive morphogenesis', *Dev Biol* 341(1): 5-19.

Schachter, K. A. and Krauss, R. S. (2008) 'Murine models of holoprosencephaly', *Curr Top Dev Biol* 84: 139-70.

Schauerte, H. E., van Eeden, F. J., Fricke, C., Odenthal, J., Strahle, U. and Haffter, P. (1998) 'Sonic hedgehog is not required for the induction of medial floor plate cells in the zebrafish', *Development* 125(15): 2983-93.

Schonbaum, C. P., Lee, S. and Mahowald, A. P. (1995) 'The Drosophila yolkless gene encodes a vitellogenin receptor belonging to the low density lipoprotein receptor superfamily', *Proc Natl Acad Sci U S A* 92(5): 1485-9.

Serluca, F. C. and Fishman, M. C. (2001) 'Pre-pattern in the pronephric kidney field of zebrafish', *Development* 128(12): 2233-41.

Shanmugalingam, S., Houart, C., Picker, A., Reifers, F., Macdonald, R., Barth, A., Griffin, K., Brand, M. and Wilson, S. W. (2000) 'Ace/Fgf8 is required for forebrain commissure formation and patterning of the telencephalon', *Development* 127(12): 2549-61.

Shinya, M., Furutani-Seiki, M., Kuroiwa, A. and Takeda, H. (1999) 'Mosaic analysis with oep mutant reveals a repressive interaction between floor-plate and non-floor-plate mutant cells in the zebrafish neural tube', *Dev Growth Differ* 41(2): 135-42.

Simon-Chazottes, D., Tutois, S., Kuehn, M., Evans, M., Bourgade, F., Cook, S., Davisson, M. T. and Guenet, J. L. (2006) 'Mutations in the gene encoding the low-density lipoprotein

receptor LRP4 cause abnormal limb development in the mouse', *Genomics* 87(5): 673-7.

Smith, D. W., Lemli, L. and Opitz, J. M. (1964) 'A Newly Recognized Syndrome of Multiple Congenital Anomalies', *J Pediatr* 64: 210-7.

Smith, J. L. and Schoenwolf, G. C. (1989) 'Notochordal induction of cell wedging in the chick neural plate and its role in neural tube formation', *J Exp Zool* 250(1): 49-62.

Smith, K. M., Ohkubo, Y., Maragnoli, M. E., Rasin, M. R., Schwartz, M. L., Sestan, N. and Vaccarino, F. M. (2006) 'Midline radial glia translocation and corpus callosum formation require FGF signaling', *Nat Neurosci* 9(6): 787-97.

Sonoda, I., Imoto, I., Inoue, J., Shibata, T., Shimada, Y., Chin, K., Imamura, M., Amagasa, T., Gray, J. W., Hirohashi, S. et al. (2004) 'Frequent silencing of low density lipoprotein receptor-related protein 1B (LRP1B) expression by genetic and epigenetic mechanisms in esophageal squamous cell carcinoma', *Cancer Res* 64(11): 3741-7.

Soriano, P. (1999) 'Generalized lacZ expression with the ROSA26 Cre reporter strain', *Nat Genet* 21(1): 70-1.

Spoelgen, R., Hammes, A., Anzenberger, U., Zechner, D., Andersen, O. M., Jerchow, B. and Willnow, T. E. (2005) 'LRP2/megalin is required for patterning of the ventral telencephalon', *Development* 132(2): 405-14.

Stenkamp, D. L., Frey, R. A., Mallory, D. E. and Shupe, E. E. (2002) 'Embryonic retinal gene expression in sonic-you mutant zebrafish', *Dev Dyn* 225(3): 344-50.

Storm, E. E., Garel, S., Borello, U., Hebert, J. M., Martinez, S., McConnell, S. K., Martin, G. R. and Rubenstein, J. L. (2006) 'Dose-dependent functions of Fgf8 in regulating telencephalic patterning centers', *Development* 133(9): 1831-44.

Storm, E. E., Rubenstein, J. L. and Martin, G. R. (2003) 'Dosage of Fgf8 determines whether cell survival is positively or negatively regulated in the developing forebrain', *Proc Natl Acad Sci U S A* 100(4): 1757-62.

Tamai, K., Semenov, M., Kato, Y., Spokony, R., Liu, C., Katsuyama, Y., Hess, F., Saint-Jeannet, J. P. and He, X. (2000) 'LDL-receptor-related proteins in Wnt signal transduction', *Nature* 407(6803): 530-5.

Tanzawa, K., Shimada, Y., Kuroda, M., Tsujita, Y., Arai, M. and Watanabe, H. (1980) 'WHHL-rabbit: a low density lipoprotein receptor-deficient animal model for familial hypercholesterolemia', *FEBS Lett* 118(1): 81-4.

Thisse, B., Heyer, V., Lux, A., Alunni, V., Degrave, A., Seiliez, I., Kirchner, J., Parkhill, J. P. and Thisse, C. (2004) 'Spatial and temporal expression of the zebrafish genome by large-scale in situ hybridization screening', *Methods Cell Biol* 77: 505-19.

Thompson, J. D., Higgins, D. G. and Gibson, T. J. (1994) 'CLUSTAL W: improving the sensitivity of progressive multiple sequence alignment through sequence weighting, position-specific gap penalties and weight matrix choice', *Nucleic Acids Res* 22(22): 4673-80.

Tian, J., Yam, C., Balasundaram, G., Wang, H., Gore, A. and Sampath, K. (2003) 'A temperature-sensitive mutation in the nodal-related gene cyclops reveals that the floor plate is induced during gastrulation in zebrafish', *Development* 130(14): 3331-42.

Tingaud-Sequeira, A., Forgue, J., Andre, M. and Babin, P. J. (2006) 'Epidermal transient

down-regulation of retinol-binding protein 4 and mirror expression of apolipoprotein Eb and estrogen receptor 2a during zebrafish fin and scale development', *Dev Dyn* 235(11): 3071-9.

Tole, S., Gutin, G., Bhatnagar, L., Remedios, R. and Hebert, J. M. (2006) 'Development of midline cell types and commissural axon tracts requires Fgfr1 in the cerebrum', *Dev Biol* 289(1): 141-51.

Trommsdorff, M., Gotthardt, M., Hiesberger, T., Shelton, J., Stockinger, W., Nimpf, J., Hammer, R. E., Richardson, J. A. and Herz, J. (1999) 'Reeler/Disabled-like disruption of neuronal migration in knockout mice lacking the VLDL receptor and ApoE receptor 2', *Cell* 97(6): 689-701.

van Straaten, H. W., Hekking, J. W., Wiertz-Hoessels, E. J., Thors, F. and Drukker, J. (1988) 'Effect of the notochord on the differentiation of a floor plate area in the neural tube of the chick embryo', *Anat Embryol (Berl)* 177(4): 317-24.

Veth, K. N., Willer, J. R., Collery, R. F., Gray, M. P., Willer, G. B., Wagner, D. S., Mullins, M. C., Udvadia, A. J., Smith, R. S., John, S. W. M. et al. (2011) 'Mutations in Zebrafish lrp2 Result in Adult-Onset Ocular Pathogenesis That Models Myopia and Other Risk Factors for Glaucoma', *PLoS Genetics* 7(2): e1001310.

Wang, Y., Song, L. and Zhou, C. J. (2011) 'The canonical Wnt/beta-catenin signaling pathway regulates Fgf signaling for early facial development', *Dev Biol* 349(2): 250-60.

Wehrli, M., Dougan, S. T., Caldwell, K., O'Keefe, L., Schwartz, S., Vaizel-Ohayon, D., Schejter, E., Tomlinson, A. and DiNardo, S. (2000) 'arrow encodes an LDL-receptor-related protein essential for Wingless signalling', *Nature* 407(6803): 527-30.

Willnow, T. E., Hammes, A. and Eaton, S. (2007) 'Lipoproteins and their receptors in embryonic development: more than cholesterol clearance', *Development* 134(18): 3239-49.

Willnow, T. E., Hilpert, J., Armstrong, S. A., Rohlmann, A., Hammer, R. E., Burns, D. K. and Herz, J. (1996) 'Defective forebrain development in mice lacking gp330/megalin', *Proc Natl Acad Sci U S A* 93(16): 8460-4.

Willnow, T. E., Petersen, C. M. and Nykjaer, A. (2008) 'VPS10P-domain receptors - regulators of neuronal viability and function', *Nat Rev Neurosci* 9(12): 899-909.

Yang, X., Zou, J., Hyde, D. R., Davidson, L. A. and Wei, X. (2009) 'Stepwise maturation of apicobasal polarity of the neuroepithelium is essential for vertebrate neurulation', *J Neurosci* 29(37): 11426-40.

Yang, Y. P., Anderson, R. M. and Klingensmith, J. (2010) 'BMP antagonism protects Nodal signaling in the gastrula to promote the tissue interactions underlying mammalian forebrain and craniofacial patterning', *Hum Mol Genet* 19(15): 3030-42.

Yang, Y. P. and Klingensmith, J. (2006) 'Roles of organizer factors and BMP antagonism in mammalian forebrain establishment', *Dev Biol* 296(2): 458-75.

Yochem, J., Tuck, S., Greenwald, I. and Han, M. (1999) 'A gp330/megalin-related protein is required in the major epidermis of Caenorhabditis elegans for completion of molting', *Development* 126(3): 597-606.

Zeng, X., Tamai, K., Doble, B., Li, S., Huang, H., Habas, R., Okamura, H., Woodgett, J. and He,

X. (2005) 'A dual-kinase mechanism for Wnt co-receptor phosphorylation and activation', *Nature* 438(7069): 873-7.

Zhang, B., Luo, S., Wang, Q., Suzuki, T., Xiong, W. C. and Mei, L. (2008) 'LRP4 serves as a coreceptor of agrin', *Neuron* 60(2): 285-97.

Zolessi, F. R. and Arruti, C. (2001) 'Apical accumulation of MARCKS in neural plate cells during neurulation in the chick embryo', *BMC Dev Biol* 1: 7.